Estimation of the Annualized Earthquake Loss (AEL) for Residential Buildings in the Greater Montreal area using HAZUS and OpenQuake

By

Xuejiao Long

Department of Civil Engineering

McGill University

Montreal, Canada

October 2022

A Thesis submitted to the
Faculty of Graduate Studies and Research
in partial fulfillment of the requirements for the degree of
Master of Engineering

Table of Contents

List of Figures

List of Tables

Executive Summary

Annualized Earthquake Losses (AEL) are estimated for residential buildings in the Greater Montreal region using two software, Hazus and OpenQuake. The loss estimation for each return period requires the following inputs: probabilistic hazard map with soil effect, building exposure model, census demographic information, and vulnerability. The losses for a range of return periods are used to calculate AEL. AEL estimates the average loss per year in a region that accounts for the variability in the location of the epicenter and the magnitude of earthquakes. It is an important information for public safety officials to identify the area most at risk as well as for determining the potential economic and human losses. AEL also provides a basis to compare the relative risk between various types of natural hazards and to prioritize risk mitigation measures. Probabilistic hazard models in Canada are provided by Natural Resources Canada (NRCan). The analysis was first performed according to the 5th generation seismic hazard model (SHM5), which is used for the 2015 Canadian National Building Code and to a limited extent with the 6th seismic hazard model (SHM6), which is used for the 2020 Canadian National Building Code. The total annualized residential earthquake loss based on SHM5 is estimated at Can$ 6.18 million with Hazus. The AEL is dominated by non-structural and content losses, which represents approximately 90% of the total AEL. A sensitivity analysis is conducted and indicates that the effect of ground motion level has the greatest effect on AEL followed by building value, construction type and code level. The result from Hazus is also compared with AEL calculated for US by FEMA, which indicates that the AEL for the Greater Montreal Area is consistent with values obtained in the US for urban areas with similar seismicity and exposure. The AEL was also estimated with OpenQuake since the software has been adopted by NRCan to implement SHM6 as well as for future generations of seismic hazard maps in Canada. Hazus uses fragility function while OpenQuake can operate with fragility functions as well as with vulnerability functions. The estimates with OpenQuake using vulnerability functions were obtained with functions provided by NRCan. The AEL of OpenQuake with the vulnerability approach is Can$ 6,16 million and is similar to AEL obtained by HazCan. The AEL of OpenQuake with the damage approach is Can$ 12.4 million and overestimates AEL in comparison to Hazus. The

discrepancy is mainly in relation to non-structural damage. Estimates of AEL with OpenQuake based on fragility analysis is obtained by calibrating the fragility functions with those of HazCan. This could be done accurately for structural losses but could only be done approximately for non-structural losses, which need to be derived separately for acceleration-sensitive and displacement-sensitive losses. The formulation of fragility curves for non-structural damage and content needs to be further investigated. Additionally, estimates of losses based on SHM6 were obtained for the return period of 2475 years. These preliminary results indicate that losses from SHM6 greatly increases for the Greater Montreal Area due to the increased average ground motions. It is recommended that the full probabilistic approach to calculate AEL be implemented as the next phase to this project. The analysis should also be extended to other populated regions of the St-Lawrence valley with high seismic hazards to provide a comprehensive assessment of residential seismic hazards in Quebec. Future applications should also provide estimates for social and other costs due to earthquakes.

Résumé Executif

Le Dommage Moyen Annuel (DMA) est estimé pour les bâtiments résidentiels de la région du Grand Montréal à l'aide de deux logiciels, Hazus et OpenQuake. L'estimation des pertes pour chaque période de retour nécessite les données d'entrée suivantes : carte probabiliste des risques avec effet de sol, modèle d'exposition des bâtiments, informations démographiques du recensement et vulnérabilité. Les pertes pour une plage de périodes de retour sont utilisées pour calculer le DMA. DMA estime la perte moyenne par an dans une région qui tient compte de la variabilité de l'emplacement de l'épicentre et de la magnitude des tremblements de terre. Il s'agit d'une information importante pour les responsables de la sécurité publique pour identifier les zones les plus à risque ainsi que pour déterminer les pertes économiques et humaines potentielles. DMA fournit également une base pour comparer le risque relatif entre divers types de risques naturels et pour hiérarchiser les mesures d'atténuation des risques. Les modèles probabilistes de risques au Canada sont fournis par Ressources naturelles Canada (RNCan). L'analyse a d'abord été effectuée selon le modèle d'aléa sismique de 5e génération (SHM5), qui est utilisé pour le Code national du bâtiment du Canada 2015 et, dans une mesure limitée, avec le modèle d'aléa sismique de 6e génération (SHM6), qui est utilisé pour le Code national du bâtiment du Canada 2020. Code du bâtiment. La perte totale annualisée du tremblement de terre résidentiel basée sur SHM5 est estimée à 6,18 millions de dollars canadiens avec Hazus. Le DMA est dominé par les pertes non structurelles et de contenu, qui représentent environ 90 % de le DMA totale. Une analyse de sensibilité est effectuée et indique que l'effet du niveau de mouvement du sol a le plus grand effet sur l'AEL, suivi de la valeur du bâtiment, du type de construction et du niveau de code. Le résultat de Hazus est également comparé à DMA calculée pour les États-Unis par la FEMA, ce qui indique que DMA pour la région du Grand Montréal est cohérente avec les valeurs obtenues aux États-Unis pour les zones urbaines avec une sismicité et une exposition similaire. DMA a également été estimée avec OpenQuake puisque le logiciel a été adopté par RNCan pour mettre en œuvre SHM6 ainsi que pour les générations futures de cartes d'aléas sismiques au Canada. Hazus utilise la fonction de fragilité tandis qu'OpenQuake peut fonctionner avec des fonctions de fragilité ainsi qu'avec des fonctions de vulnérabilité. Les estimations avec

OpenQuake utilisant des fonctions de vulnérabilité ont été obtenues avec des fonctions fournies par RNCan. Le DMA d'OpenQuake avec l'approche par vulnérabilité est de Can$ 6,16 millions et est similaire à DMA obtenue par HazCan. Le DMA d'OpenQuake avec l'approche des dommages est de Can$ 12,4 millions et surestime DMA par rapport à Hazus. L'écart concerne principalement les dommages non structurels. Les estimations de le DMA avec OpenQuake basées sur l'analyse de fragilité sont obtenues en calibrant les fonctions de fragilité avec celles de HazCan. Cela pourrait être fait avec précision pour les pertes structurelles, mais ne pourrait être fait qu'approximativement pour les pertes non structurelles, qui doivent être dérivées séparément pour les pertes sensibles à l'accélération et sensibles au déplacement. La formulation de courbes de fragilité pour les dommages non structuraux et le contenu doit être étudiée plus avant. De plus, des estimations des pertes basées sur SHM6 ont été obtenues pour la période de retour de 2475 ans. Ces résultats préliminaires indiquent que les pertes de SHM6 augmentent considérablement pour la région du Grand Montréal en raison de l'augmentation des mouvements moyens du sol. Il est recommandé que l'approche probabiliste complète pour calculer DMA soit mise en œuvre dans la prochaine phase de ce projet. L'analyse devrait également être étendue à d'autres régions peuplées de la vallée du Saint-Laurent à fort aléa sismique afin de fournir une évaluation complète de l'aléa sismique résidentiel au Québec. Les applications futures devraient également fournir des estimations des coûts sociaux et autres dus aux tremblements de terre.

Acknowledgement

I would like to express my gratitude, first and foremost to Professor Luc E. Chouinard for giving me the opportunity to work in this project. His guidance and time to time advice and constructive discussions throughout this project have been invaluable.

I would also like to thank Dr. Philippe Rosset. His superb mentorships and continuous supports lead me to a stimulating research program. I sincerely appreciate his contributions of time and ideas, which allowed me to conduct my research in a self-dependent way.

I also wish to thank my parents for their encouragement and support. Last but not the least I would like to thank all my friends and colleges at McGill for being supportive.

1. Introduction

1.1 Significance of Earthquake Loss Estimation

Earthquakes, as a major natural hazard, regularly affects living environment in high-seismic areas worldwide and induced large social and economic losses. Some of the largest earthquakes of the past decades includes the M9 Tōhoku earthquake and the following induced tsunami in Japan (2019), the M8.8 Chile earthquake (2010)., and the M7.9 Sichuan earthquake (2008)In general, large magnitude earthquakes which occurred in densely populated or less developed regions will cause more significant damages and losses than in rural areas or developed countries (e.g. Wyss et al. (2021)). The top ten earthquakes in terms of economic losses listed in Table 1 represent more than US$670 billion losses in total.

Table 1. List of top ten earthquakes in terms of economic losses

Rank	Losses Billion US$	Magnitude	Name	Year	Location	Date
1	360	9	Tōhoku	2011	Japan	11-Mar-11
2	150	7.9	Sichuan	2008	China	12-May-08
3	40	6.1	Christchurch	2011	New Zealand	22-Feb-11
4	28	6.8	Chūetsu	2004	Japan	23-Oct-04
5	16	6.3	L'Aquila	2009	Italy	06-Apr-09
6	15.80	5.8	Emilia	2012	Italy	20-May-12
7	15—30	8.8	Chile	2010	Chile	27-Feb-10
8	14.10	5.3	Zagreb	2020	Croatia	22-Mar-20
9	10	7.8	Gorkha	2015	Nepal	25-Apr-15
10	7.8—8.5	7	Haiti	2010	Haiti	12-Jan-10

In Canada, the seismic network of Natural Resources Canada detects approximately 4000 earthquakes each year (Trevor I. Allen et al., 2020). The map in Figure 1 locates significant earthquakes since 1663 in Canada with a magnitude higher than 4.0. In these events, bridges, buildings, and dams will experience major damages close to the earthquake source. Damages occur typically when the earthquake magnitude is above 4, depending on the epicentral distance, local soil conditions, building construction, etc (USGS, 2022). In particular, old and poor-designed buildings are particularly vulnerable to structural damage from earthquakes, which may cause additional human casualty (Parisi & Piazza, 2015; Rozman & Fajfar, 2009; Saretta et al., 2021).

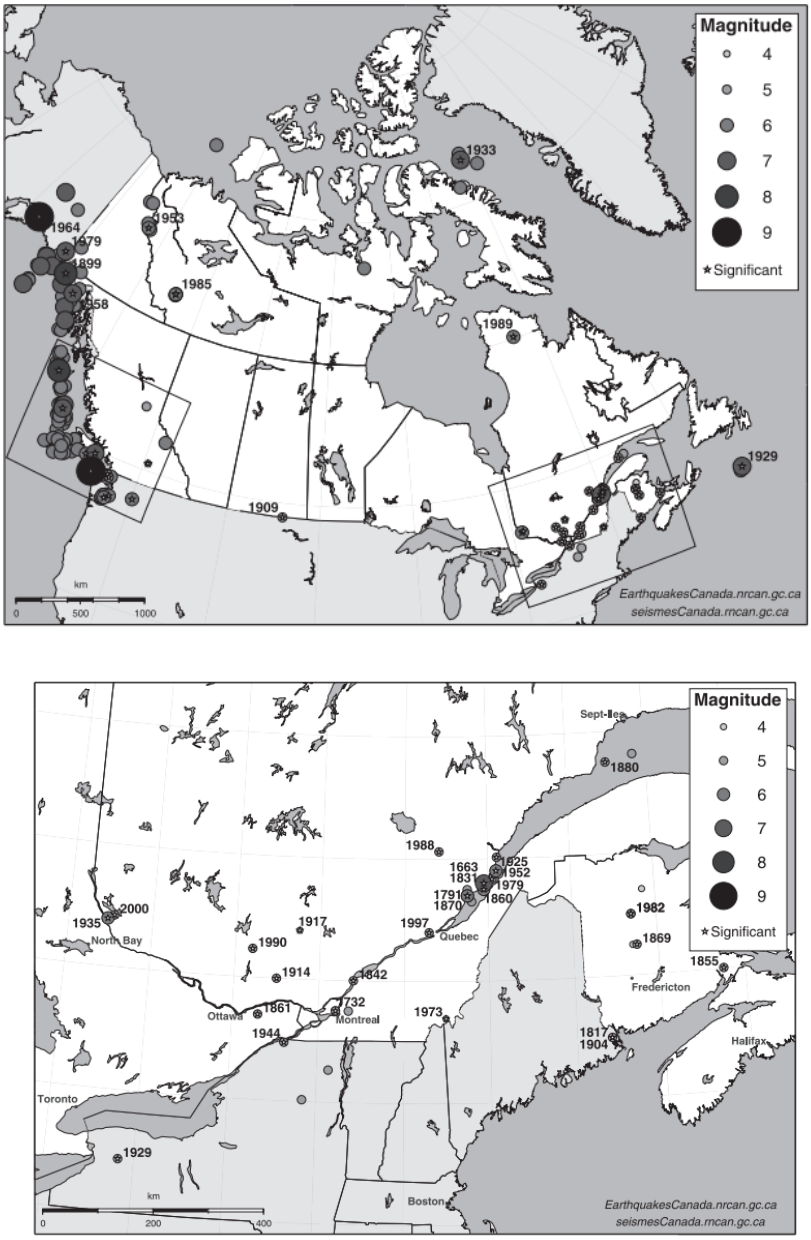

Figure 1. Significant earthquakes in Canada (top) and in or near southeastern Canada (Bottom) 1663-2006 (From Lamontagne et al., 2008)

Many national research associations, such as the Federal Emergency Management Agency in United States (FEMA), Natural Resources Canada (NRCan), and China Seismological Bureau, conduct risk assessment for risk mitigation and earthquake emergency response. For example, NRCan generates the seismic hazard map and updates the National Building Code on a five-year basis. A simulation of a large (M7.1) earthquake in eastern Canada conducted by the Insurance Bureau of Canada concluded that possible losses could reach Can$ 61 billion, with over Can$ 46 billion of losses from building properties (AIR,

2013). Studies on seismic damages and losses provide local policy makers and engineers with key outputs for disaster preparedness, mitigation, and response.

1.2 Seismic risk

In order to estimate seismic induced losses, a seismic risk assessment is conducted. Dowrick (2009) defined seismic risk as "the probability that social or economic consequences of earthquakes will equal or exceed specified values at a site, at several sites, or in an area, during a specified exposure time." It is the result of the combination of three components (Figure 2):

RISK=HAZARD*VULNERABILITY*EXPOSURE

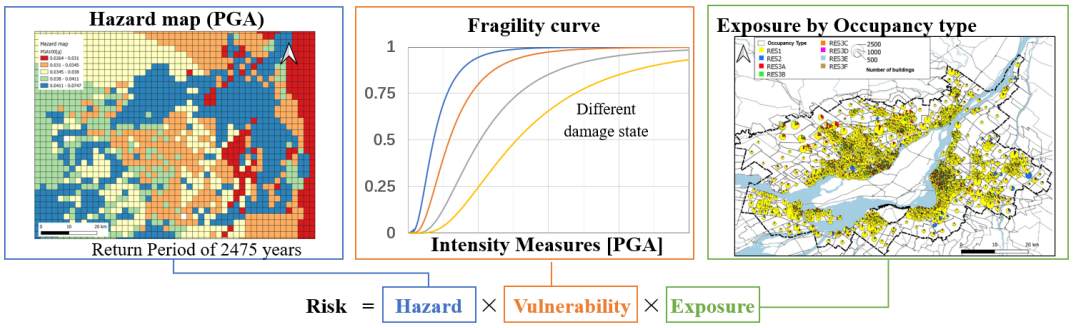

Figure 2. Components contributing to seismic risk calculation

Seismic risk analysis could be used for decision-making processes or risk management to decrease the potential for future adverse social and economic consequences. Government may use these results to make decisions on planning of land use, economic funding distribution, or social emergency response to earthquakes. Quantifying seismic losses in an appropriate manner is the first step to develop effective mitigation plans and making decisions in comparison to other natural hazards. By using different risk analysis software, different hazard and risk analysis method could be evaluated to obtain seismic loss using the most feasible and efficient approach.

1.3 Seismic Hazard

A seismic hazard is defined as "any physical phenomenon (e.g., ground shaking, ground failure) associated with an earthquake that may produce adverse effects on human activities" (Dowrick, 2009). Two main approaches are used to estimate the seismic hazard of a given region, the Deterministic Seismic Hazard Assessment (DSHA) and the Probabilistic Seismic Hazard Analysis (PSHA). Both methods use seismic sources, which could be represented by

a single point coordinate, a line, or an area (Figure 3).

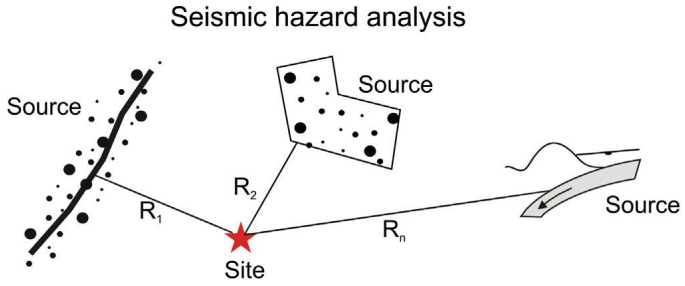

Figure 3. Types of seismic sources (Parvez and Rosset, 2014)

DSHA uses a single earthquake to determine the worst-case ground motion levels (Kramer, 1996). For that, one selects the earthquake source that can produce the strongest shaking at the site among the seismic sources that significantly affect the study area and source-to-site distance parameter for each source (right side of the Figure 4). DSHA accounts only the ground shaking uncertainties, given the occurrence of a single earthquake source or a limited set of specific earthquake sources (e.g., the "maximum expected earthquakes"), regardless of the probability of occurrence of these sources.

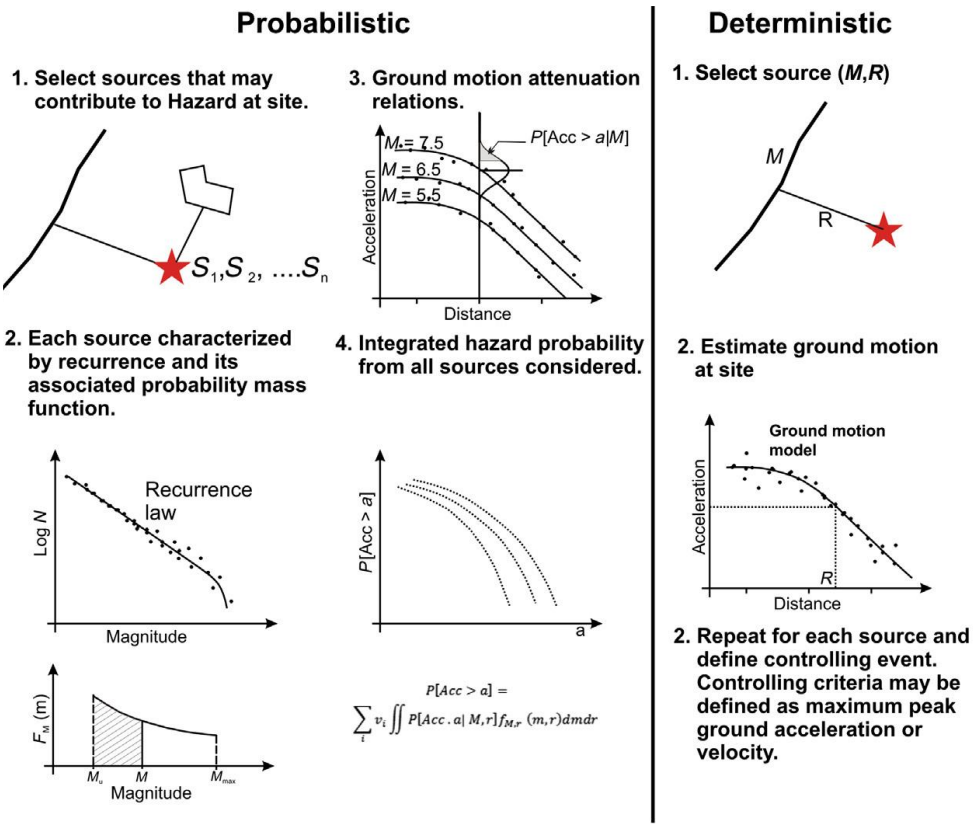

Figure 4. Schematic procedure used in probabilistic and deterministic seismic hazard assessment (Parvez and Rosset, 2014)

Unlike DSHA considering the worst-case ground motion, PSHA calculates the probability of exceedance of different levels of ground motion from all possible earthquake events (Baker, 2013).

A PSHA follows the main steps:

- First, identify all earthquake sources around the study area. For that, an earthquake catalog, which includes recorded and reported earthquakes of all magnitude, is used to determine earthquake regions with similar tectonic context. These seismic sources are linked to faults, which are typically observed from geological evidence, or regions where earthquakes occur frequently (Adams et al., 2015).
- Next, the recurrence rate and distribution in magnitude for earthquakes in each source are defined.
- Given a location where hazard has to be estimated, the attenuation of the earthquake motions is a function of the epicentral distance and local soil conditions. Ground motion prediction equations (GMPEs) are function that provide estimates for ground motion intensity, such as Peak Ground Acceleration (PGA), Peak Ground Velocity (PGV), and Spectra acceleration (Sa) for different periods as a function of the magnitude of the earthquake and epicentral distance (Baker, 2013).

It is now well known that local site conditions can amplify or de-amplify ground shaking at certain frequencies, and then influence the level of ground motion at a given site (Filiatrault, 2013; Hunter & Crow, 2015). By identifying the soil condition, one can adjust ground motion intensity by applying an amplification or de-amplification coefficient at the investigated sites.

The ground motion intensity calculated by PSHA at a site are often represented by the hazard curve, showing the mean annual frequency of exceedance of the corresponding intensity measure (IM). An example of the large scatter around those ground motion prediction models is seen in Figure 5, which shows spectral acceleration values at 1s that were observed in a past earthquake, the 1999 Chi-Chi, Taiwan (Mw7.6) event (Campbell & Bozorgnia, 2008).

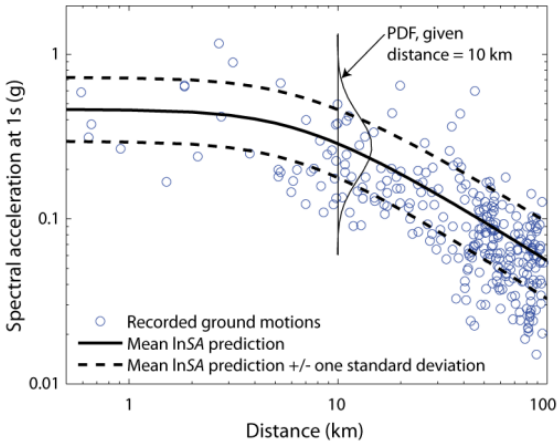

Figure 5. Ground motion prediction model: Observed spectral acceleration values from the 1999 Chi-Chi, Taiwan earthquake (Campbell & Bozorgnia, 2008)

The ground motion intensity could be also represented through hazard maps, showing the spatial distribution of expected ground motion intensity for an assigned return period (Parvez & Rosset, 2014). Seismic hazard map can be expressed in qualitative or quantitative terms. For example, the seismic hazard map for Canada produced in 1953 was a qualitative zoning map, while the map produced in 1970 and later were probabilistic seismic hazard maps showing the spatial distribution of PGA and Sa as illustrated in the Figure 6 (Adams, 2011).

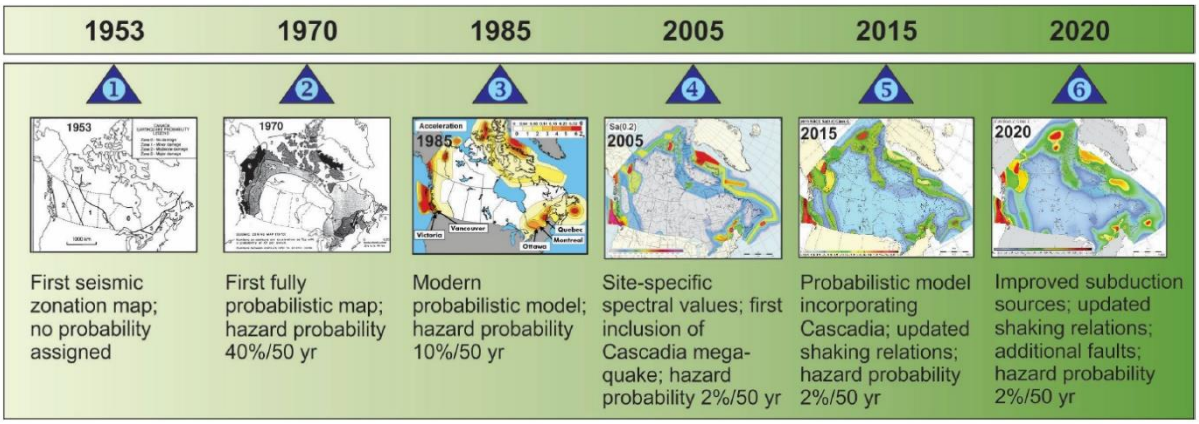

**Year of the* seismic hazard model is indicated on the top (Kolaj, Adams, et al., 2020)

Figure 6 Evolution of the PSHA mapping in Canada since 1953

Typically, seismic hazard maps are built at national scale, but larger-scale global seismic event maps are developed in the last decades in order to identify the high-seismicity regions in the world. The most recent project is the one developed by Global Earthquake Model (GEM), which is an international collaboration between multiple countries using the open-source software OpenQuake (V. Silva et al., 2014).

1.4 Vulnerability

In eastern Canada, old existing buildings were designed according to outdated versions of seismic design codes. Vulnerability of theses building under seismic events needs to be studies for loss estimation. Vulnerability or fragility is defined as the likelihood of a given damage level caused by a given level of ground motion (Dowrick, 2009). Damages are often divided in four levels: slight, moderate, extensive, and complete. Figure 7 shows an example of fragility curves for the four levels of damage. For a given level of ground shaking (the vertical dashed lines in Figure 7), the probability of each damage state is represented by the differences between the exceedance probabilities of two damage states.

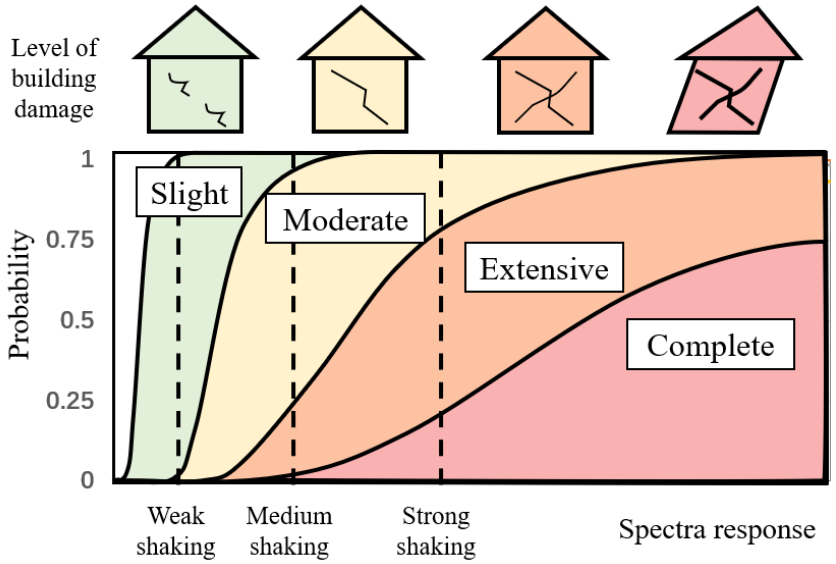

Figure 7. Example fragility curve for different damage states (modified from FEMA(2020)

Fragility curves depend on the types of the building and the construction material of the building frame. The building categories used in this thesis are discussed in section 3.4. Fragility curves are also influenced by the year of construction since an old building is more vulnerable than a recent one, due to evolution of seismic design code. For a given building type and construction material, Hazus provides fragility curves for different code levels.

Seismic loss estimates combine a consequence function to fragility functions. After estimating the damage from the fragility functions, the consequence function links the damage level to the building repair or replacement cost.

1.5 Exposure

Exposure is used to quantify the elements at risk. It includes the spatial distribution of the

number of buildings, their occupants, and replacement cost, characterized in terms of building classes. The development of building exposure models follows two main steps: (1) define the types of buildings and occupancy classes that are applicable for a region, (2) identification of the types of buildings, their location, replacement cost, and number of occupants, census data, past research projects, or local database such as the property tax roll (V. Silva et al., 2020). Detailed structural surveys are resource intensive and are performed only for complex or major buildings (Dell'Acqua et al., 2013). Conversely, in the absence of available data bases, a subjective approach is through interviews, expert judgements and comparisons with previously surveyed cities (Wieland et al., 2015).

1.6 Annualized Earthquake Loss (AEL)

Using the information on hazards, vulnerability, and exposure, estimates of direct economic loss, casualties, and shelter needs are computed. Direct economic losses are usually the monetary value of losses caused directly by earthquake. The direct economic losses from a PSHA associated with a given probability of occurrence can then be used to estimate the annualized earthquake loss (AEL), which is defined as "a long-term average loss per year in a specified geographic area due to earthquakes" (Chen et al., 2016). It is an indicator of relative regional earthquake risk and, therefore, facilitates understanding and comparison of earthquake risk among different communities and other sources of hazards. Earthquake loss estimates support stakeholders in preparing emergency response plans, developing earthquake-hazard mitigation strategies, and establishing earthquake insurance policies.

AEL is computed by numerically integrating the loss-probability curve linking the loss assessment for several return periods as shown in Figure 8. FEMA (2008) conducted a sensitivity analysis of AEL estimates as a function of the number of return periods for 10 metropolitan regions using 5, 8, 12, 15, and 20 return periods. They concluded that the difference in the AEL results using 8, 12, 15, and 20 return periods was negligible. Two assumptions were made in the choice of the return periods; first, the losses of ground motion with return periods greater than 2,500 years were assumed to be no worse than the losses for a 2,500-year event. Second, the losses for ground motion with less than a 100-year return period were assumed to be generally small enough to be negligible (FEMA-USGS-PDC,

2017).

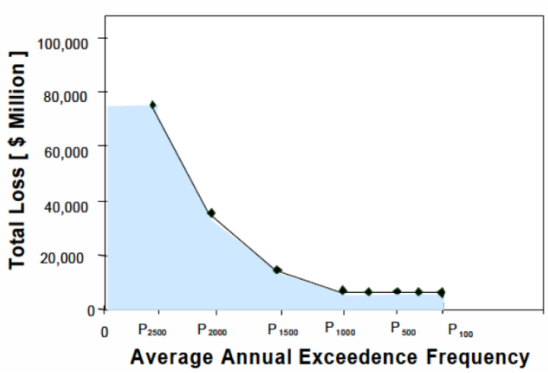

Annual probability	Probability (%) in 50 years	Return period (years)
0.02	63.6	50
0.01375	50.0	73
0.01	40.0	100
0.00445	20.0	225
0.0021	10.0	475
0.001	5.0	1000
0.0005	2.5	2000
0.000404	2.0	2475

Figure 8. Scheme to calculate AEL: Average AEL Computation Probabilistic Loss Curve (left); Return period used to compute the loss curve (right)

In the FEMA's estimate done in 2017, losses were calculated for the probabilistic ground motions associated with eight return periods: 100, 225, 475, 750, 1000, 1500, 2000, 2475 years using software HAZUS 3.0 (FEMA-USGS-PDC, 2017). The annual probability and probability of exceedance in 50 years of the return periods are shown in the right table of Figure 8. AEL was computed by multiplying losses calculated by HAZUS by respective annual probability (annual frequencies of occurrence), and then integrated the values for all eight return periods as explained in Table 2.

Table 2. Method to calculate AEL by FEMA (2017).

#	Return period	Annual probability	Differential probabilities		Annual Losses	Average losses	Annualized losses
			Formula	Values			
1	2500	0.00040	P2500	0.00040	L2500	L2500	P2500 x L2500
2	2000	0.00050	P2000-P2500	0.00010	L2000	(L2500+L2000)/2	P2100-P2500 x (L2500+L2000)/2
3	1500	0.00067	P1500-P2000	0.00017	L1500	(L1500+L2000)/2	P1500-P2000 x (L1500+L2000)/2
4	1000	0.00100	P1000-P1500	0.00033	L1000	(L1000+L1500)/2	P1000-P1500 x (L1000+L1500)/2
5	750	0.00133	P750-P1000	0.00033	L750	(L750+L1000)/2	P750-P1000 x (L750+L1000)/2
6	500	0.00200	P500-P750	0.00067	L500	(L500+L750)/2	P500-P750 x (L500+L750)/2
7	250	0.00400	P250-P500	0.00200	L250	(L250+L500)/2	P250-P500 x (L250+L500)/2
8	100	0.01000	P100-P250	0.00600	L100	(L100+L250)/2	P100-P250 x (L100+L250)/2
Annualized earthquake loss (AEL)°							**Sum ∑( )**

FEMA calculated Annualized Earthquake Losses based on the hazard maps from 2001, 2008, and 2017 (Federal Emegency Management Agency (FEMA), 2001, 2008; FEMA-USGS-PDC, 2017). The earliest studies (FEMA 2001), published in 2001, used the 1996 version of the seismic hazard maps provided by the US Geological Survey (USGS), and estimated the AEL of $4.4 billion US dollars at the national level. California accounted for 75% of the losses, at $3.3 billion. The second study (FEMA 2008) incorporates the 2002 hazard maps and uses up-to-date inventory data. It predicts annualized losses of $5.3 billion US dollars and California again carries the majority of losses annualized with $3.5 billion. The most recent published version calculated the annualized loss and annualized loss ratio for USA and evaluated the geographical distribution of the losses. Western US will experience the most losses, especially in California as shown in the map of the Figure 9. Jaiswal et al. (2017) compared the results of the calculated AEL for the 2008 and 2017 reports showing that earthquake risk continues to grow with increased population and vulnerability of old buildings even though the earthquake hazard has remained relatively stable. . Chen et al. (2016) further examined the effects of site amplification on AEL in California. The statewide AEL estimate is in- sensitive to alternate assumptions of site amplification while differences in AEL were observed for smaller geographic units.

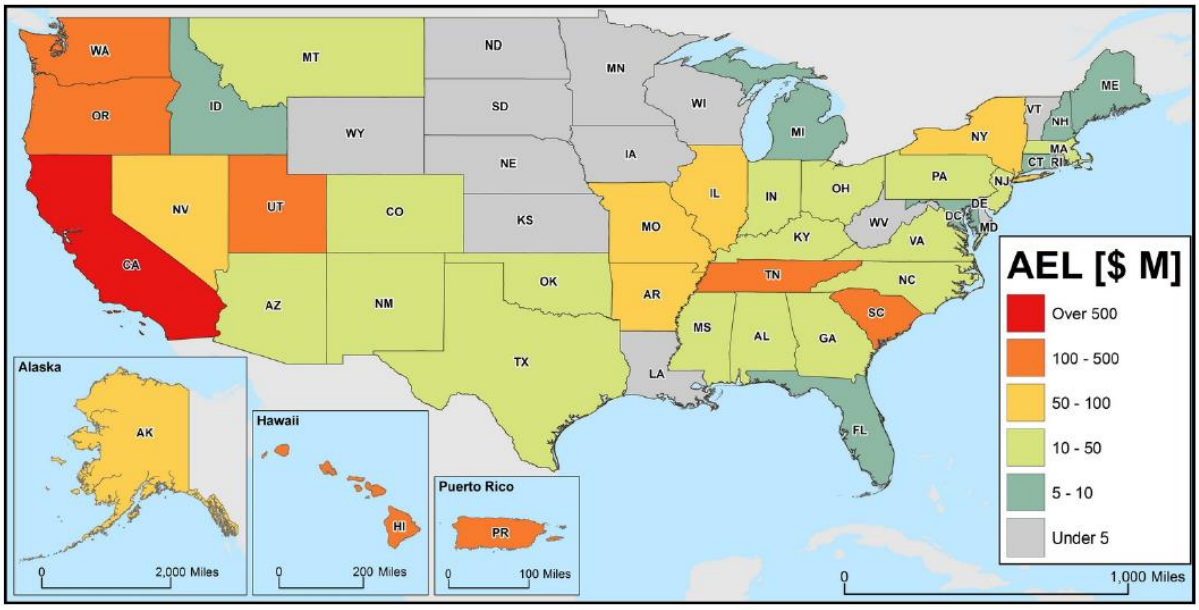

Figure 9. Annualized Earthquake Losses by State (FEMA-USGS-PDC, 2017)

For scientists and engineers, AEL allows them to assess the socioeconomic losses,

determine and prioritize the possible risk mitigation alternatives. For decision makers such as government agency and insurance companies, the annualized loss gives a measure of total losses that account for appropriate discounting for events far into the future. It provides guidelines for community risk assessment and a standard to rank risk management options. Therefore, conducting an AEL estimation for the region of interest is expected to be valuable and necessary.

1.7 Objectives

The main objective of the thesis is to estimate AEL for residential buildings in the Greater Montreal Area (see chapter 3) with two risk assessment software: Hazus (FEMA, 2020) and OpenQuake (GEM, 2021). This thesis aims at quantifying the annualized earthquake loss for residential buildings in the Greater Montreal area and provide insights on the feasibility of carrying out risk assessments by the two software. Hazus is a multi-hazard (flood, hurricane and earthquake) loss estimation tool commonly used mainly in USA developed by FEMA, while OpenQuake is a new developed open-source platform by GEM that performs both seismic hazard and risk assessments worldwide.

This thesis is divided into seven chapters: first, it starts with an introductory chapter that provides a brief overview of the topic studied, introducing methodology for seismic risk assessment and calculation of AEL. Then, the second chapter provides comprehensive state-of-art review on risk assessments using HAZUS and OpenQuake. The third chapter discusses the case study of the residential buildings in Montreal region, where the components to evaluate risk and procedures to calculate AEL are detailed. The results from both software are analyzed and discussed in chapters 4 and 5, followed by a comparison of the approaches using the two software and a comparison of the results from different generations of seismic hazards in chapter 6. The last chapter presents the main conclusions, discussion of the results, and recommendations for future studies.

2. The use of Hazus and OpenQuake to calculate AEL

In recent years, various software was developed to perform seismic risk analysis. The major seismic risk software includes: Hazus, Ergo, SELENA, OpenQuake and ER2 (Hosseinpour et al., 2021). Two of the major software, Hazus and OpenQuake, are used in this thesis to conduct loss estimation and provide a comprehensive comparison of their results.

2.1 HAZUS

Hazus has been developed by FEMA and the National Institute of Building Sciences (NIBS) since 1992 to produce estimates of human and economic consequences of earthquakes, hurricanes, and floods (FEMA 2012). It has a user-friendly Graphical User Interface (GUI) to input data and presents output in GIS-based platform connected to ArcGIS software. This tool also performs loss estimation for a number of infrastructures (i.e., lifelines, essential facilities and transportation systems), as well as the damage evaluation from fires following earthquake and indirect economic losses (FEMA, 2020).

A multi-hazard version, Hazus MH, was released in 2004 (HAZUS-MH, 2004). It is used for various hazards including earthquakes, floods, and hurricanes. It has been applied in most of the case studies for seismic loss estimation and at various spatial scales in the USA. Examples of previous studies are Dargush et al. (2001) for New York State, (Field et al., 2005) for a blind-thrust earthquake in Los Angeles, California, Moffatt and Cova (2010) for the Salt Lake County, Utah, and Chen et al., (2006) on the sensitivity of seismic losses in California due to soil amplification. Hazus MH was updated several times and now is a well-developed tool for seismic loss estimation. It has been widely used the last decade in many regions around the world. Bendito et al. (2014) used the USGS ShakeMaps scenarios for two potential earthquake events to evaluate the influence of large earthquakes in Mérida State in Venezuela. Similarly, seismic loss estimations for Israel and Turkey were performed by (Levi et al., 2015) and (Ansal et al., 2009). Damage assessments for individual buildings using HAZUS data were obtained for buildings in Northern Israel (Felsenstein et al., 2021) and in Iran (Firuzi et al., 2019).

Hazus Canada (HazCan) is the Canadian version of the HAZUS software for regional hazard loss estimation. It has been adapted from the US version since 2011 for seismic risk

assessment and loss estimation (Ulmi et al., 2014). Although many studies on seismic loss comparison between estimated and observed damage using HazUS have been conducted for US earthquakes, little has been done in the Canadian context. One example from the US is the study conducted by Kircher et al. (2006), in which a comparison of estimated and actual damage and loss due to the 1994 Northridge earthquake was discussed. In the paper, trends in direct economic losses to residential buildings are similar to those observed in residential insurance claims.

The Canadian version HazCan (Ploeger et al., 2010), is based on version 2.1 of Hazus, which does not include the latest developments of the 4.2 version such as the output exporting module. The default population and building database for Canada is from 2008 (Ulmi et al., 2014). The input data units refer to US customary unit system (inches and feet) which required a conversion from the international unit system applied in Canada.

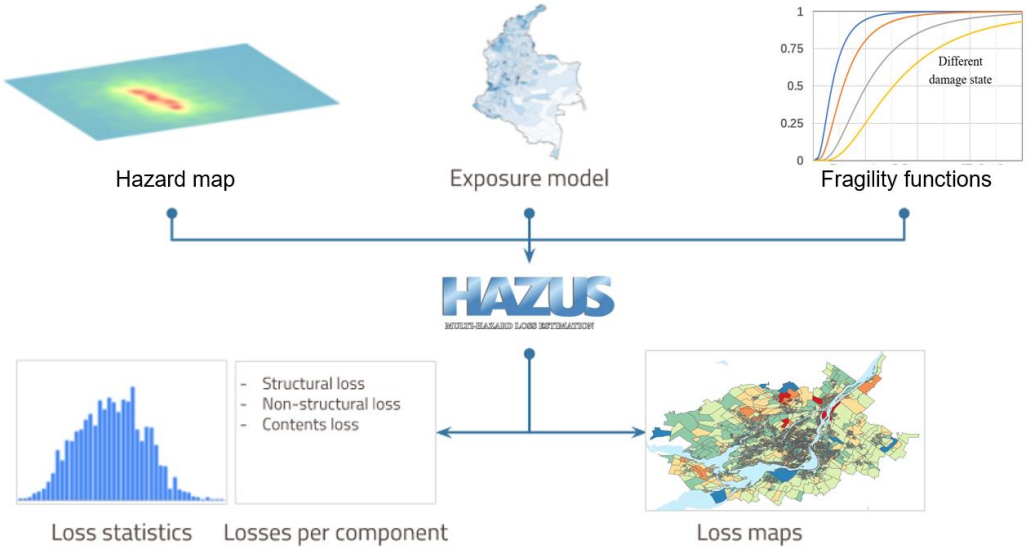

Figure 10. Scheme for Hazus seismic analysis

The databases required in HazCan to perform seismic risk analyses are: (1) the building inventory, (2) the distribution of population at three different times of the day, (3) fragility functions, and (4) ground motion hazard maps defined in a probabilistic or deterministic modes (Rozelle et al., 2019). The loss statistics and loss maps can be obtained from running the model, scheme shown in Figure 10. HazCan has been applied for risk assessment and loss estimation in various regions in Canada, especially in urban areas, such as Ottawa (Ploeger et al., 2010) and Montreal (Rosset et al., 2022; Yu et al., 2016; Rosset et al., 2019. For the

Montreal region, Rosset et al. (2022) performed a seismic risk assessment for residential buildings considering a repetition of the 1732 M5.8 Montreal earthquake.

2.2 OpenQuake

OpenQuake is a seismic hazard and risk assessment platform developed by the Global Earthquake Model (GEM) consortium that offers an integrated environment for modelling, viewing, exploring, and managing earthquake risk (GEM, 2021). Unlike Hazus, which is a closed source software accompanied by comprehensive users and technical manuals, OpenQuake is opensource coded in the Python programming language. The most updated version is OQ 3.7.1. OpenQuake targets to calculate the hazard and risk using the same method for anywhere across the world (V. Silva et al., 2014), in the hopes of achieving a uniform standard. More importantly, it can also include the spatial correlation of the ground motion residuals in hazard analysis and uncertainty in the vulnerability for risk assessment (GEM, 2021). The major calculation algorithms of the OQ engine include the scenario risk calculator, scenario damage calculator, classic PSHA-based risk, probabilistic event-based (PEB) risk and retrofitting benefit–cost ratio (GEM, 2021).

The scenario risk calculator can be used for calculation of individual asset loss of an earthquake scenario, taking into account aleatory and epistemic uncertainty. The input data consists of the ground motion fields, exposure model of the regions of interest, and the vulnerability model (Figure 11(a)). The losses are calculated based on these three components and presented via statistics or spatial maps.

The Classical Probabilistic Seismic risk calculator is an integrated risk assessment that includes the PSHA and risk analysis components (Figure 11(b)). The PSHA components allows calculation of hazard curves and hazard maps following the classical integration procedure formulated by Field et al. (2003). A seismic source logic tree is used to create a seismic source input model and a ground motion model (GEM, 2021). Once the Hazard curves are obtained from PSHA, they are combined with the exposure model and vulnerability functions to calculate losses and associated risk (Figure 11(b)).

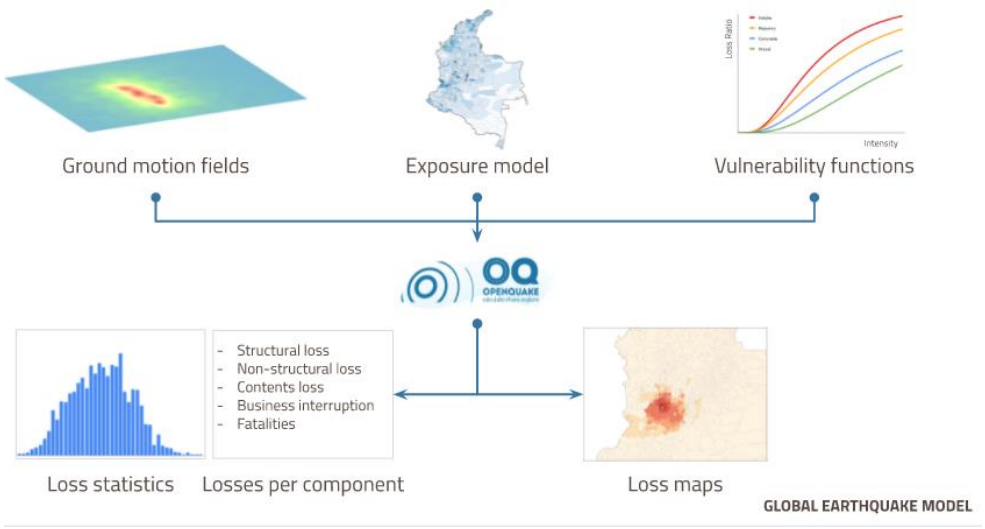

(a)

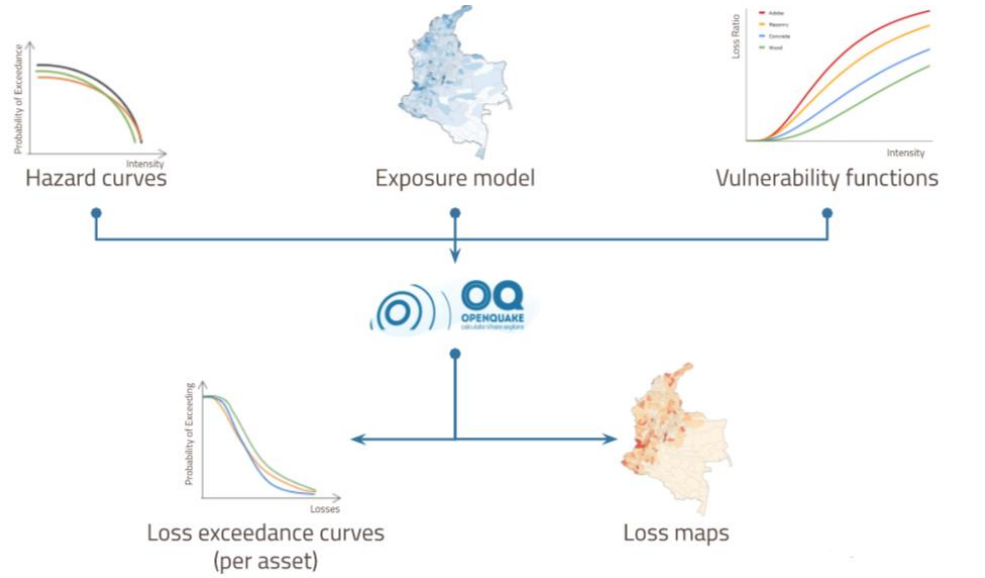

(b)

Figure 11. Scheme for (a) scenario risk calculator and (b) PSHA risk calculator (GEM, 2021)

The Probabilistic Event-Based (PEB) calculator is the most innovative calculation mode in OQ with respect to other lost estimation software. In PEB, the Monte Carlo method is used to generate the stochastic event set (SES), which represents a potential realization of seismicity, with a ground motion field calculated for each event contained in SES.

The classical and PEB calculator has the advantage of carrying out hazard and risk analysis within one iteration, eliminating the preparation process for the hazard data. However, the lack of vulnerability information, as well as the computationally intensive procedure make the classical and PEB calculator less feasible for the study area of this thesis. Then, for our calculation of the annualized loss, we will use the scenario calculator

individually for each of the eight-selected return period; each hazard map of a return period representing one scenario.

Seismic hazard analysis has been conducted using OpenQuake in several countries such as Canada, Italy, or Turkey. For example, a fully probabilistic hazard and risk assessment was carried out for mainland Portugal (Burton & Silva, 2016) Furthermore, in addition to the ground motion in PSHA, seismic-induced liquefaction has been examined using the OpenQuake hazard and risk model to estimate regional losses (Yilmaz et al., 2021).

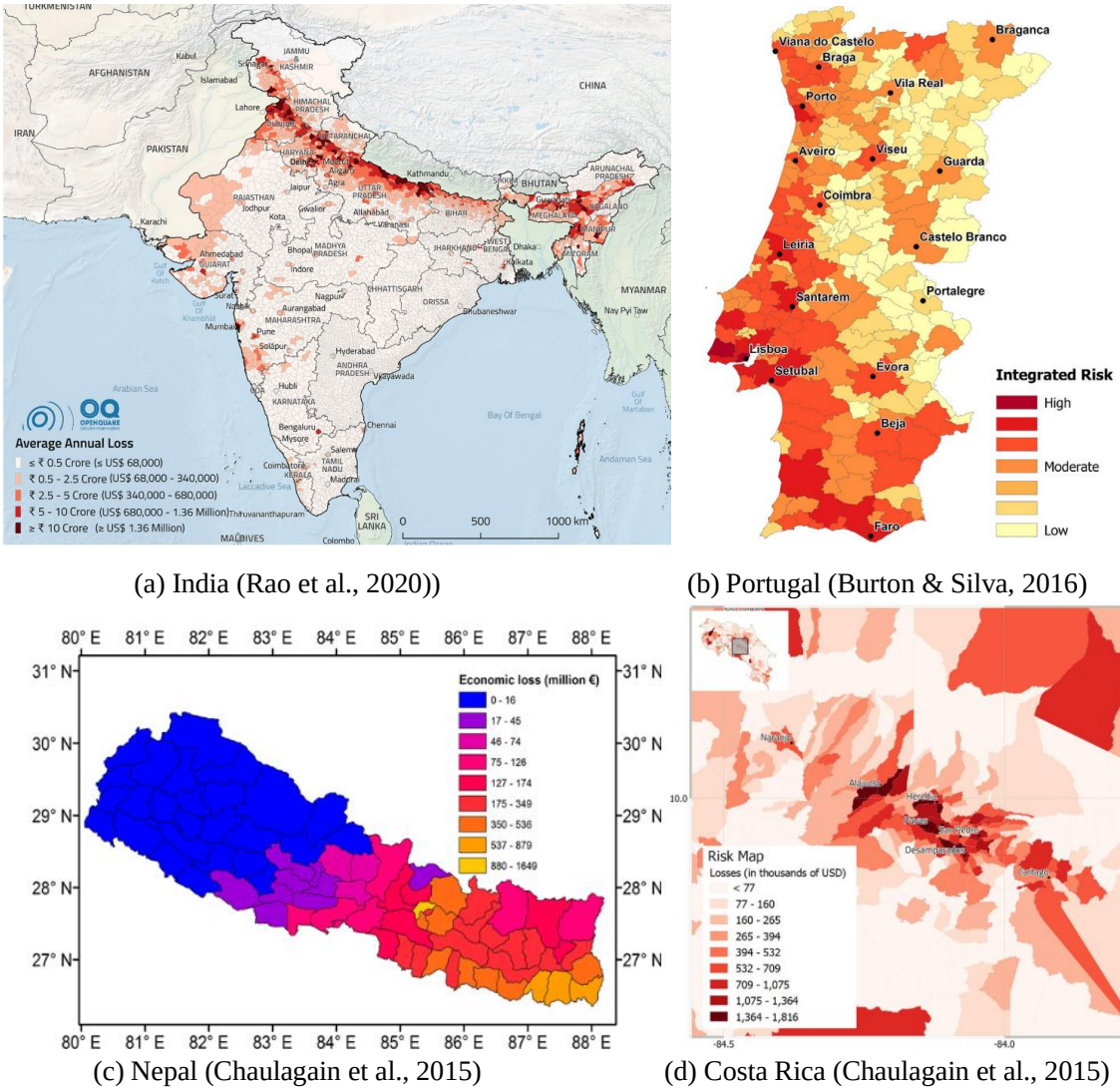

(a) India (Rao et al., 2020)) (b) Portugal (Burton & Silva, 2016)

(c) Nepal (Chaulagain et al., 2015) (d) Costa Rica (Chaulagain et al., 2015)

Figure 12. Loss map from various studies in four regions in the world

However, there is a lack of studies associated with seismic risk. Risk assessment and loss estimation has been calculated in terms of economic and social attributes. The average annual loss (AAL) is the economic loss divided by the number of years of the seismic event set. The

PEB risk analysis calculated AAL for India (Rao et al., 2020) using vulnerability functions developed by past studies in India. The losses occurred in northern India, which is close to the plate boundary. Costa Rica (Calderon & Silva, 2019) and Nepal (Chaulagain et al., 2015) used vulnerability functions converted from a combination of fragility and consequence functions. AAL is disaggregated by district for metropolitan areas for Costa Rica and Nepal. This provided the overview of the regional risk distribution and a general economic loss estimation. Besides estimation of direct physical risk such as human or economic losses, the socioeconomic characteristics of populations is also evaluated. For Portugal, demographic characteristics (age, gender, and nationality, etc.), economy indicators (purchasing power and labor force per household, etc.), education indicators, governess indicators (for example, crime rate) are combined into the risk model to form a social risk distribution map in Figure 12 (b) (Burton & Silva, 2016).

OpenQuake can be also used to estimate seismic losses for specific structures, such as precast RC structures in Italy (Rodrigues et al., 2018). The most recent published loss estimation is a scenario-based probabilistic seismic risk assessment for the Republic of Cyprus (Kazantzidou-Firtinidou et al., 2022). Stochastic event-based hazard analysis is first developed, followed by a selection of seismic scenarios for given return periods. Although this considered the scenario for different return period of 475 and 2500 years, there is no up-to-date studies of AEL calculations using OpenQuake.

The major challenge to use OpenQuake to conduct risk analysis is the construction of the proper fragility or vulnerability function. There are various ways to obtain the vulnerability. Some studies used push over analysis to obtain the fragility models (Calderon & Silva, 2019), while others are obtained from design code or analytical relationships (Rao et al. 2020; Chaulagain et al. 2015).

OpenQuake is more flexible compared with HAZUS, as it can generate large datasets for testing and ensuring that desired results are obtained following any changes or additions to the code base (V. Silva et al., 2014). However, the flexibility of selecting currently available fragility curves can be very subjective and applying the GEM framework necessitates an in-depth knowledge and data about the structural dynamic response and evaluated fragility

curves. For example, the risk assessment for India by Rao et al. (2020) has limited information about the fragility function for the specific building type such as rubble-stone masonry buildings, reinforced concrete buildings, or bamboo buildings.

In Canada, OpenQuake has been adopted by NRCan to develop the new generation of seismic hazard models for the National Building Code of Canada (Allen et al., 2020). The earliest application of OpenQuake is the damage estimation for the western coast in Victoria, British Columbia done by Bebamzadeh et al. (2019). In their study, a deterministic seismic hazard analysis for the City of Victoria was carried out, followed by risk assessment. The city's most at-risk buildings and infrastructure and damage distribution are discussed. However, they did not calculate any seismic induced losses such as economic or social losses. For eastern Canada, Chien et al., (2021) first proposed a scenario-based hazard calculation using OpenQuake for the region of Montreal considering the potential activation of existing faults from earthquake sources inversion without conducting any risk analysis. Hobbs et al. (2021) proposed a framework and carried out associated risk analysis for three earthquake scenarios: a M7.0 event in the Strait of Georgia near Vancouver, BC; a M7.3 event on the Leech River Fault near Victoria, BC; and a M7.5 event in Gatineau, QC, near Ottawa. The latter provides some information about the losses in Gatineau region, but there are still no related studies for Montreal region using OpenQuake.

3. Case study in Greater Montreal

3.1 Region studied

Around 4000 earthquakes are recorded in Canada each year by the seismic network operated by Natural Resources Canada. These events are mainly concentrated in two regions: the west coast of British Columbia and southeastern Canada, mainly the southeastern Ontario and southern Québec region. Although these two seismic source zones consist of only a small fraction of Canada in terms of territory area, they concern about 40% of the national population.

In 2002, Adams et al. calculated the seismic risk for urban areas in Canada considering their population and the level of ground shaking for the return period of 475 years. At this time, Montreal was ranked second after Vancouver (Adams et al. 2002). In Quebec, the seismic activity is attributed to the reactivation of an ancient normal rift faults along the St. Lawrence and Ottawa Rivers (the Iapetan Rift Margin -IRM) as well as the passage of an ancient hot spot beneath the region (the Gatineau region-GAT) as shown in Figure 13. Low-magnitude seismic events delineate the St. Lawrence Rift, which is at the origin of the main large earthquakes marked by white stars. The black arrows indicate areas of low seismic activity in the middle of the active areas of Montreal (MNT), Charlevoix (CHV) and Bas Saint-Laurent (BSL) within the IRM region (Kolaj et al., 2020).

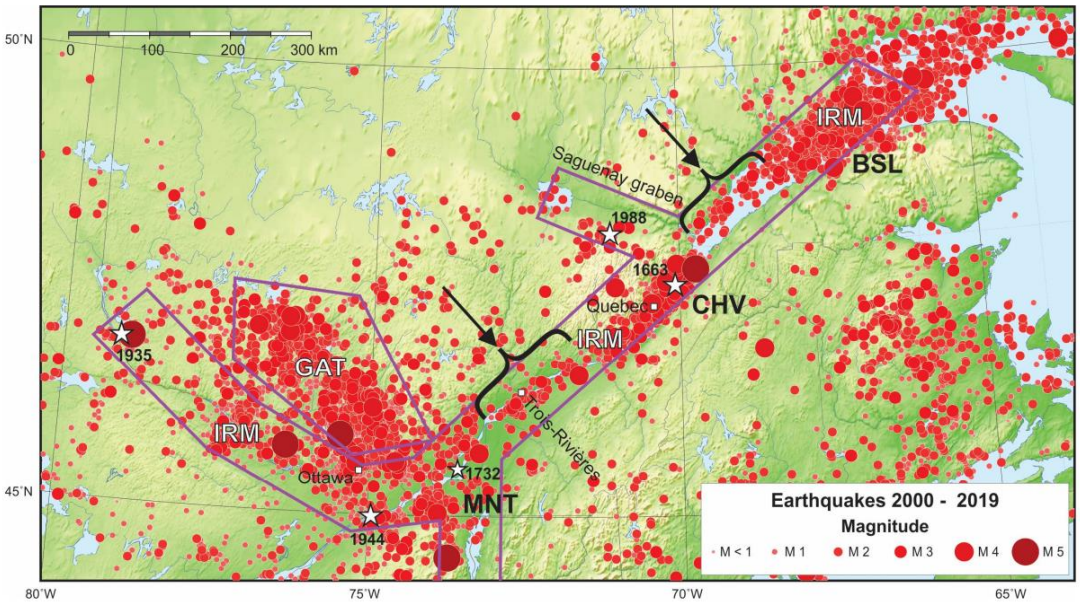

Figure 13. Local earthquakes in Southeast Canada between 2000-2019 (Kolaj et al., 2020).

In addition, the residential buildings in Greater Montreal are particularly vulnerable under seismic events since part of them were designed according to standards that predate modern seismic design codes (Yu et al., 2016). Several scientific papers have been published that quantify the risk inherent to this seismicity on the Montreal area for residential buildings (e.g., Rosset et al., 2022a; Rosset et al., 2019a and 2019b; Yu et al., 2016) for both probabilistic and deterministic seismic hazard inputs.

According to Rosset et al., (2019a, 2019b, 2022a), depending on the seismic scenarios considered, the results for the Montreal Metropolitan Community (MMC) show that:

- The damage and losses between the island of Montreal and the surrounding municipalities are due to the differences in building typology.

- The damage (from slight to complete) could affect 21 to 42% of the residential buildings with 1 to 16.5% of the buildings being heavily damaged.

- The total cost of structural and non-structural damage could represent 1.5 to 7.1% of the total value of the residential building stock (approximately Can$196.5 billion) and that approximately 80% of this cost would be related to non-structural damage.

- The amount of debris generated could vary from 0.4 to 8 million tons, 60% of which is wood and brick.

- The number of injuries is small and often not significant. However, depending on the scenario considered, the number of people requiring hospital care could vary from several hundred to several thousand.

- The number of people requiring temporary accommodation could vary from 4,000 to 50,000.

These facts show the necessity of developing appropriate measures in order to mitigate and reduce the seismic risk. For that, studies of the Annualized Earthquake Loss (AEL) and Annualized Earthquake Loss Ratio (AELR) are important risk evaluation metrics.

Our study area is the Montreal Metropolitan Community (MMC) which includes 6116 Dissemination Areas (DAs) as shown in Figure 14. It comprises the Montreal Island region divided into 3201 DAs, and the municipalities outside Montreal (grouped in Regional County Municipality or RCM) divided into 2915 DAs. Each DA is associated to a Census

subdivision code as shown in the table in Appendix A. More than 50% of the DAs in the Montreal Island belong to the Montreal RCM and they have a relatively dense distribution of population and buildings within this RCM. 46% of the total population lives on the Island of Montreal.

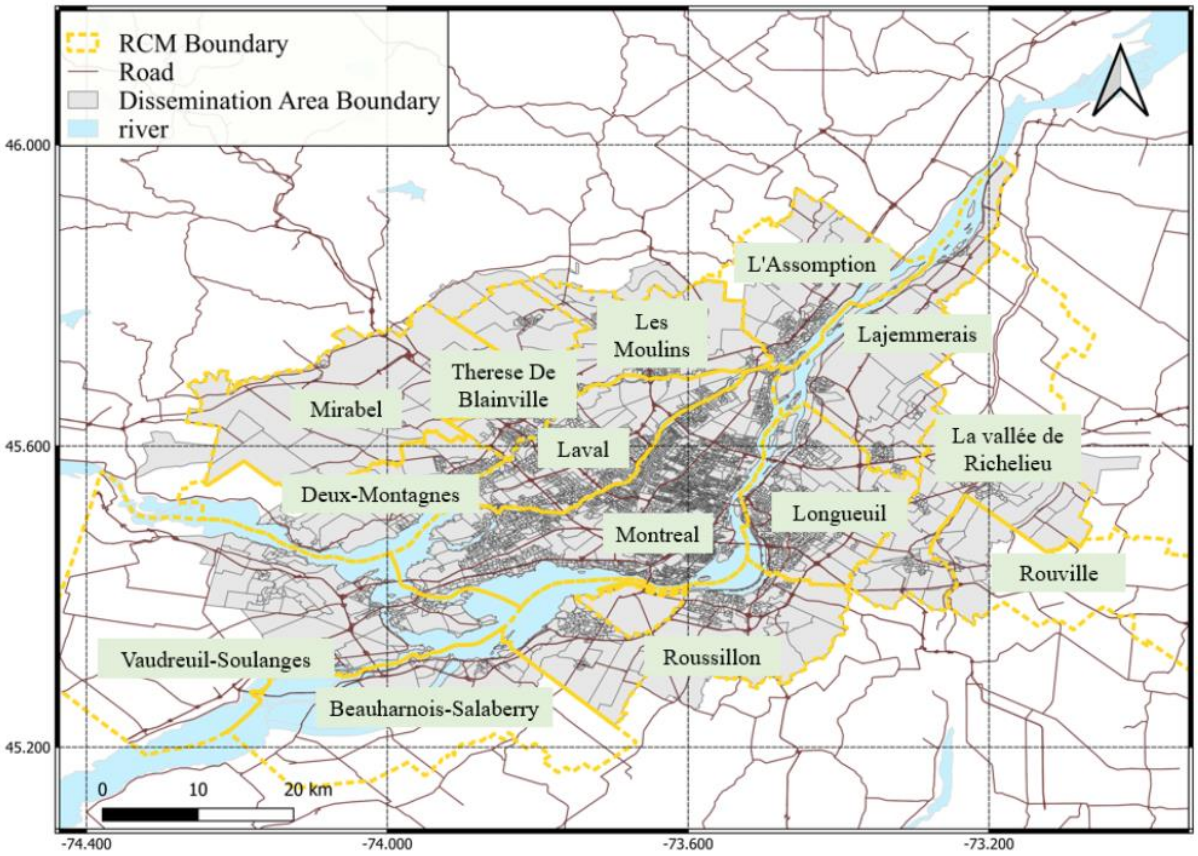

Figure 14. Limit of the study region divided into Dissemination Area and Regional County Municipality (RCM)

3.2 Seismic and geological context

Most parts of the Montreal region are built on recent unconsolidated marine deposits and till, attested by geological information as shown in Figure 15. Soft soil layers on the island of Montreal are mainly associated with thick (up to 50 m) Holocene-age Champlain Sea sediments and more recent sediments deposited from the Saint-Lawrence River. Soft soil deposits such as clay and sand tend to amplify earthquake shear waves. Shear wave velocities within a soft soil layer are much lower than the ones in the underlying bedrock due to the velocity contrast between two layers (Khaheshi Banab et al., 2012). The degree of amplification or deamplification is dependent on several factors, including shear wave

velocity of the soil layers, their thickness, and contrast with base rock. Thus, the structure of the underlying soil has an impact on the ground motions (Rosset et al., 2015; Rosset & Chouinard, 2009).

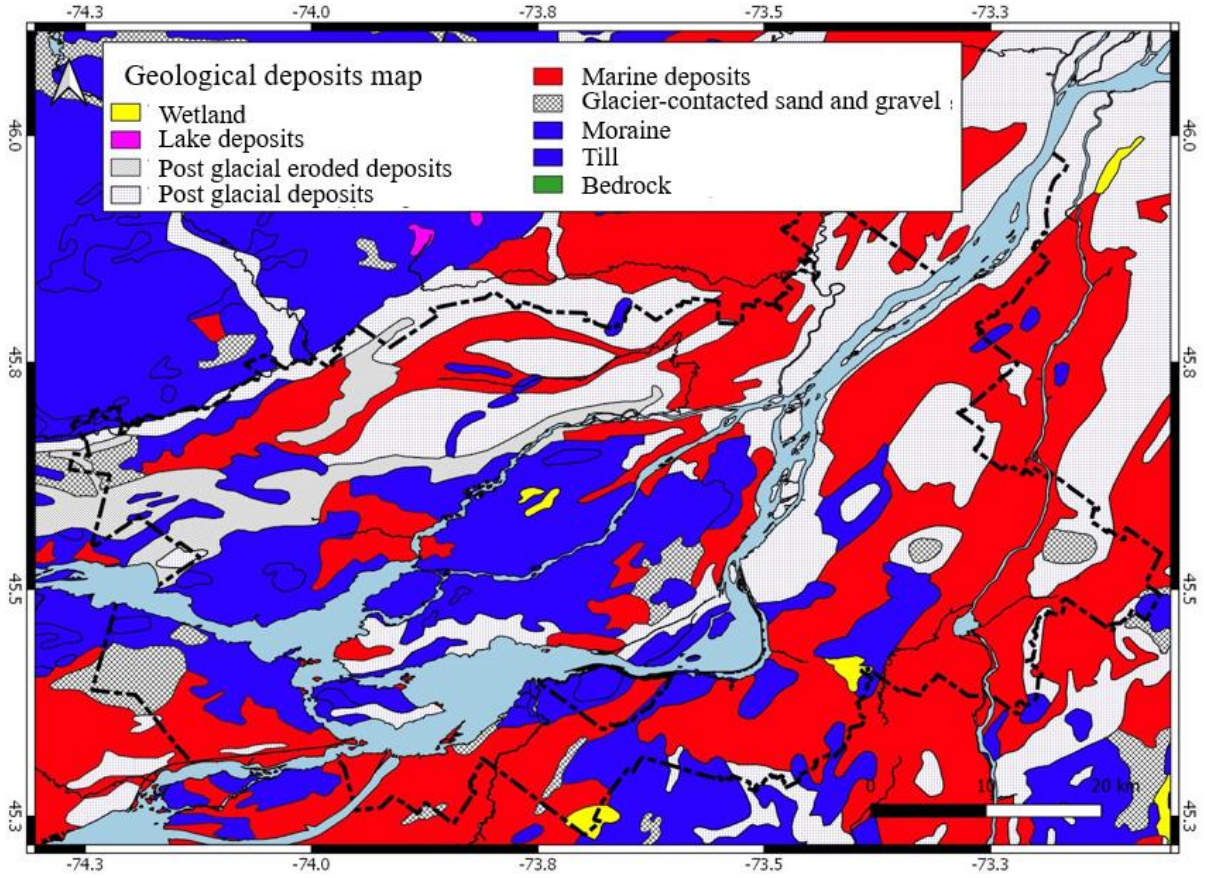

Figure 15. Geological deposit of Montreal region (Rosset et al., 2022b)

The Western Quebec seismic zone (WQSZ) has a moderate seismicity and is the major source of seismic hazards for Montreal. Historically, the province of Quebec has experienced several damaging earthquakes: in 1663 near Charlevoix with a magnitude close to 7, in 1732 near Montreal with a magnitude estimated from reports around 5.8, in 1944 in Cornwall (M=5.8) and in 1988 near Chicoutimi (M=6.0) (Figure 16). This seismicity is related to the normal Cambrian faults generated during the formation of the Iapetan Rifted Margin (IRM) in the Grenville province and the rupture from the Montérégiennes hills to the Baskatong reservoir (200 km to the northwest of Montreal) (Rosset et al., 2022b).

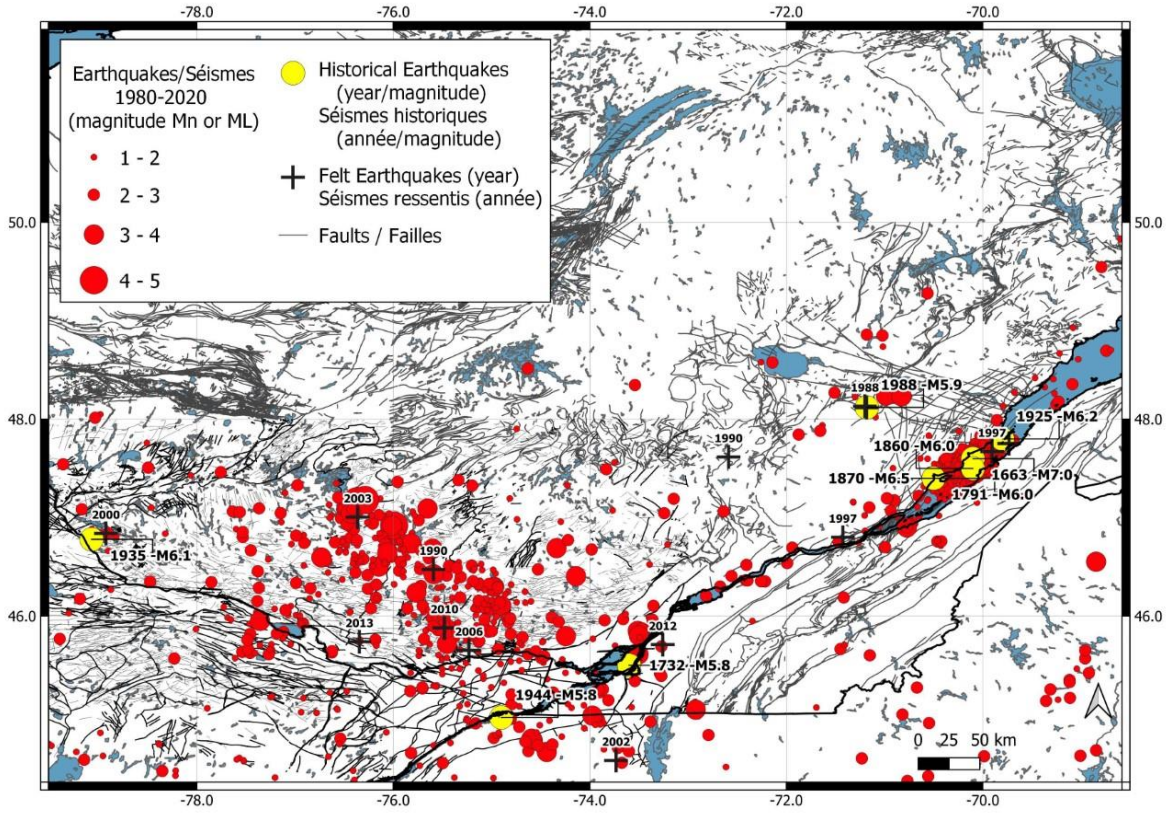

Figure 16. Seismo-tectonic map of the Western Quebec Seismic Zone (Rosset P., 2022b)

3.3 Past studies for Montreal region

For the Montreal region, most of the previous risk analyses are based on deterministic scenarios. For given earthquake scenarios, economic losses and various socioeconomic impacts were evaluated such as the shelter demand associated with evacuations and the response of first responders (hospitals and firemen) (Tamima & Chouinard, 2016). Yu et al. (2016) used Hazus to estimate the seismic losses for 12-earthquake scenarios compatible with the disaggregation of seismic threats at the 2% in 50 years level according to the 2010 national seismic hazard model. Rosset et al. (2019a, 2019b) calculated losses in Montreal for six scenarios combining the identification of potential seismic sources from background seismicity and disaggregation of seismic threats at the 2% in 50 years level according to the 2015 national seismic hazard model. Rosset et al. (2022) calculated the losses in the MMC for a repetition of the M5.8 1732 Montreal earthquake. In this thesis, the annualized earthquake loss for residential buildings in greater Montreal region will be investigated.

3.4 Models used for the Montreal region

The risk analysis can be divided into three levels according to Hazus based on the level of data inputs available (Figure 17). Level 1 analyses use only baseline inventory data and can provide only preliminary evaluations of the local seismic risk. It can be improved greatly with some locally developed inputs such as maps of soil conditions, local expertise to modify the mapping scheme, and demographic information from the regional census (levels 2 to 3). In this thesis, a combination of local and baseline information was used for the MMC.

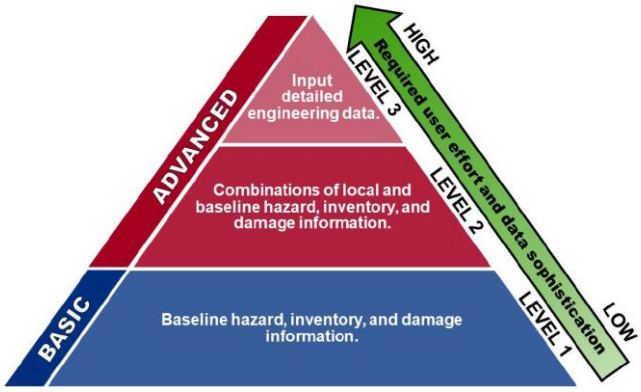

Figure 17. Levels of Analysis (FEMA-USGS-PDC, 2017)

The approach proposed in (FEMA-USGS-PDC, 2017) is selected to calculate the annualized earthquake loss in HazCan. The flow chart in Figure 18 shows the different steps and required models for loss estimation. The next sections will detail the data and models used for the calculation of AEL.

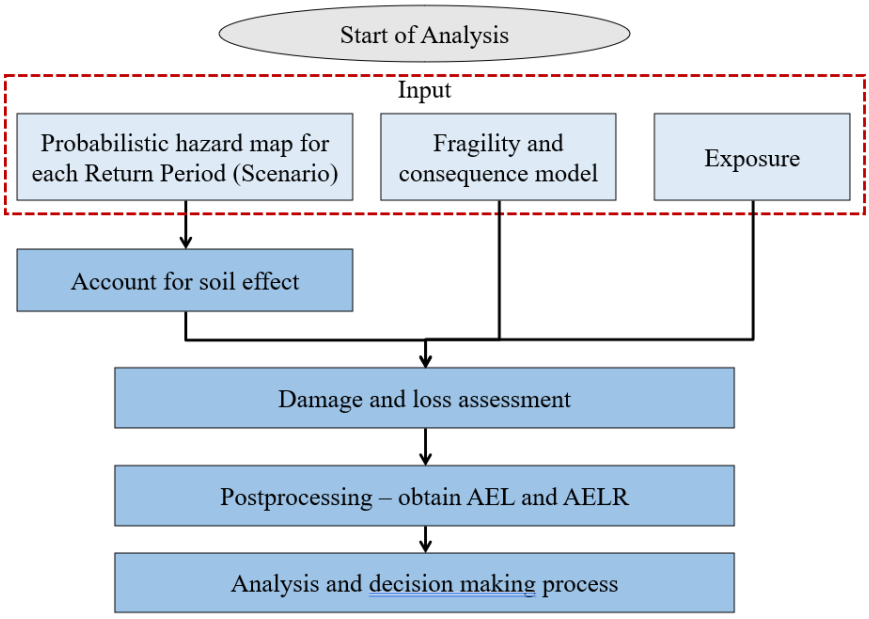

Figure 18 Workflow of the study

3.4.1 Hazard Model and site effect

Natural Resources Canada is responsible for assessing national seismic hazard that is used to define the design criteria in the National Building Code of Canada (NBCC) (Figure 6).

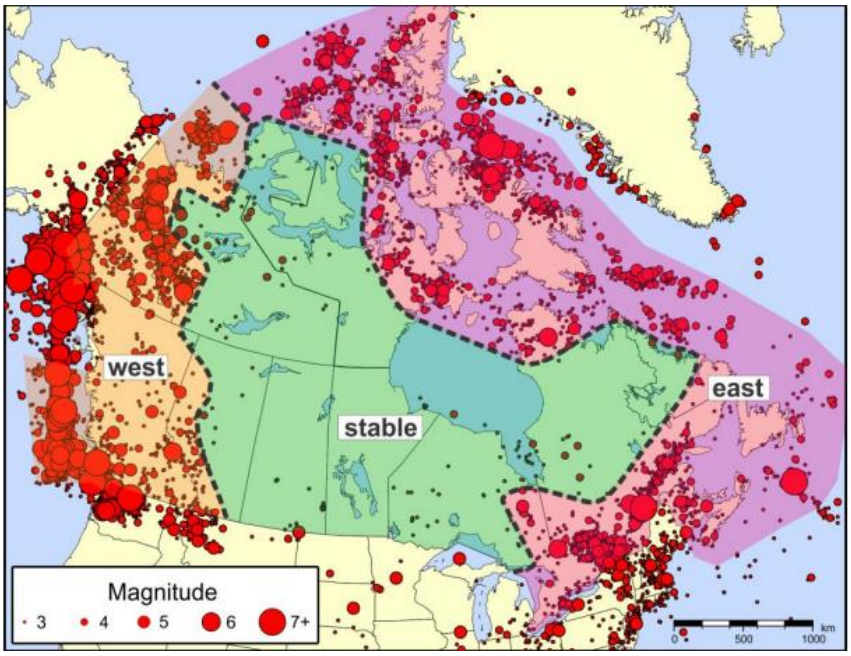

Figure 19. Map of Canada showing the earthquake catalog used for the 5th Generation model; dashed lines dividing seismic regions into three regions

The Fifth Generation of the Seismic Hazard Model of Canada (SHM5) was developed with the software GSCFRISK and provides peak ground acceleration (PGA), Peak Ground Velocity (PGV) and Sa(T) for the period T= 0.05, 0.1, 0.2, 0.3, 0.5, 1.0, 2.0, 5.0 and 10.0s across Canada at various recurrence intervals (Allen et al., 2020). SHM5 uses a probabilistic model that considers uncertainty on source models (historical cluster (H), regional seismotectonic (R) models, floor (F) model and Cascadia subduction zone (C)), seismic parameters for each source, maximum magnitude for each source, and attenuation functions (Canada is divided into three regions due to the difference in propagation properties of seismic waves). Figure 19 shows the earthquake catalog and the seismic zones divided into western, central(stable), and eastern regions. For southeastern Canada, an additional type of hybrid source between H and R was used (Allen et al., 2017). The Gutenberg-Richter magnitude-frequency distribution (MFD) is used as the earthquake recurrence for each earthquake source:

$$N(m) = N_0 e^{-\beta m}[1 - e^{-\beta(M_{max}-m)}]$$

Where N is the cumulative number of earthquakes greater than magnitude m; N_0 is the number of earthquakes per year with magnitude greater than or equal to 0; M_{max} is the maximum magnitude considered; $\beta = b\ ln(10)$ and b is the Gutenberg-Richter b-value (Halchuk et al., 2014). To account for the uncertainty, a logic tree with different weighted branches is defined as shown in Figure 20. The logic tree includes the branches with different weights for the source model, MFD (MFD in the red box is simplified into one branch), hypocentral depth, and ground motion model.

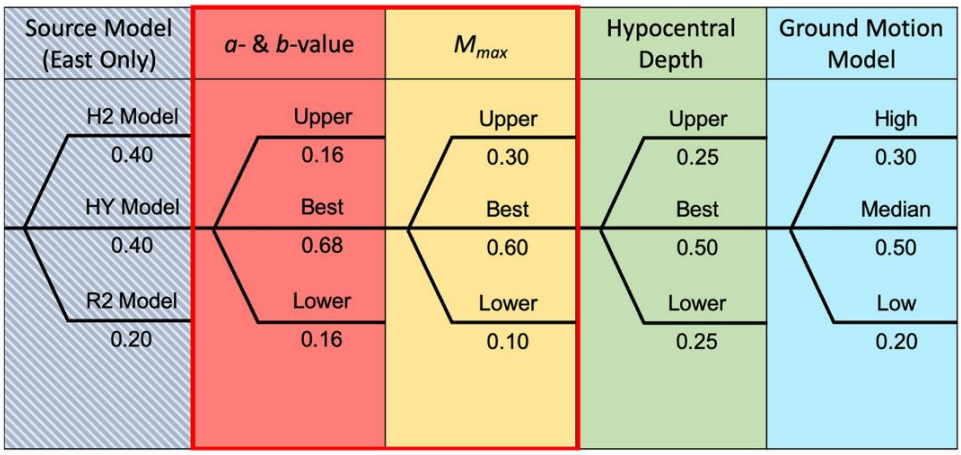

Figure 20. Logic tree and associated weights used for the 2015 Fifth Generation model as implemented in GSCFRISK for the 2015 NBCC (Trevor I. Allen et al., 2020)

Due to the lack of relevant data in the magnitude–distance range, the GMPEs used for eastern Canada is a combination of five different GMPEs including Pezeshk et al.'s (2011) used for hard-rock site, two GMPE models updated in Atkinson & Boore (2011), and single corner and double corner point-source models from W. Silva et al. (2002). The five GMPEs are defined by a combination of three relationships: for ground motions, for the geometric mean and its standard deviation of the magnitude–distance–period (Atkinson & Adams, 2013). Seismic hazard values were calculated in a grid format within Canada on a uniformly 10km by 10km spaced grid of sites. These data points are represented as the largest ground shaking likely to occur in a region at a given probability.

In 2020, the 5th Generation national seismic hazard model has been calculated using OpenQuake. The values calculated by OpenQuake are consistent with the hazard values from GSCFRISK, with a difference lower than 2%–3% (Allen et al., 2020).

For our purposes, seismic hazard values (for site class C sites) are calculated for PGA

and PGV, and spectral acceleration (Sa) at different periods in a grid format. Since some of the dissemination areas studied are smaller than the grid resolution provided by GSC, an interpolation of the current grid data has been performed to obtain a higher resolution and a more refined ground shaking map. For that, two interpolation methods were investigated: the inverse distance weighting (IDW) and the cubic spline interpolation.

The IDW, known as the Shepard's Method, is an interpolation procedure using the point estimation technique based on weighting as a function of relative distance (Lu & Wong, 2008). The points are expressed in terms of geographic coordinates (latitude and longitude in degrees using the WGS1984 projection system) and the value of ground motion parameters, such as PGA, at a given location. First, one needs to calculate the distance $d(x_0, x_i)$ between the point we want to interpolate (x_0) and the existing points xi around x_0 as shown in Figure 21.

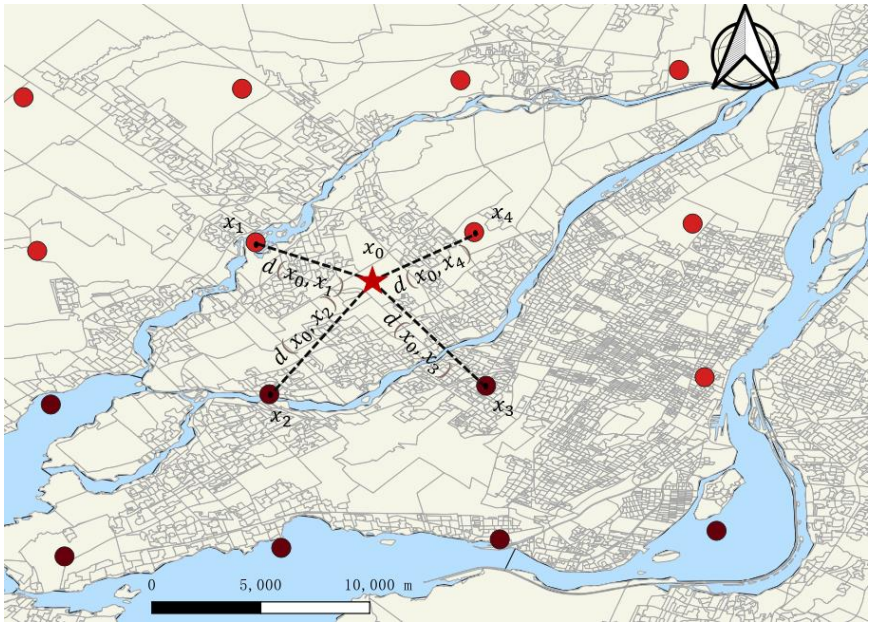

Figure 21. Illustration of the inverse distance weighting interpolation using the grid points from The Fifth Generation of Seismic Hazard Model

A weight $w(x_0, x_i)$ is attributed to each xi point around the point x_0 according to the distance $d(x_0, x_i)$ using the following relation:

$$w(x_0, x_i) = \frac{d(x_0, x_i)^{-p}}{\sum_{i=1}^{n} d(x_0, x_i)^{-p}} \qquad 3-1$$

Where n represents the surrounding control points that contribute to the interpolation, and p is a factor defining the power function for the weights as a function of the distance between the

points (Guan and Wu, 2008).

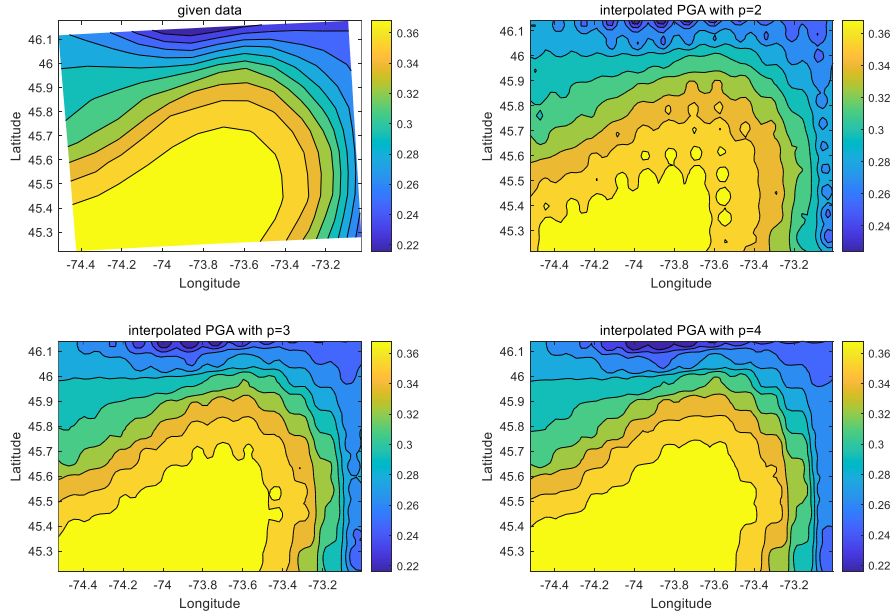

Figure 22. Influence of the p factor on the IDW interpolation (Initial data from Natural Resources Canada).

The maps in Figure 22 show the initial contour map based on a grid of points of 10km by 10km, and the interpolated ones at a 2km-by-2km scale for p values of 2, 3, and 4. As shown in Figure 22, as p increases, the shape of the contour map for interpolated PGA is closer to the original contour map. The relative error, mean relative error and standard deviation are used to evaluate the accuracy of the interpolation for n points using the following equations:

$$Relative\ error = \frac{interpolated\ value - given\ Geotiff\ value}{given\ Geotiff\ value} \qquad 3-2$$

$$Mean\ relative\ error = \frac{\text{relative error for each point}}{n} \qquad 3-3$$

$$Standard\ deviation = \sqrt{\frac{\sum (\text{interpolated}\ Value - \text{the given}\ Geotiff\ value)^2}{n-1}} \qquad 3-4$$

The calculated parameters for the different p values are listed in Table 3. The mean error and standard deviation for p=3 are reduced to about 50% instead of the one from default value p=2. However, the mean error for p=4 did not decrease much, only 0.07% and the standard deviation remains constant. Therefore, a p value of 3 is selected to have a balance between accuracy and calculation efficiency.

Table 3. Mean error and standard deviation of interpolated PGA value using p=2, 3, 4

	p=2	p=3	p=4
mean relative error	3.14%	1.47%	1.40%
standard deviation	0.0126	0.0062	0.0062

The second method is cubic spline interpolation, a curving fitting method (McKinley & Levine, 1998). A series of unique polynomials of degree three are fitted based on the input data points. These cubic splines can then be used to determine the new points of interest. The interpolation was done in MATLAB to use the included cubic spline interpolation function. Figure 23 compares the interpolated PGA in a 2x2km interval using the IDW method with p=4 (left contour map) and the cubic spline interpolation (right map). The cubic spline interpolation gives a smoother curve and a more precise interpolation result than the map obtained with the IDW method.

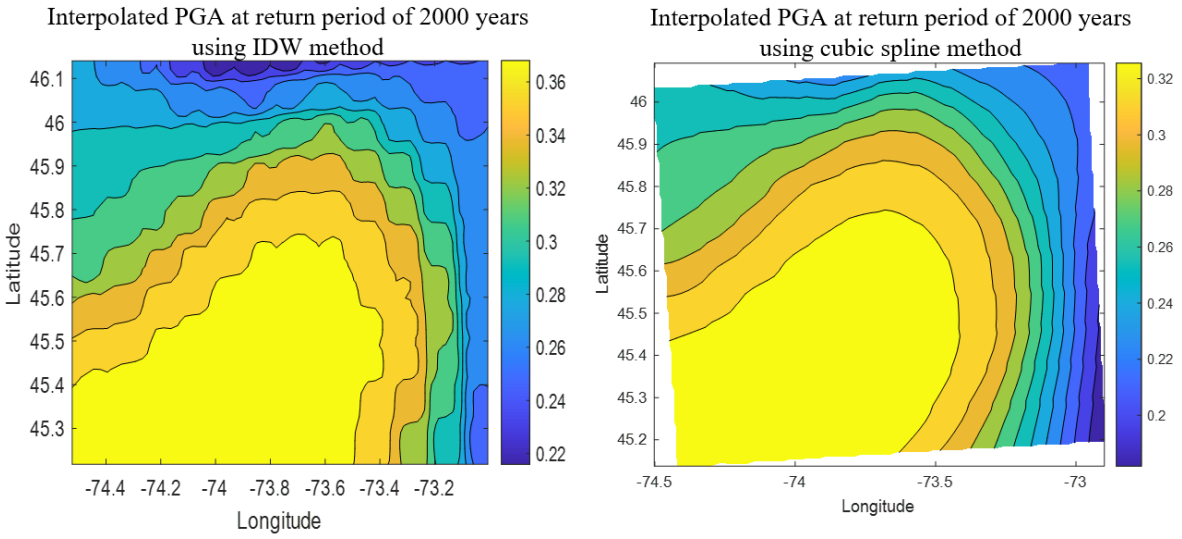

Figure 23. Contour map of given data from Geological Survey Canada in 10kmx10km and interpolated PGA for return period of 2000 years

PGA, PGV and spectra acceleration Sa(T) for T=0.3s and 1.0s are interpolated using both IDW and cubic spline methods from the grid data of 10 by 10 km at return period of 2475 years. The result is in a resolution of 2 by 2 km. This can be compared with the GeoTIFF hazard map from the report of GSC, which is also obtained cubic spline interpolation (SciPy.org) in a resolution of 5km by 5km. Note that the grid values (10 by 10 km) in the tabulated gird files are definitive and calculated from the hazard model, whereas the

GeoTIFFs are derived by interpolation of the grid values. Therefore, instead of interpolating using smaller resolution GeoTIFFs, the GeoTIFFs are only used for comparison to illustrate the precision of the interpolation used in this study. Mean error and standard deviation with respect to 5km-by-5km hazard are calculated for the PGA, PGV, Sa(0.3s), and Sa(1.0s) as listed in Table 4. The mean error and the standard deviation from Cubic Spline interpolation is smaller for the four seismic hazard values. All of the mean errors from Cubic Spline interpolation range from 0.94% to 1.28%, which is a negligible error. The standard deviations are below 0.007, which indicates a good consistency of all the data obtained from interpolation.

Table 4. Mean error and standard deviation of PGA, PGV Sa(0.3s) and Sa(1.0s)

		PGA	PGV	Sa=0.3s	Sa=1.0s
IDW method	mean error	1.404%	1.190%	1.373%	1.009%
	standard deviation	0.006196	0.003476	0.006965	0.001699
Cubic Spline interpolation	mean error	1.275%	1.097%	1.263%	0.940%
	standard deviation	0.005607	0.003168	0.006338	0.001560

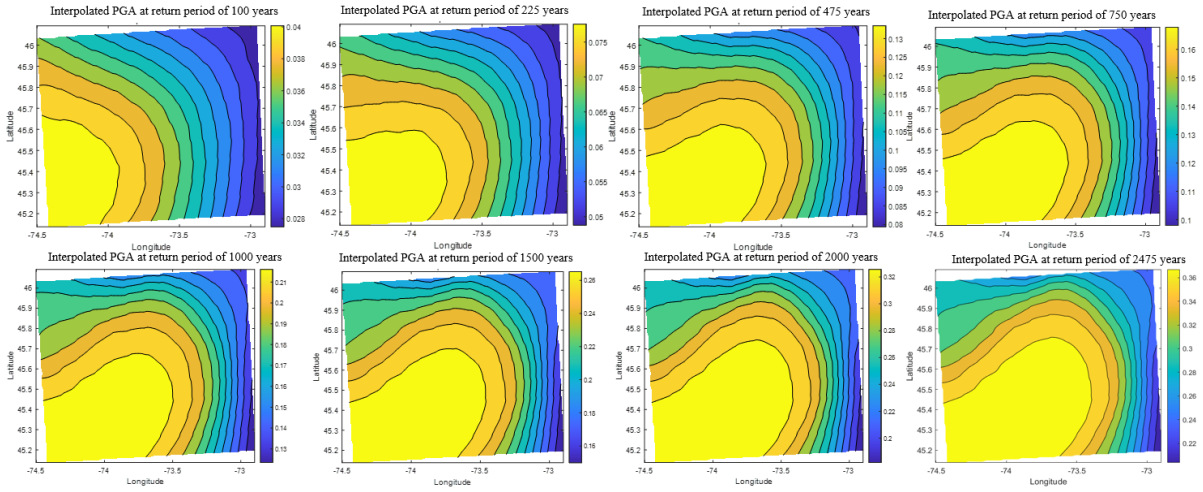

Figure 24. Contour map for cubic spline interpolated PGA for eight return periods

Therefore, the cubic spline interpolation is taken as the interpolation method. The hazard values, PGA, PGV, Sa(0.3s) and Sa(1.0s), are interpolated for eight return periods shown in Figure 24. These interpolated hazard values, adding the soil effect based on the microzonation map, will form the new hazard map as an input to carry out risk analysis in Hazus and OpenQuake.

Local site conditions can significantly affect the ground motion values and consequently the seismic loss. The seismic microzonation map developed by (Rosset et al., 2020) combines

information from various seismic measurements and borehole data, and has been used to account for the soil effect in the Greater Montreal region (Figure 25). It characterizes soil conditions in terms of average shear wave velocity for the first 30 m of soil (V_{s30}). NBCC2015 uses the NEHRP classification system to classify site conditions into five classes (A to E, shown in Table 5), each class corresponding to a range of V_{s30} values and a type of site.

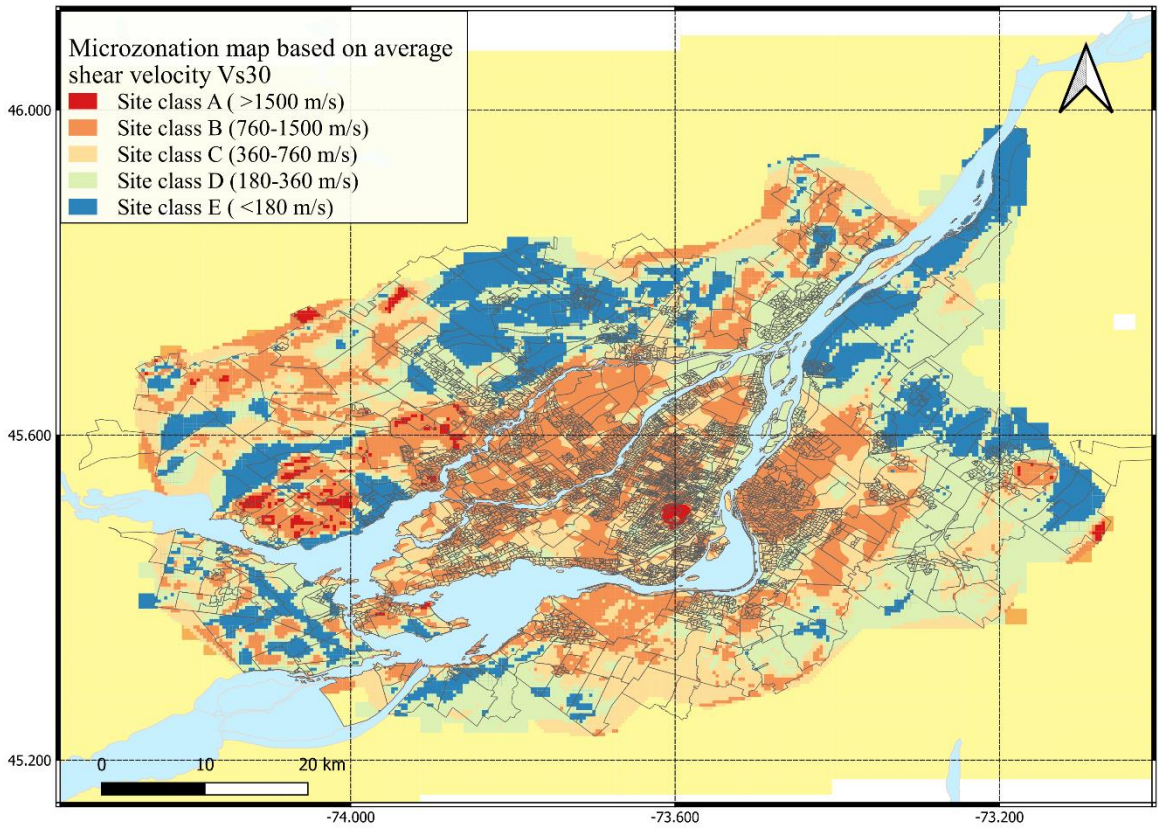

Figure 25.Microzonation Map in terms of site classes based on V_{s30}

Table 5 NBCC site classification.

Site class	Description	Vs_{30} (m/s)	
		Minimum	Maximum
A	Hard rock	1500	
B	Rock	760	1500
C	Very dense soil and soft rock	360	760
D	Stiff soil	180	360
E	Soft soil		180

The soil effect is added to the probabilistic hazard map using a foundation factor (F)

based on the corresponding soil conditions. The applied factor is based on the updated NBCC 2015 (CCBFC, 2015). The factors F(T) are adjusted on the PGA and the spectral periods T (e.g., F(T=0.2s)) using site class and PGA_{ref} (0.8×PGA) when the ratio Sa (0.2)/PGA < 2.0 and PGA otherwise) (CCBFC, 2015).

Table 6. Amplification factor for PGA, PGV, Sa(0.3s), and Sa(1.0s) provided in NBCC2015

(a) Value of F(PGA) as a function of cite class and PGA_{ref}

PGA	⩽0.1	0.2	0.3	0.4	⩾0.5
A	0.9	0.9	0.9	0.9	0.9
B	0.87	0.87	0.87	0.87	0.87
C	1	1	1	1	1
D	1.29	1.1	0.99	0.93	0.88
E	1.81	1.23	0.98	0.83	0.74

(b) Value of F(PGV) as a function of cite class and PGA_{ref}

PGA	⩽0.1	0.2	0.3	0.4	⩾0.5
A	0.62	0.62	0.62	0.62	0.62
B	0.67	0.67	0.67	0.67	0.67
C	1	1	1	1	1
D	1.47	1.3	1.2	1.14	1.1
E	2.47	1.8	1.48	1.3	1.17

(c) Value of F(0.3) as a function of cite class and PGA_{ref}

PGA	⩽0.1	0.2	0.3	0.4	⩾0.5
A	0.65	0.65	0.65	0.65	0.65
B	0.73	0.73	0.73	0.73	0.73
C	1.00	1.00	1.00	1.00	1.00
D	1.32	1.16	1.07	1.01	0.97
E	1.92	1.43	1.19	1.05	0.96

(d) Value of F(1.0) as a function of cite class and PGA_{ref}

PGA	⩽0.1	0.2	0.3	0.4	⩾0.5
A	0.57	0.57	0.57	0.57	0.57
B	0.63	0.63	0.63	0.63	0.63
C	1	1	1	1	1
D	1.55	1.39	1.31	1.25	1.21
E	2.81	2.08	1.74	1.53	1.39

*linear interpolated from F(0.2) and F(0.5)

The PGA values calculated for a return period of 750 years (Figure 26) and 2475 years (Figure 27) provide a direct illustration that the site condition greatly affects seismic hazard distribution. Since most of the regions are class B and C, the amplification is equal or less than 1.0 decreasing the original PGA. In the northern and eastern part of MMC, some regions have site class D and E, which will have a large amplification factor. This indicates that the softer soil amplifies more ground motion. Similar trends are observed for Sa(0.3s) and Sa(1.0s). The hazard maps calculated with and without soil effect for the other selected return periods are shown in Appendix B.

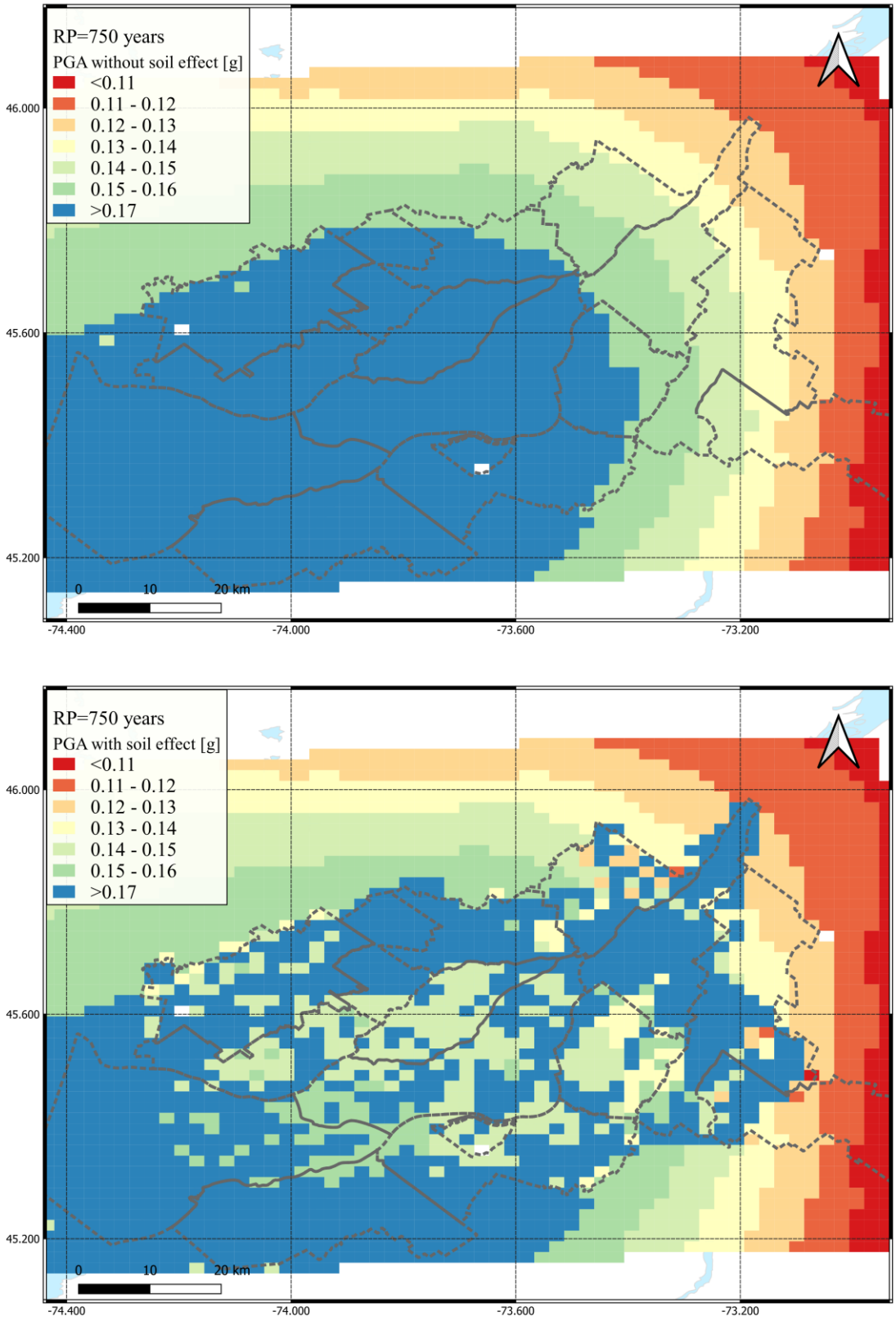

Figure 26. Comparison of PGA before adding site condition (above) and after adding site condition (below) for the return period of 750 years

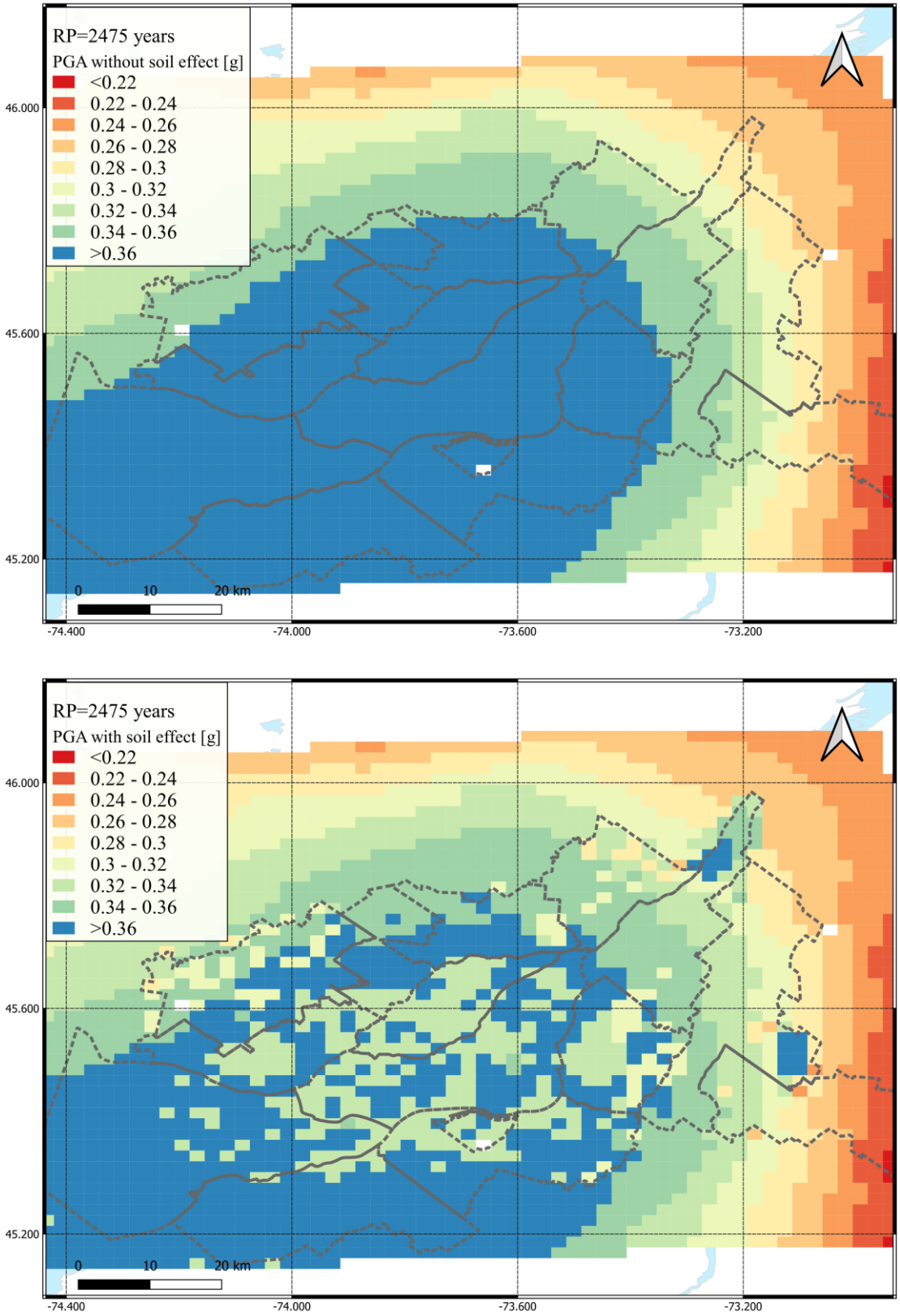

Figure 27. Comparison of PGA before adding site condition (above) and after adding site condition (below) for the return period of 2475 years

The plot in Figure 28 shows the average, minimum, and maximum PGA for the dissemination areas (DA) within the Greater Montreal region for the eight return periods used to calculate the AEL. It shows, obviously, that PGA increases with the return period. Since ground motion parameters (PGA, Sa(0.3s), and Sa(1.0s)), are amplified by the local site conditions, the maximum PGA values do not increase linearly as the average shown due to the soil amplification. For example, the maximum PGA at a return period of 1000 years is 0.339g, which is larger than the maximum PGA at return period of 1500 years.

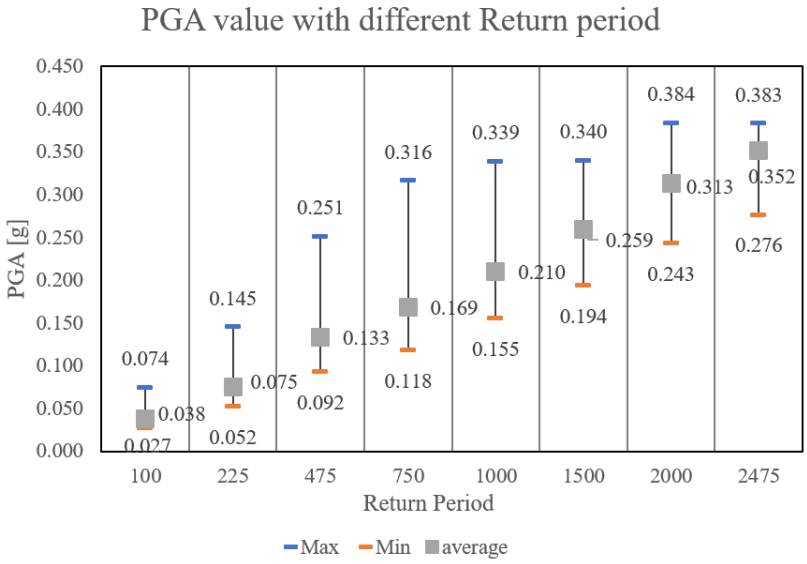

Figure 28. Corrected PGA based on site condition for different return periods.

After incorporating the soil effect, the adjusted PGA, Sa(0.3s) and Sa(1.0s) gridded values are used as an input map for the risk analysis. Indeed, HAZUS and OpenQuake can implement the hazard input in terms of user-supplied ground motions. In HAZUS, a spatial hazard map is imported, while in OpenQuake the average ground motion value in each Dissemination Area is calculated and imported as an input.

3.4.2 New generation of seismic hazard Model SHM6

At the time of the thesis, the details of SHM6 data were not officially published and were only briefly presented in three conference papers (Kolaj et al., 2020a, Adams et al., 2019 and Kolaj et al., 2020b). The same methodology used in SHM5 (Cornell-McGuire methodology) was used for the 6th generation seismic hazard model and implemented within the OpenQuake platform. The SHM6 model includes two major changes. The first one is the adoption of new Ground Motion Models (GMMs) included in a logic tree. Compared to

SHM5, which used the same aleatory model for GMMs in all regions, SHM6 used aleatory model for each GMM to better consider the epistemic variability. The second change is the selection of the site amplification model. SHM6 proposes a new approach that account for the site conditions as a function of continuous Vs30 values instead of discretized V_s30 per site classes. This new approach avoids the discrete jump from one site class to another as in the SHM5 model as shown in the graphs in Figure 29. This change in the consideration of site conditions and the calculation of the hazard in the SHM6 will surely modify (increase) the results of the AEL calculation compared to the SHM5 model used in this thesis.

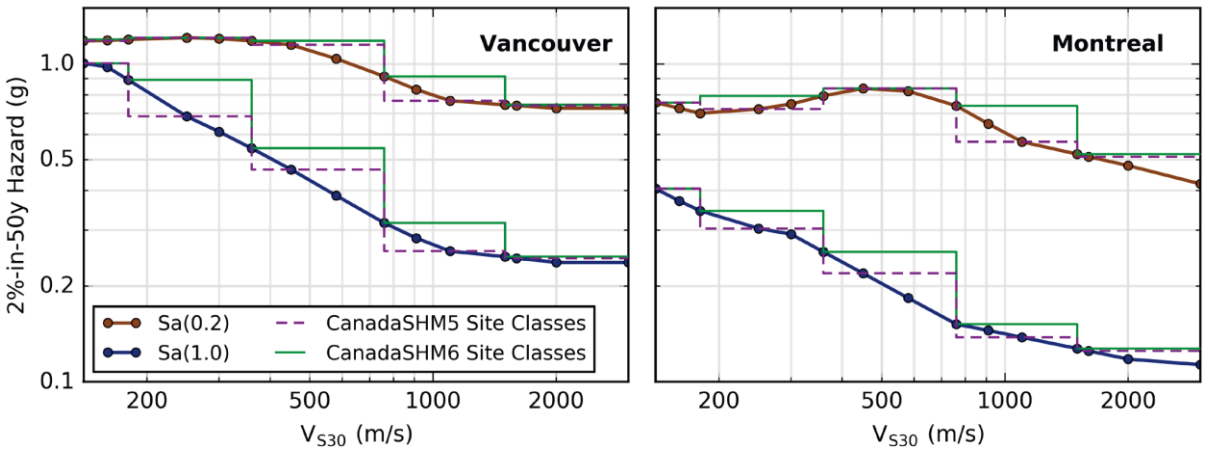

Figure 29. Spectral acceleration values for different periods calculated for the center of Montreal and Vancouver for a return period of 2475 years (From Kolaj et al., 2020)

The Logic Tree Processor is used for processing data in a PSHA input model. In this model (Figure 30), a seismic source model is constructed using a series of branching levels. The first branching level selects an initial seismic source model from historical (H2), hybrid (HY), and regional (R2) with a probability equal to the uncertainty weight. Epistemic uncertainties for the maximum magnitude and the magnitude recurrence are defined in subsequent branching levels. The sampling of the ground-motion logic tree takes place by looping over the different tectonic region types and by randomly selecting a GMPE according to its weight for each of them. The final set of samples will contain therefore a ground-motion model for each tectonic region type considered in the source model (Pagani et al., 2014).

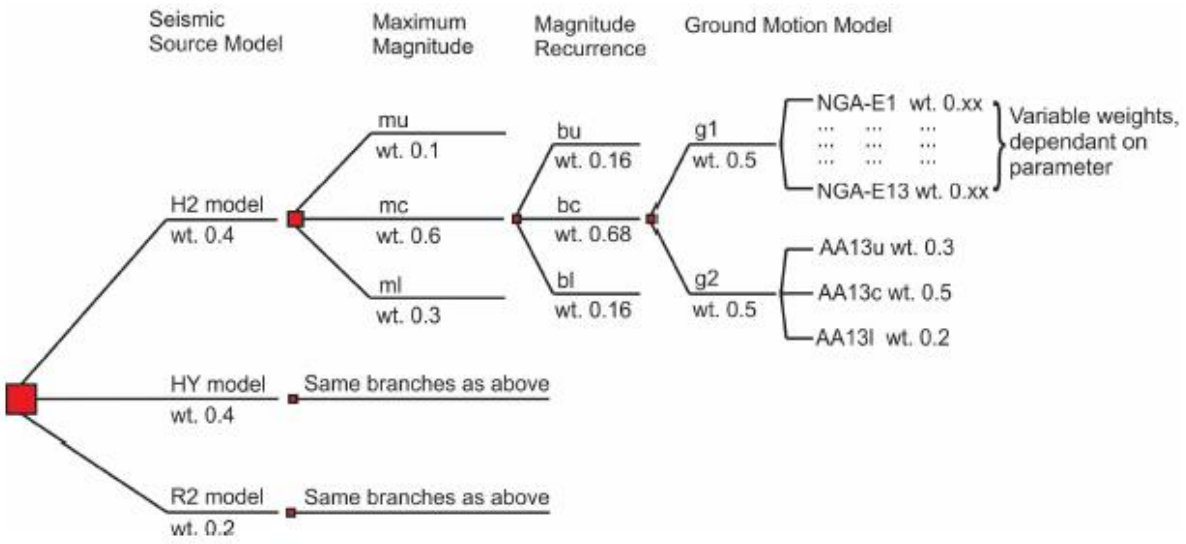

Figure 30. Logic tree in CanadaSHM6 for eastern Canada (Kolaj et al., 2020)

The seismic hazard values are calculated based on the hazard model presented in Figure 30. The PGA and Spectra acceleration obtained in both SHM5 and SHM6 are plotted in Figure 31. Overall, the PGA and Spectral acceleration values calculated in the SHM6 increased for a given PoE relative to those of the SHM5. The SHM6 PGA values are 42% larger than SHM5 PGA values. For large probabilities of exceedance such as 10% in 50 years, the PGA value doubled. This incremental increase in hazard values will have an impact on the seismic damage when using SHM6 data.

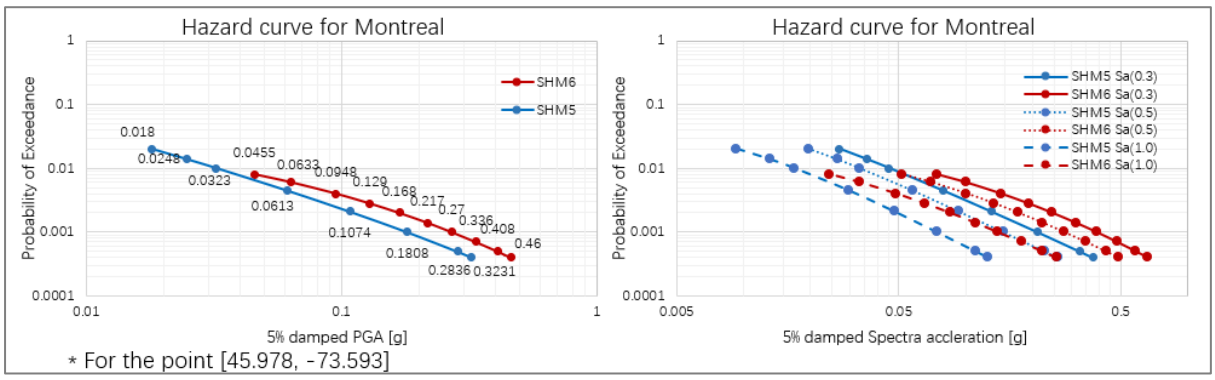

Figure 31. PGA and spectral hazard curves from SHM5 and SHM6 in Montreal

In particular, the hazard map of a 2% probability of exceedance (PoE) in 50 years is shown in Figure 32. Comparing this map with the one from SHM5 (Figure 27 with soil effect), there is a notable increase in the hazard values (especially PGA). However, the general trend is very similar. The southwestern region has a larger PGA and decreases as it forwards northeast. Since SHM6 already includes the site condition during hazard analysis,

there is no need to incorporate the amplification factor in the post-processing of the hazard values. However, the same interpolation procedure to have a good resolution is taken to convert the hazard grid data into the hazard map that Hazus required.

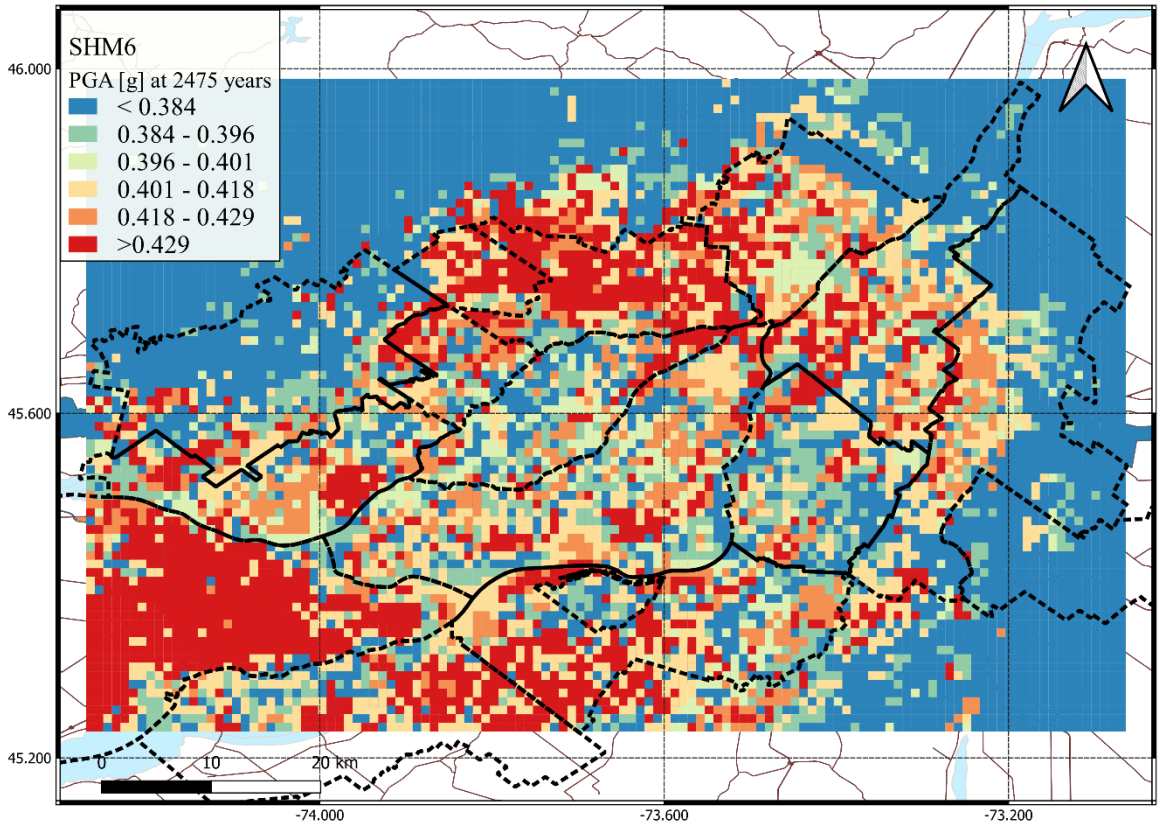

Figure 32. Hazard map for PGA of Great Montreal Region with a PoE = 0.000404 (return period of 2475 years) based on SHM6

3.4.3 Building Inventory

The exposure model includes the general building information for given demographic characteristics and economic data. Demographic information is essential for estimating human losses from earthquakes and calculating the economic loss per capita. The distribution of population by DA from the 2018 Census is shown in Figure 33.

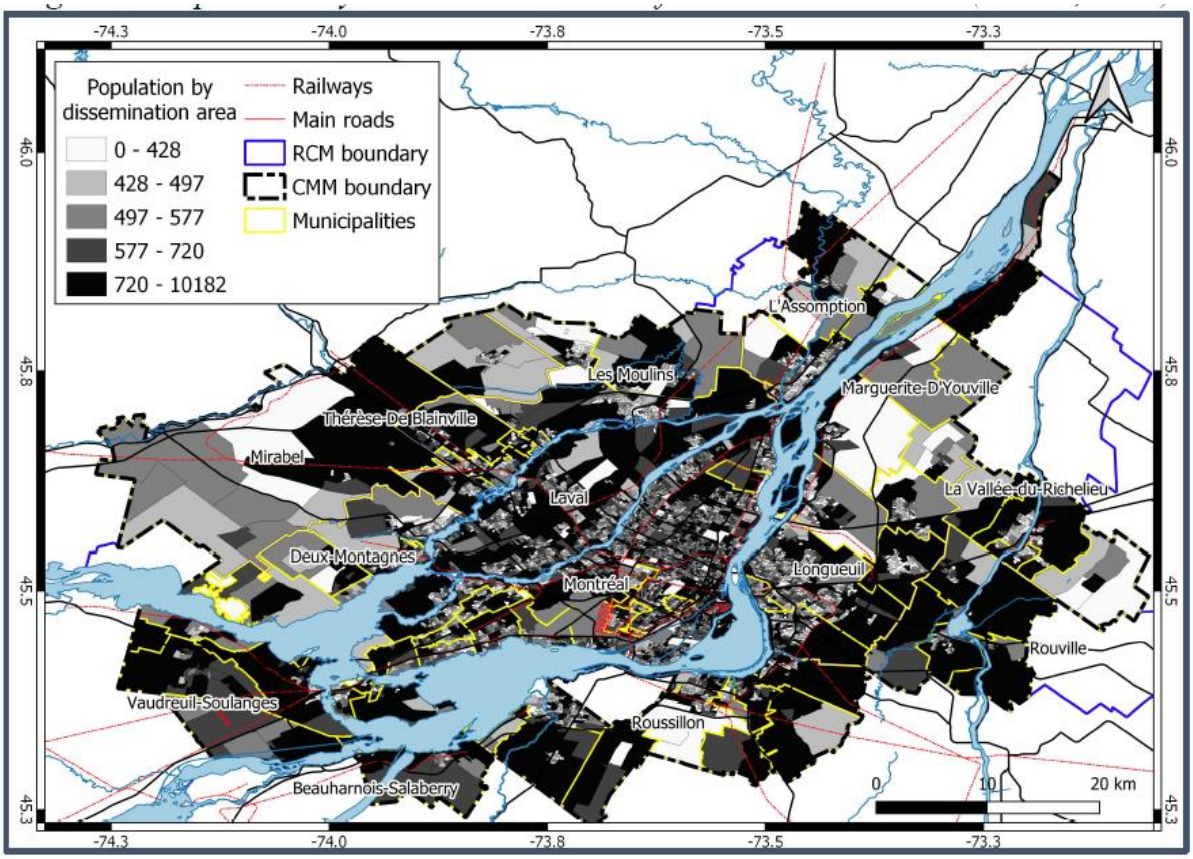

Figure 33. Population distribution by dissemination area (Rosset et al., 2022b)

To construct the exposure model, a building has to be defined according to its characteristics. In this study, only residential buildings are studied. The exposure model related to residential buildings is created from the 2016 and 2018 municipal property rolls for Montreal and the MMC. Around 872 000 buildings were grouped by occupancy types and building types within each DA (Rosset et al., 2022b). Five general building materials are distinguished within the MMC: wood, steel, concrete, unreinforced masonry, and mobile housing. The Taxonomy used in both HAZUS and OpenQuake tools is listed in Table 7. They are divided into subcategories based on three characteristics: building type (W, C, S, URM, and MH), construction frame (moment frame, shear wall etc.), and building height (low-rise, medium-rise, and high-rise).

Table 7. Taxonomy by building type used in HAZUS and OpenQuake and associated structural systems

HAZUS building taxonomy	OpenQuake building taxonomy	Definition
W1	W+WLI/LFM	Light wood moment frame
C1L	CU/LFM/HBET:1,2	Low-rise concrete moment frame
C1M	CU/LFM/HBET:4,7	Medium-rise concrete moment frame
C1H	CU/LFM/HAPP:8	High-rise concrete moment frame
C2L	CU/WAL/HBET:1,2	Low-rise concrete shear walls
C2M	CU/WAL/HBET:4,7	Medium-rise concrete shear walls
C2H	CU/WAL/HAPP:8	High-rise concrete shear walls
C3L	CR+CIP/LFINF/HBET:1,3	Low-rise concrete frame with unreinforced masonry infill walls
S1L	S/LFM/HBET:1,2	Low-rise steel moment frame
S1M	S/LFM/HBET:4,7	Medium-rise steel moment frame
S1H	S/LFM/HAPP:8	High-rise steel moment frame
S2L	S/LFBR/HBET:1,2	Low-rise steel braced frame
S2M	S/LFBR/HBET:4,7	Medium-rise steel braced frame
S2H	S/LFBR/HAPP:8	High-rise steel braced frame
URML	MUR/LWAL/HBET:1,2	Low-rise unreinforced masonry bearing walls
URMM	MUR/LWAL/HBET:4,7	Medium-rise unreinforced masonry bearing walls
MH	MATO/RES+RES5	Mobile home

Table 8 shows the distribution of buildings by construction type as given in Rosset et al., (2022b). There are in total 522,316 residential buildings outside Montreal and 349,358 buildings in Montreal. The building inventory for MMC is dominated by wood light frame buildings, in total 796,965 buildings. The type of building that has second largest number is unreinforced masonry building, which consists of 5.7% of the total buildings in the region. Steel buildings and mobile homes are only 0.7% and 0.6% of the total buildings, respectively. If the buildings are divided by their location, wood buildings are 96% of the total residential buildings outside of Montreal and 84.6% of the total buildings in Montreal. The majority of the concrete buildings are mainly outside Montreal region (97% of total concrete buildings) and only 3% are located in Montreal. In contrast, a majority (96%) of the unreinforced masonry buildings are within Montreal, which is also the second largest (by number) type of residential buildings. There are only 5743 steel buildings for MMC, which are located all in

Montreal, and 4879 mobile housing, which makes up 0.9% of the buildings located outside Montreal.

Table 8. Building inventory distribution by building type (From Rosset et al., (2022b))

Building Types	Structural frame	Outside Montreal Number	Outside Montreal %	Montreal Number	Montreal %*	Total Number	Total %
W	Wood	501,363	96.0	295,602	84.6	796,965	91.4
C	Concrete	14,051	2.7	448	0.1	14,499	1.7
URM	Unreinforced masonry	2,023	0.4	47,562	13.6	49,585	5.7
S	Steel	-	-	5,743	1.6	5,743	0.7
MH	Mobile home	4,879	0.9	3	-	4,882	0.6
Total		**522,316**		**349,358**		**871,674**	

Buildings can be classified by occupancy types as well. Most of the residential buildings are individual dwellings, while some of them may form multiplexes. Table 9 shows the breakdown of buildings by occupancy types. For the residential buildings in this study, three main types are studied: Single Family Dwelling, Mobile House, and Multi Family Dwelling. Most of the buildings are single family dwellings, which is 60% of the total number of buildings. As a direct illustration, the total building number for mobile house (RES2) in Table 8 is equal to the building number for RES2 in Table 9. Sometimes, multiple dwellings share the same geographical location; it is more accurate to group these dwellings into multiplexes.

Table 9. Building Occupancy Classes

HAZUS Occupancy type	Occupancy class	Number of buildings	Percentage (%)
RES1	Single Family Dwelling	850	0.16
RES2	Mobile Home	648617	86.38
RES3A	Duplex	4882	0.93
RES3B	Triplex	114227	5.92
RES3C	Multiplex/apartment, 4 to 11 floors	57988	3.89
RES3D	Multiplex/apartment, 5 or more floors, 3 or less floors without commercial use	35593	1.84
RES3E	Multiplex/apartment, 12 or more floors, 4 or more floors without commercial use	7944	0.55
RES3F	Condominium	2808	0.24
		Total: 871,674	

Table 10.Distribution of occupancy types by building types in Montreal from Rosset et al., (2022b)

Occupancy types	Building types* (in %)											
	W1	C1H	C1L	C1M	C2H	C2L	C2M	S1L	S1M	URML	URMM	MH
RES1	94.6	-	-	-	-	-	-	-	-	5.3	-	-
RES2	-	-	-	-	-	-	-	-	-	-	-	100
RES3A	77.3	-	-	-	-	-	-	-	-	22.5	0.2	-
RES3B	62.9	-	-	-	-	-	-	-	-	36.1	1.0	-
RES3C	71.7	-	-	-	-	0.9	-	14.2	0.2	12.5	0.5	-
RES3D	95.5	0.2	0.3	0.4	0.3	0.1	0.3	-	-	2.2	0.7	-
RES3E	44.2	17.5	0.2	8.9	5.6	0.2	3.8	0.7	0.4	7.3	11.2	-

* W1= Light wood frame; URM= Unreinforced masonry; MH= mobile home; C1= Concrete Moment Frame; C2= Concrete Shear Walls; S1= Steel Moment Frame; L = 1-2 floors; M=4-7 floors; H= 8+ floors

Table 11. Distribution of occupancy types by building types for municipalities outside Montreal from Rosset et al., (2022b)

Occupancy types	Building types* (in %)									
	W1	URMM	URML	MH	C2M	C2L	C2H	C1M	C1L	C1H
RES1	99.4	-	0.6	-	-	-	-	-	-	-
RES2	-	-	-	100	-	-	-	-	-	-
RES3A	99.2	-	0.8	-	-	-	-	-	-	-
RES3B	99.4	-	0.6	-	-	-	-	-	-	-
RES3C	-	0.2	1.5	-	-	25.5	-	0.2	72.6	-
RES3D	-	0.3	0.3	-	-	30.8	-	0.6	68.0	-
RES3E	-	0.1	0.1	-	0.9	28.5	-	2.5	67.9	-
RES3F	-	0.2	-	-	6.7	32.8	1.9	12.5	40.5	5.4

* The same legend as Table 10.

In Hazus, the percentage of the building by occupancy type (OT) in terms of building type (BT) and code level is defined in the occupancy mapping. Since the distribution of buildings by OT and BT varies between RCMs in Montreal and outside Montreal, two sets of occupancy mapping scheme are defined corresponding to the DA of the region. These percentages by BT and OT are given in Table 10 and 11 for Montreal and municipalities outside Montreal, respectively. Wood buildings (W1) consists of more than 95% single-family houses (RES1) and concrete buildings (C1 and C2) are mostly multiplexes. The majority of the unreinforced masonry buildings are single family dwellings, duplexes, and

triplexes. Steel buildings are either apartment of 4-11 floors or large condos (RES3C and RES3E) and they are all concentrated within the Montreal Island.

Table 12. Distribution of design code levels by construction types for the municipalities in Montreal (Rosset et al., 2022b)

Occupancy Type	Level of design code (in %) by construction types										
	W1	**URMM**	**URML**	**S1L**	**C3L**	**C2M**	**C2L**	**C2H**	**C1M**	**C1L**	**C1H**
RES1	PC: 51 LC: 31 MC: 18		PC: 99 MC: 1								
RES3A	PC: 89 LC: 11		PC: 100								
RES3B	PC: 65 LC: 24 MC: 11		PC: 100								
RES3C	PC: 47 LC: 29 MC: 24		PC: 100	PC: 100		MC: 3	MC: 27			LC: 67 MC: 3	
RES3D	PC: 42 LC: 21 MC: 37	PC: 3	PC: 97		MC: 2	MC: 15	MC: 8	LC: 1 MC: 2	PC: 10 LC: 20 MC: 8	PC: 2 LC: 1 MC: 2	PC: 2 LC: 9 MC: 18
RES3E	PC: 46 LC: 19 MC: 35	PC: 63	PC: 35 LC: 1 MC: 1	PC: 90 MC: 10	MC: 1	LC: 1 MC:16	MC: 1	LC: 2 MC:20	PC: 9 LC: 7 MC: 6	PC: 1 MC: 1	PC: 17 LC: 15 MC: 3

Note : PC=Pre-code; LC= Low-code; MC= Moderate-code

Table 13. Distribution of design code levels by construction types for the municipalities outside Montreal (Rosset et al., 2022b)

Occupancy Type	Level of design code (in %) by construction types									
	W1	**URMM**	**URML**	**MH**	**C2M**	**C2L**	**C2H**	**C1M**	**C1L**	**C1H**
RES1	PC: 24 LC: 41 MC: 35		PC:100							
RES2				PC: 11 LC: 71 MC: 18						
RES3A	PC: 42 LC: 21 MC: 37		PC:100							
RES3B	PC: 42 LC: 28 MC: 30		PC:100							
RES3C		PC: 11	PC: 89			MC: 28			PC: 23 LC: 44 MC: 5	
RES3D		PC: 50	PC: 50			MC: 33			PC: 9 LC: 52 MC: 6	
RES3E		PC: 67	PC: 33		MC:1	MC: 32		PC: 9 LC: 50	PC: 1 LC: 2 MC: 5	
RES3F		PC:100			MC: 8	MC: 39	MC: 2	LC: 11	PC: 2 LC: 28 MC: 4	LC: 5 MC: 1

Note : PC=Pre-code; LC= Low-code; MC= Moderate-code

The fragility curves defined for each building type consider the level of seismic design of the buildings established according to the year of construction. For Quebec, three levels of seismic design code are applied to residential buildings; 1970 is the year to differentiate building's code level because the capacity-based design and structural ductility considerations have been introduced for building seismic design at this date. Structures built before 1970 are defined as pre-code. There are new seismic requirements in several design standards introduced in 1990, which also affected seismic durability for buildings. The buildings built after 1970 but before 1990 are defined as low code. The highest level of seismic design considered for residential buildings constructed after 1990 is defined as moderate code. For a given BT and OT, the distribution by code levels is shown in Table 12 for municipalities in the Montreal region and Table 13 for municipalities outside of Montreal. Unreinforced masonry was mostly used in the pre-code period and not commonly used in recent decades.

Once the building inventory is defined, the exposure data are inputted into the two software. In HAZUS, the exposure data is transferred using the Comprehensive Data Management System (CDMS), which helps update and manage datasets from previous studies. In OpenQuake, the exposure data are re-formatted using MATLAB code from the Hazus datasets to comply with the OpenQuake format. This conversion combines buildings of the same occupancy type together for a given building type and code level.

3.4.4 Fragility Model

There are two risk procedures that can be used to calculate the seismic loss. The first one is to use fragility functions to calculate the probability of damage associated to a given damage level and then estimate the loss ratio for a given damage level using damage-loss ratio curves (consequence model). Fragility curves are an estimate of the cumulative probability of being in, or exceeding, each damage state for the given level of ground shaking (or ground failure) over each of the five damage levels: none, slight, moderate, extensive, and complete (Figure 34). They are building-type specific. The consequence model provides the information of the replacement cost for a given damage level (cost-damage ratio), which is used to estimate the damage costs.

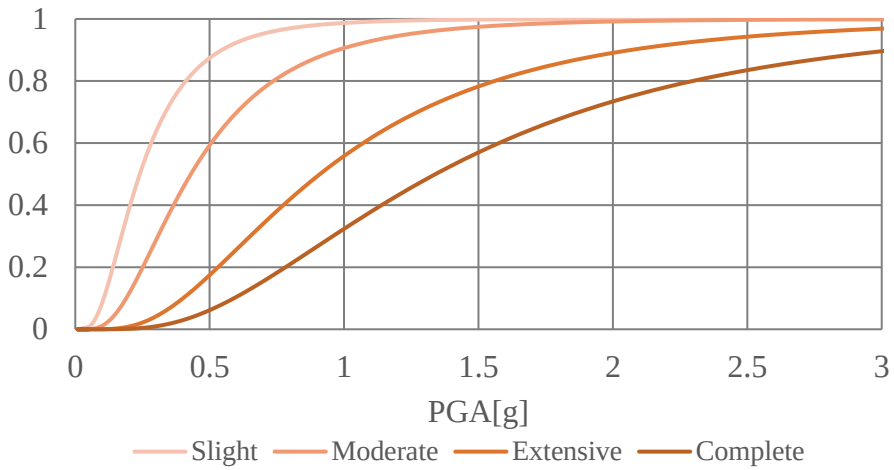

Figure 34. Example of fragility curve by levels of damage for W1 Moderate Code Seismic Design Level (FEMA, 2020)

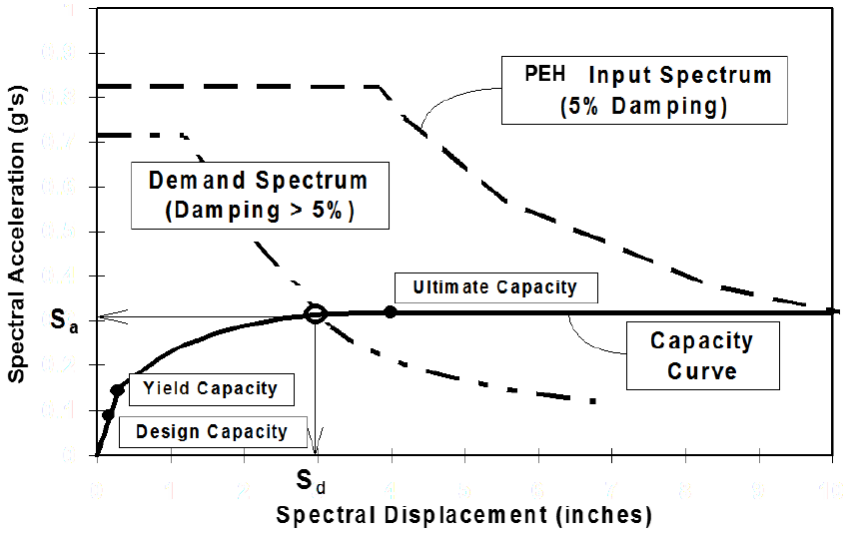

Figure 35. Illustration of the capacity spectrum method (FEMA, 2020)

Hazus uses the Capacity Spectrum Method to estimate the building damage (FEMA, 2020). The peak building response, in terms of spectral displacement or spectral acceleration, is defined as the intersection of the building capacity curve for a given building type and its respective demand spectrum (Figure 35). The building capacity curve, also known as a push-over curve, is the lateral displacement of a given building type against applied earthquake load. Design capacity, yield capacity, and ultimate capacity are the three controlling points that describe each curve. The demand spectrum is the damped Potential Earthquake Hazards (PEH) spectrum, which will be reduced for effective damping greater than 5%. The fragility curves are analytically defined by the median value of peak ground displacement (PGD) and the variability associated with that damage state. For each given damage state, the fragility

curves are defined as a continuous lognormal distribution function with a median value and a logarithmic standard deviation. The value used to generate the fragility function for each building type and level of damage are listed in the Table 5-29, 5-30 and 5-31 of Appendix C.

OpenQuake uses directly fragility curves for a specific ground motion parameter. Hazus provides with equivalent PGA fragility parameters calculated for the Western USA seismic context (FEMA, 2020). The medians of equivalent-PGA fragility curves are based on the medians of spectral displacement for the four damage states and are very sensitive to the shape assumed for the demand spectrum. A method is proposed to correct the given parameter, taking into account the average magnitude and distance of earthquake events in the study area. The formula 3-1 of the FEMA technical manual (FEMA, 2020) helps to calculate the correcting factor calculate the medians PGA, $\overline{PGA}$, from the reference spectrum, $\overline{PGA}_{ref}$. It is as follow:

$$\overline{PGA} = \overline{PGA}_{ref} \times \frac{PGA}{S_{A1}} \times \left(\frac{1.5}{F_v}\right) \qquad 3-5$$

Where PGA/S_{A1} is the spectrum shape ratio based on earthquake source, earthquake magnitude, and distance from source to site as shown in Table 14. Fv is taken as 1.3, the soil amplification given in Appendix E.

Table 14. Spectrum Shape Ratio for central-eastern US and rock condition applied for the MMC

Hypocentral Distance	PGA/S_{A1} Given Magnitude, M:			
	≤ 5	6	7	≥ 8
≤ 10 km	7.8	3.5	2.1	1.1
20 km	8.1	3.1	2.1	1.7
40 km	6.1	2.6	1.8	1.6
≥ 80 km	4.3	1.9	1.4	1.3

The earthquake magnitude and distance from source to site for the Montreal Metropolitan Community are used to estimate PGA/S_{A1}. According to the disaggregation of SHM5 for Montreal as shown in Figure 36, the mean magnitude of the earthquake and mean hypocentral distance are defined for PGA at 100, 475, 1000 and 2475 years return periods. Using the mean magnitudes and the mean hypocentral distances, the values PGA/S_{A1} for

eight return periods will be linearly interpolated using the corresponding values in Table 14.

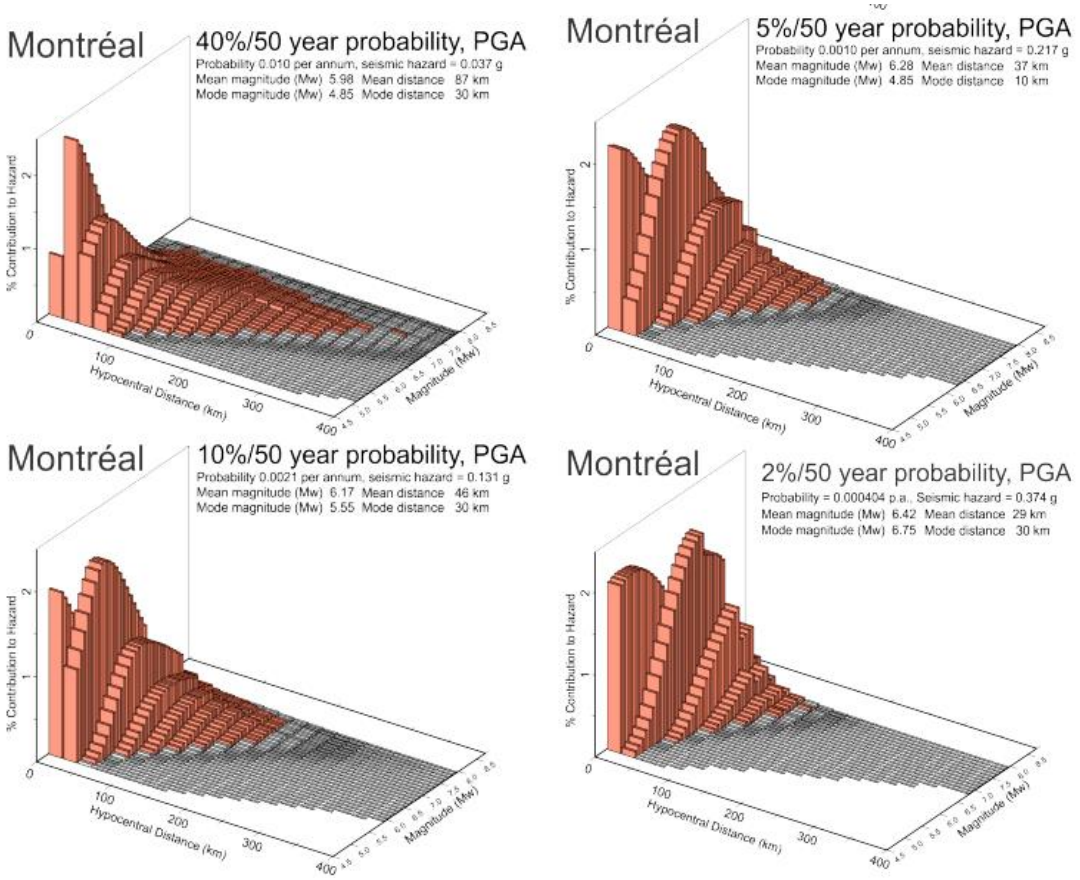

Figure 36. Disaggregation of the Montreal region for 4 return periods (Halchuk et al., 2019)

The amplification factor for $\overline{PGA}_{ref}$ is calculated for eight return periods shown in Table 15 below:

Table 15. Parameters used to calculate the PGA-factor of amplification. The stars indicate the return period for which mean magnitude and distance are provided by disaggregation from Halchuk et al. (2019)

RP	Mean magnitude	Mean distance	Mean Sa (1.0)	PGA/S_{A1}	Fv	PGA amplification
2475*	6.42	29	0.04	2.49	1.5	2.49
2000	6.42	29	0.08	2.49	1.5	2.49
1500	6.28	37	0.13	2.44	1.5	2.44
1000*	6.28	37	0.17	2.44	1.5	2.44
750	6.17	46	0.21	2.37	1.5	2.37
475*	6.17	46	0.26	2.37	1.5	2.37
225	5.98	87	0.31	1.95	1.5	1.95
100*	5.98	87	0.35	1.95	1.5	1.95

Fragility curves used in OpenQuake converts the normal mean and standard deviation used in Hazus, which are the median M and logarithmic standard deviation Φ. The following formulae convert M and Φ to the mean μ and normal standard deviation σ:

$$\mu = e^{\ln M + \frac{\Phi^2}{2}} \qquad 3-6$$

$$\sigma = \sqrt{(e^{\Phi^2} - 1) \times e^{2lnM + \Phi^2}} \qquad 3-7$$

This procedure is applied for each structural type and design code level.

A consequence model defines a set of consequence functions describing the distribution of the loss ratio conditional on a set of discrete damage levels. The consequence models used in this thesis are defined as the ratio of repair to replacement cost described in the Hazus Inventory Technical Manual (FEMA, 2020). The full consequence models used in both Hazus and OpenQuake are based on the HAZUS Repair Cost Ratios (in % of building replacement cost) for structural, non-structural, and content components shown in Appendix D.

Since the consequence model is defined by occupancy type only, it is necessary to relate it to building type as well during the conversion of input used in OpenQuake. In OpenQuake, a consequence model is defined based on the percentage of buildings in each occupancy type for a given building type. The percentage of buildings in each occupancy type combining Table 8 and 9 is presented in Table 16.

Table 16. Combined building percentage distribution by building type and occupancy type

Occupancy types	Building types* (in %)											
	W1	C1H	C1L	C1M	C2H	C2L	C2M	C3L	S1L	URML	URMM	MH
RES1	80.5	-	-	-	-	-	-	-	-	19.8	-	-
RES2	-	-	-	-	-	-	-	-	-	-	-	100
RES3A-F	19.5	100	100	100	100	100	100	100	100	80.2	100	-
Total building	796179	254	9241	955	136	4338	169	8	3652	51762	226	5794

Based on the ratio of buildings in each building type for RES1, 2 and 3, the consequence model for each building type is calculated as Table 17 shows. The full calculated consequence model for OpenQuake is presented in Appendix F.

Table 17. Consequence model combining for all occupancy type

Building types	Occ. types
W1	0.8RES1 + 0.2 RES3
URMM	RES3
URML	0.2RES1+0.8RES3
S1L	RES3
MH	RES2
C3	RES3
C2	RES3
C1	RES3

Based on the elements of interest, damages are calculated separately for structural, nonstructural, and content components. Structural elements are the main components that serve for structural stability, such as beams, columns, and girders. Non-structural elements are those that does not serve as primary or secondary structural elements, such as stairs, cables, veneers, chimneys, and exterior wall panels. It is divided into acceleration sensitive components and drift sensitive components (Table 18). Building damage is the sum of damage of the structural and non-structural elements. The content of the building includes equipment and furnishings.

Table 18. Typical Nonstructural Components and Contents of Buildings (Hazus, 2021)

Type	Item	Drift-Sensitive	Acceleration-Sensitive
Architectural	Nonbearing Walls/Partitions	P	S
	Cantilever Elements and Parapets		P
	Exterior Wall Panels	P	S
	Veneer and Finishes	P	S
	Penthouses	P	
	Racks and Cabinets		P
	Access Floors		P
	Appendages and Ornaments		P
Mechanical and Electrical	General Mechanical (boilers, etc.)		P
	Manufacturing and Process Machinery		P
	Piping Systems	S	P
	Storage Tanks and Spheres		P
	HVAC Systems (chillers, ductwork, etc.)	S	P
	Elevators	S	P
	Trussed Towers		P
	General Electrical (switchgear, ducts, etc.)	S	P
	Lighting Fixtures		P
Contents	File Cabinets, Bookcases, etc.		P
	Office Equipment and Furnishings		P
	Computer/Communication Equipment		P
	Nonpermanent Manufacturing Equipment		P
	Manufacturing/Storage Inventory		P
	Art and other Valuable Objects		P

**Primary cause of damage is indicated by "P", secondary cause of damage is indicated by "S"*

In general, seismic loss for a given return period is calculated as the sum of probability under the given damage state times the repair cost ratio times the building value. For structural damage, losses are calculated by the following equation:

$$\text{structural Loss} = \sum_{ds,i}\left\{BRC_i \times \left(\sum_i PSTR_{ds,i} \times RCS_{ds,i}\right)\right\} \qquad 3-8$$

Where BRC is the building replacement cost; PSTR is the probability of being in four structural damage state; RCS is the structural repair cost ratio in % of the building replacement cost under each damage state, which is the consequence model in Appendix F.

Developing fragility curves for each possible nonstructural component is not practical for the purposes of regional loss estimation, due to the sheer number of possible components and the lack of sufficient data to develop all the fragility curves. Hence, in Hazus methodology, nonstructural building components are grouped into drift-sensitive and acceleration-sensitive component groups as shown in Table 18, and the damage functions estimated for each group are assumed to be "typical" of its subcomponents. Losses are calculated based on the two components of the non-structural damages-acceleration sensitive and drift sensitive.

$$\text{non}-\text{structural Loss}_{\text{acc}} = \sum_{ds,i} BRC_i \times \left\{\sum_i RCA_{ds,i} \times PONSA_{ds,i}\right\} \qquad 3-9$$

$$\text{non}-\text{structural Loss}_{\text{drift}} = \sum_{ds,i} BRC_i \times \left\{\sum_i RCD_{ds,i} \times PONSD_{ds,i}\right\} \qquad 3-10$$

Where BRC is the building replacement cost; RCA is acceleration-sensitive non-structural repair cost ratio (in % of building replacement cost) in each damage state, ds; RCD is drift-sensitive non-structural repair cost ratio (in % of building replacement cost) in each damage state PONSA is the probability of being in acceleration sensitive non-structural damage for each of the four damage states; PONSD is the probability of being in drift sensitive non-structural damage for each of the four damage levels.

Most content damage is a function of building acceleration. For example, overturning of furniture, or items sliding off from tables and counters are considered as content damages. Therefore, acceleration-sensitive nonstructural damage is considered as a good indicator of content damage.

$$content\ Loss = \sum_{ds,i} CRC_i \times \left\{ \sum_{i} CD_{ds,i} \times PONSA_{ds,i} \right\} \qquad 3-11$$

Where CRC is the content replacement cost; CD is the content damage ratio in % of the building replacement cost under each damage state, which is the consequence model; PONSA is the probability of being in acceleration sensitive non-structural damage for four damage states.

3.4.5 Vulnerability model

Vulnerability models combine fragility functions and consequence functions to directly estimate building loss. It is the relationship of mean damage ratio (also known as loss ratio) over a set of intensity measure levels (IM). In this thesis, the vulnerability functions follow the same building taxonomy as Hazus has done. There are 312 vulnerability functions defined based on given building types, occupancy types, and code level. Figure 37 shows one example of the vulnerability used for the loss calculation obtained for concrete building type C1H. It is the curve of mean loss ratio against spectral acceleration of 1.0s. Older buildings (Pre-code) have a higher mean loss ratio at a given ground motion value than more recent buildings.

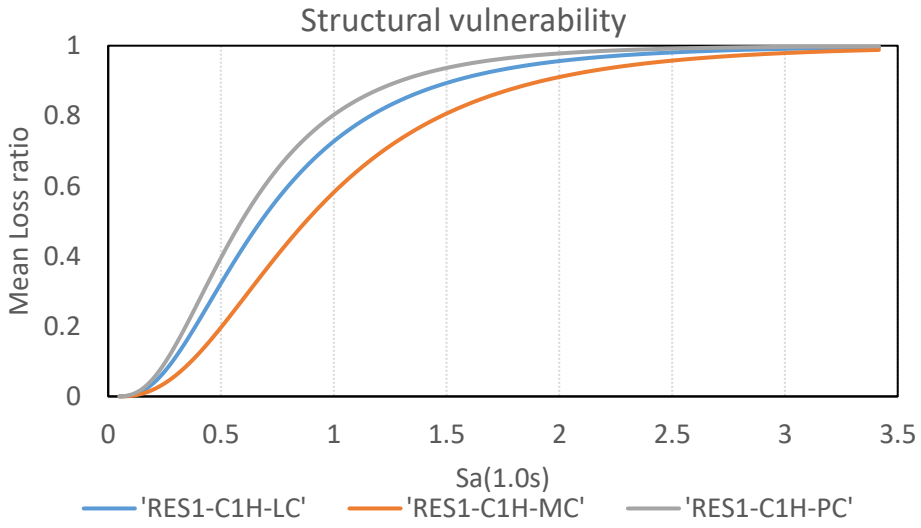

Figure 37. Structural vulnerability curves for single family house concrete buildings (RES1-C1H) for the three code levels

4. Hazus Result

4.1 Hazus result based on SHM 5

4.1.1 Damage

HAZUS determines the probability of damage to the general building inventory, and then converts these probabilities into number of damaged buildings. From the output in terms of the total number of damaged buildings for each return period, the damage increases as the return period become longer (Table 19). The seismic hazard for the return period of 2475 years gives the greatest amount of damage (24% of the total building). The percentages of buildings with slight and moderate damage exceed the ones for extensive and complete damage for every given return period. These results indicate that buildings mostly suffer slight and moderate earthquake damage.

Table 19. Number and percentage of buildings by levels of damage for different return periods

Return period	Building damage (All Design Levels)					
	None	Slight	Moderate	Extensive	complete	Total damaged building
	(%)	(%)	(%)	(%)	(%)	(%)
2475	663,377	185,681	22,643	988	25	209,337
	76.0%	21.3%	2.6%	0.1%	0.0%	24.0%
2000	711,555	145,367	15,222	561	10	161,160
	81.5%	16.7%	1.7%	0.1%	0.0%	18.5%
1500	768,091	96,052	8,326	242	4	104,624
	88.0%	11.0%	1.0%	0.0%	0.0%	12.0%
1000	813,133	55,503	3,986	93	1	59,583
	93.2%	6.4%	0.5%	0.0%	0.0%	6.8%
750	838,056	32,542	2,078	39	0	34,659
	96.0%	3.7%	0.2%	0.0%	0.0%	4.0%
475	856,265	15,607	830	11	0	16,448
	98.1%	1.8%	0.1%	0.0%	0.0%	1.9%
225	870,423	2,207	84	1	0	2,292
	99.7%	0.3%	0.0%	0.0%	0.0%	0.3%
100	872,557	152	5	0	0	157
	100.0%	0.0%	0.0%	0.0%	0.0%	0.0%

In terms of building type, wood frame houses have the greatest amount of damage at all return periods. This damage pattern is expected because wood buildings dominate the building inventory (Table 8 in section 3.4.3). The building type with the least amount of damage is steel. Steel buildings have durable and flexible frames that have good performance in past earthquakes occurring in Eastern Canada (Bagatini Cachuço, 2021). In Figure 38, the

percentage of buildings under a given damage state is calculated for each building type at return period of 2475 years. Among all the buildings that experienced extensive and complete damage, most of them were unreinforced masonry buildings (URM). Traditionally during eastern Canadian earthquakes, masonry buildings are the most seismically vulnerable. They experience the greatest amount of damage due to their lack of structural integrity (Ploeger et al., 2010). The result obtained aligned with the past studies that unreinforced masonry buildings is more vulnerable than other types of buildings. Among all the buildings that experienced slight and moderate damage, the majority were wood buildings Over 93% of all the building with no damage and 88% of the slight damaged buildings are wood buildings. This indicates that wood buildings mostly experience slight damage. The full table for all return periods can be found in Appendix G.

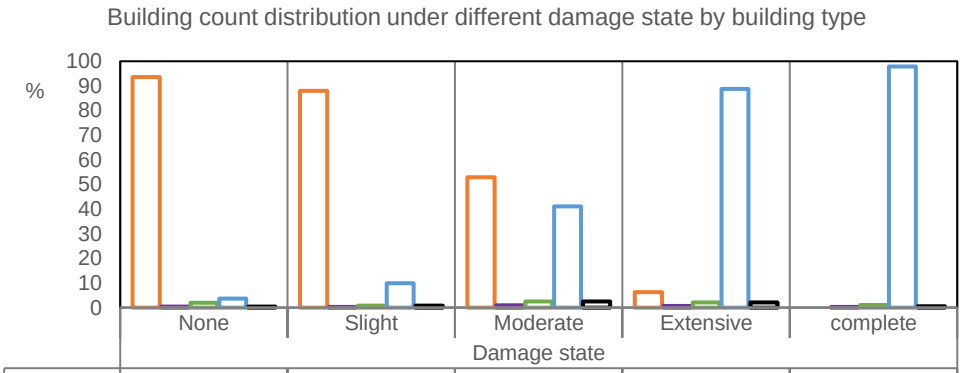

	None	Slight	Moderate	Extensive	complete
Wood	93.56	88.06	52.9	6.34	0
Steel	0.43	0.3	0.94	0.75	0.35
Concrete	1.94	0.88	2.58	2.07	1.14
URM	3.65	9.96	41.05	88.76	97.92
MH	0.42	0.79	2.53	2.09	0.58

Figure 38. Percentage of Building by damage levels and building types for a return period of 2475 years

4.1.2 AEL

Table 20 presents the direct economic losses for eight return periods. As expected, the highest loss value is obtained for the return period of 2475 years and the lowest one for the return period of 100 years. Based on the method discussed in Chapter 3, the total annualized earthquake loss is calculated as $6.19 million Canadian Dollars. It is further broken down into structural (Can$ 0.27 million), non-structural (Can$ 3.80 million), and content losses (Can$ 2.12 million).

Table 20. Structural, non-structural, and content economic losses for eight return period and associated AEL as calculated with Hazus

return period	structural losses for each RP(in k$)	non-structural losses for each RP (in k$)	content losses for each RP (in k$)	total
100	161	3,736	2,348	6,244.0
225	2,410	54,993	32,810	90,213.1
475	18,378	341,063	196,720	556,160.8
750	40,300	665,279	379,995	1,085,574.8
1000	71,514	1,111,792	615,438	1,798,744.6
1500	132,525	1,842,422	1,019,226	2,994,172.9
2000	216,713	2,750,171	1,512,373	4,479,257.8
2475	298,006	3,507,569	1,924,933	5,730,508.6
total AEL	274.9	3,796.3	2,119.2	6,190.4

The distribution of AEL by dissemination area is shown in Figure 39. Southwest of Montreal has a larger AEL. If the AEL distribution is compared with the distribution of the hazard map (Appendix B with soil effect), it is shown that the distribution follows a similar trend. The PGA value is larger in the southwest region and decreases gradually to the northeastern of the Greater Montreal region. The dissemination area with the largest AEL is area 24071710034 in the Vaudreuil-Soulanges region, which has an AEL of Can$ 29,800, and the areas in Les Moulins region have the second and third largest AEL, respectively. These two dissemination areas in red are the only two DAs with AEL over Can$ 20,000, as they contain buildings with large exposure over Can$ 600 million. It is noted that there are five areas with occupants but with no residential buildings, and one area with residential buildings but no occupants. This misalignment requires some further check for the exposure database because the building data and demographic data were from two sources. As a result, the AEL is estimated as 0 for these regions. Compared to the scenario-based study from (Rosset et al., 2022a; Yu et al., 2016) that estimates the maximum loss for an event, AEL provides a better interpretation of the expected loss combining the effects of seismic losses with probability of exceedance.

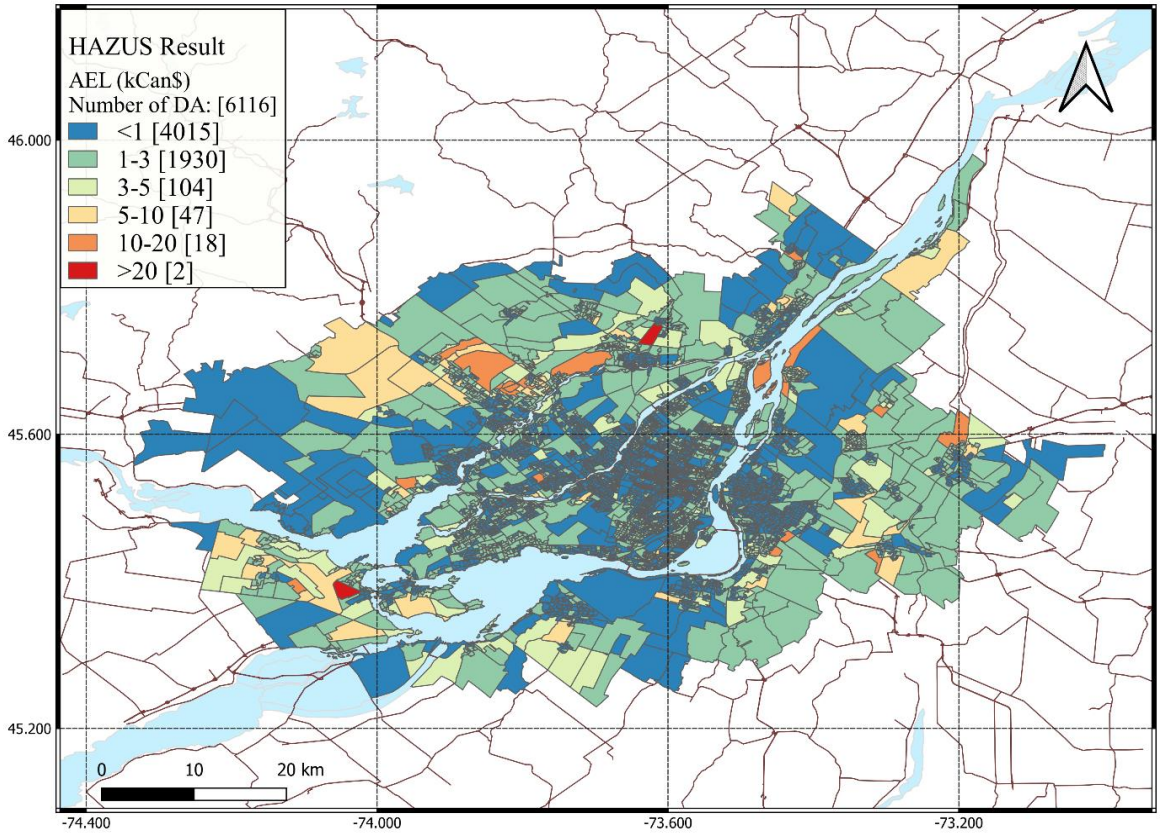

Figure 39. Distribution of Annualized Earthquake Loss (AEL) by Dissemination Area obtained from Hazus

4.1.3 AELR

While the AEL measures the annualized earthquake losses, the AELR addresses seismic risk in relation to the value of the buildings in the study area. By connecting annualized loss with the replacement value for a given DA, the AELR provides a consistent measure to compare seismic risk. The distribution of AELR by Dissemination Area is shown in Figure 40. It is shown that the AELR is high in four RCMs, Therese De Blainville, Les Moulins, Vaudreuil-Soulanges, and Lajemmerais. More than 50% of the DA in these municipalities have AELR higher than Can$ 60 per million Canadian dollars (mCan$) of building value. The DAs with largest AELR are area 24060600031 and area 24060600034 in L'Assomption RCM. The DA with largest AELR is Can$ $8213.9 per mCan$, which is more than 200 times of the average AELR per DA, Can$ 34.4 per mCan$. These two DAs generate the greatest amount of building damage as they have high loss over buildings with low values.

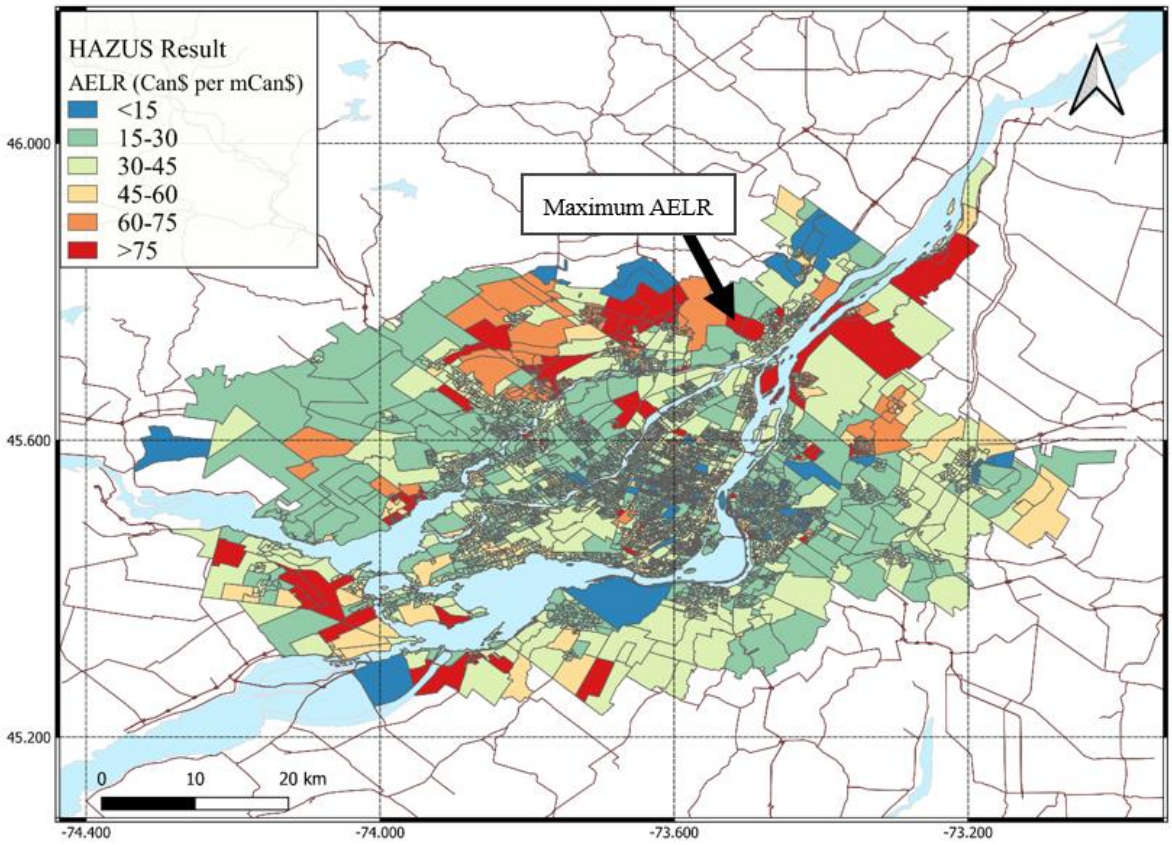

Figure 40. Distribution of Annualized Earthquake Loss Ratio (AELR) by Dissemination Area obtained from Hazus

4.1.4 AEL per capita and per building

The ability to correlate building density and population density with annualized earthquake loss is useful from a perspective of socio-economic impact of earthquakes. These figures also show annualized loss in relation to 2018 population distribution and reveal two important facts: the map in Figure 41 shows the geographic distribution of AEL relative to the number of residents by dissemination area and the map in Figure 42 shows the distribution of AEL relative to the number of residential buildings by DA. The average value of AEL per capita is of the order of Can$ 1.6 and the average AEL per building is Can$ 7.1. The largest AEL per capita is Can$ 100.7 in the DA 24066663382 due to a low population (5 people) in the area.

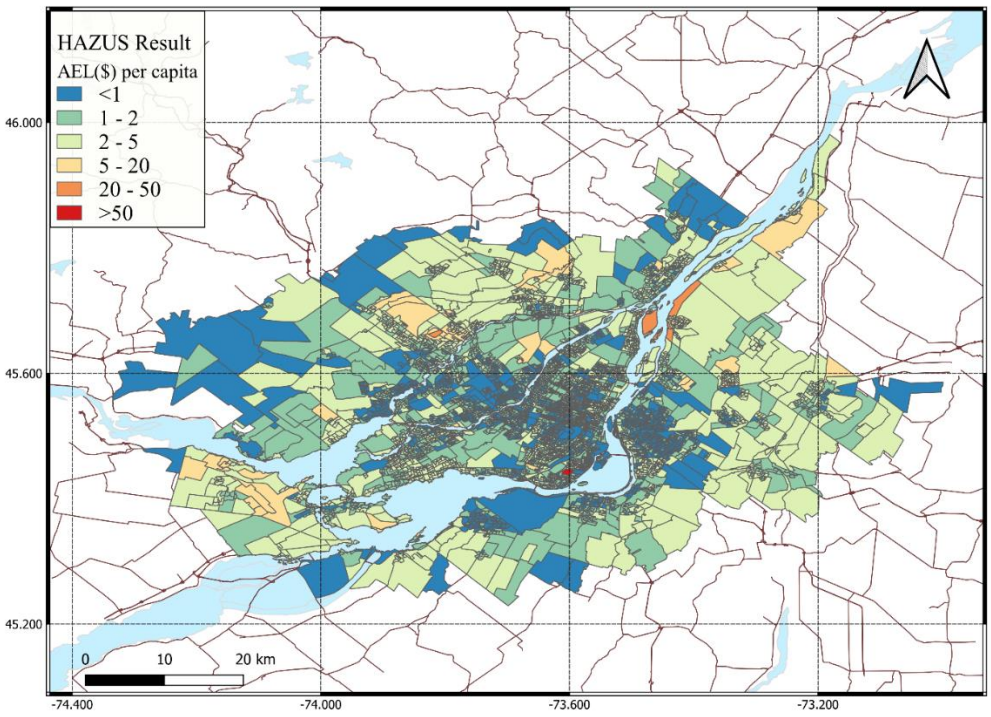

Fi

Figure 41. Distribution of AEL per capita by Dissemination Area obtained from Hazus

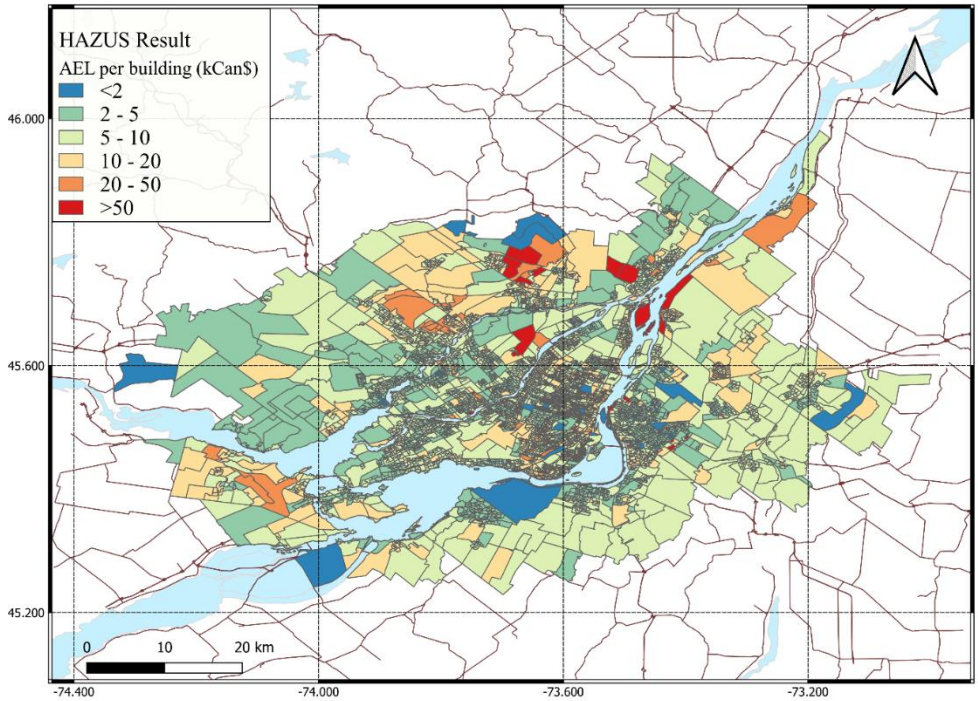

Figure 42. Distribution of AEL per building by Dissemination Area obtained from Hazus

4.1.5 Comparison with the US study

Since Quebec is close to the northeastern US, some studies from the US could be used for comparison and analysis. Three studies were conducted at the national level. The earliest studies (FEMA 2001), published in 2001, used the 1996 version of the seismic hazard maps provided by the US Geological Survey (USGS), and estimated the AEL of $4.4 billion US dollars at the national level. California accounted for 75% of the losses, at $3.3 billion. The second study (FEMA 2008) incorporated the 2002 hazard maps and used up-to-date inventory data. It predicted annualized losses of $5.3 billion US dollars and California again carried the majority of losses annualized with $3.5 billion. The most recent published version calculated the annualized loss and annualized loss ratio for USA and evaluated the geographical distribution of the losses. The western US would experience the most losses, especially in California.

The AEL calculated for US regions with similar geological location and within similar seismicity provides some insights for comparison and the accuracy of the result. Comparing the hazard map for the US in Figure 43 with the hazard map for the Montreal region in Figure 27, it is seen that the region of northern New York State and northern Maine has a similar seismicity as Montreal.

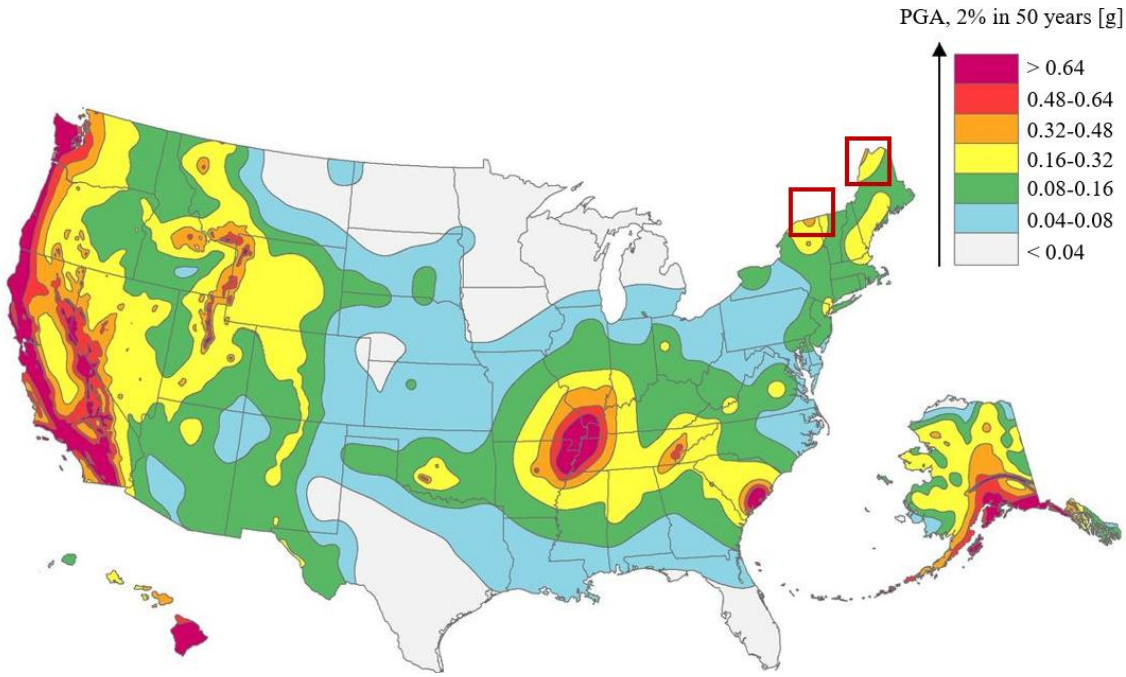

Figure 43. USGS 2018 earthquake hazard map showing PGA[g] 2% in 50 years (return period of 2475 years) (Powers et al., 2021)

The AEL for New York state was calculated to be US$25.4 million (FEMA, 2017). The AEL for the greater Montreal region was calculated to be US$4.75 million (Can$ 6.19 million), which is much lower than that calculated for major urban regions in Eastern US such as New York-Newark-Jersey region ($70.1 million) with a similar level of seismic hazard. The AEL is hard to compare because the region covered in FEMA (2017) by state has larger exposure in total compared to the Greater Montreal region. Another reason that causes the difference in AEL is that the report by FEMA (2017) calculated the AEL for residential, commercial, and industrial buildings. In this thesis, AEL is only studied for residential buildings, which was only be a portion of the study in FEMA (2017).

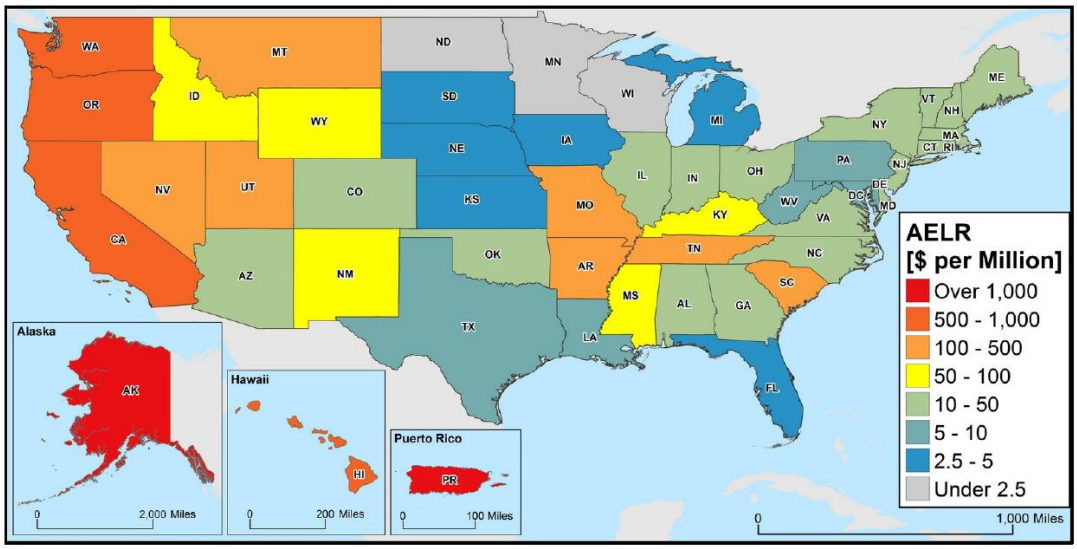

Figure 44. Annualized Earthquake Loss Ratio by State (FEMA-USGS-PDC, 2017)

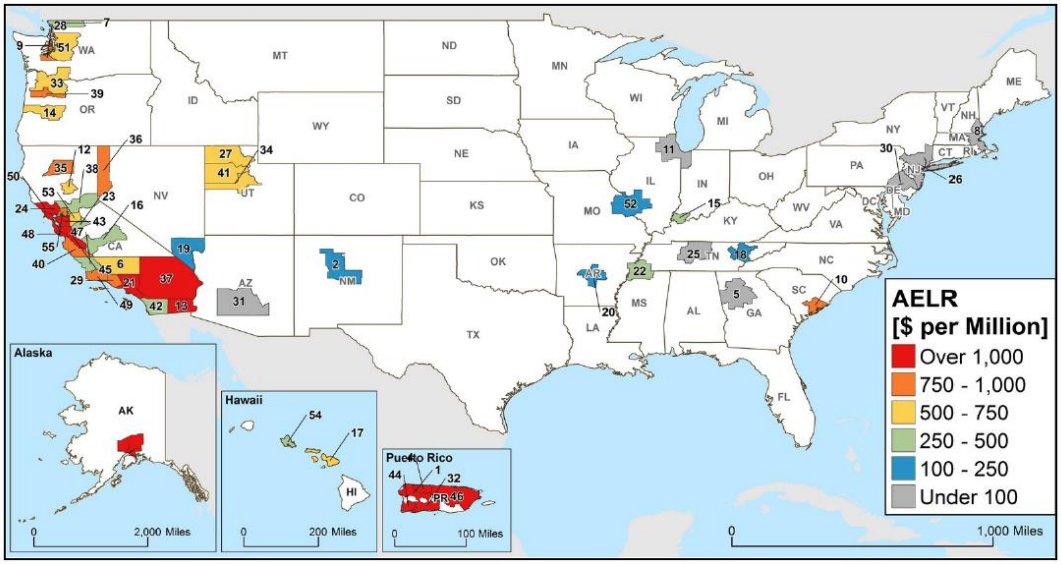

Figure 45. Metropolitan Areas with AELR over 10 million USD (FEMA-USGS-PDC, 2017)

The comparison for AELR could provide some insights as this is the losses per building value. For a region of similar seismicity, the AEL is independent of the building exposure. The average AELR for greater Montreal region is US$25.3 (Can$ 34.4) per million, and the AELR for New York State is US$28.7 per million (Figure 45). Since New York is relatively close to Montreal, this indicated a consistent result between the two regions with adjacent geological location.

It is also meaningful to compare the AEL with respect to population in Montreal and in northeastern US. The value of AEL per capita for greater Montreal region is US$1.3 (Can$ 1.6) per capita, which is lower than that calculated for counties in upstate New York (US$ 5-10) with similar geographic location and similar level of seismic hazard. The difference may be due to the high population density in downtown New York.

Table 21. Comparison between losses from Montreal and New York

	AEL [US$]	AELR [US$ per million]	AEL [US$] per Capita
Montreal	4.75	25.3	1.3
New York	25.4	28.7	5-10

4.2 Sensitivity analysis of Seismic losses with the different parameters

The graph in Figure 47 indicates the relationship among the hazards in terms of Peak Ground Acceleration (PGA) with a RP of 2475 years, the exposure of the building stock, and the estimated building loss represented by the circle with diameter proportional to the loss value. It shows that the building loss depends on both building values and hazard value (PGA). The building loss is the largest with high PGA and exposure value, which is the right upper corner of the graph. Building loss is more sensitive to the building exposure than to the hazard value. For a given hazard (x=axis), building loss increases with the exposure (y=axis) by a factor of 3 to 5. Building loss increases with the increasing PGA value by a factor of only 1.2 to 2.

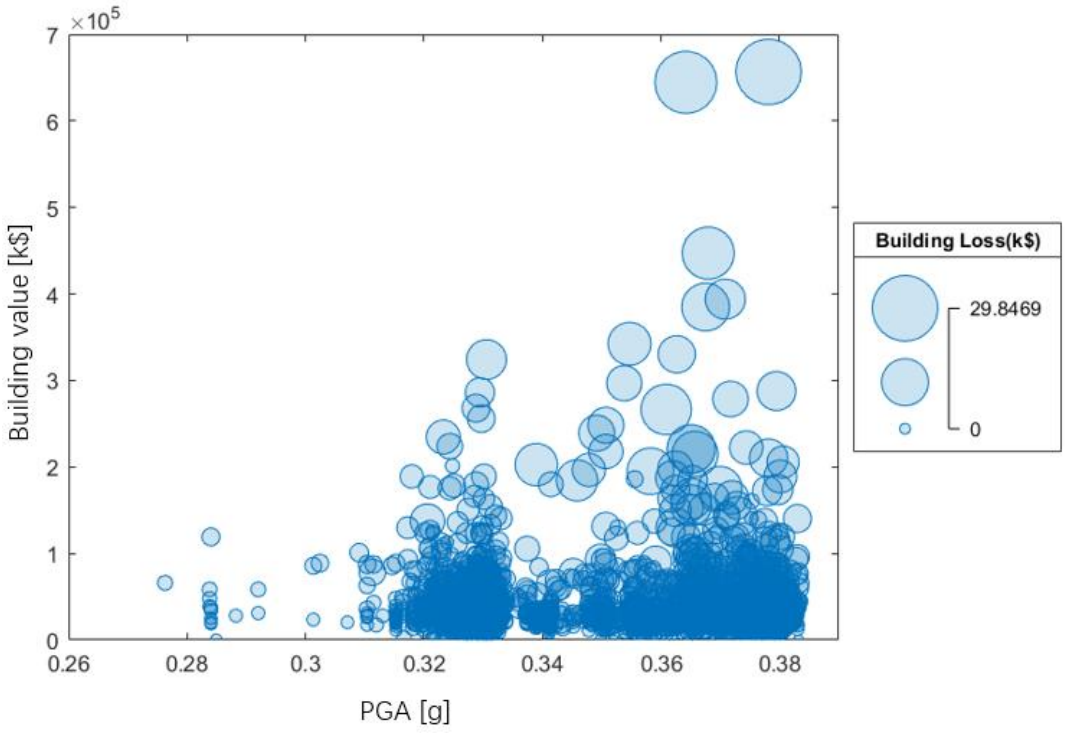

Figure 46. Relationship between AEL (in kCan$), PGA (RP=2475years in g) and building exposure (in kCan$)

4.2.1 Ground motion parameters

The graphs in Figure 48 plot the relationship between the AEL and PGA values calculated for the return periods of 100, 475, 1,000, and 2,475 years. Data by DA are grouped in intervals of 1,000 Can$ for the AEL and plotted as a box chart. It contains the median (horizontal red line), the range between 25 and 75 percentiles (blue box), as well as the minimum and maximum values (whiskers) calculated for the PGA values of the AEL intervals. It also includes the outliers for each interval, which are represented by red crosses. At the dissemination area scale, there is an increase in the value of PGA with the average value of AEL for the return periods of 100, 475, and 1500 years. This positive trend between AEL and PGA values is not found for the 2,475-year return period which shows an uncorrelated distribution, related to the PGA distribution that considers the site conditions in Figure B1 to Figure B8 in Appendix B. For low return periods such as 100 years and 475 years, the outliers appear above 25 percentiles at low-value AEL intervals, and for a return period of 2475 years, the outliers appear below 25 percentiles at low-value AEL intervals.

Because the AEL depends on not only ground motions but building exposure as well, these outliers indicated the DAs that are more sensitive to the building exposure.

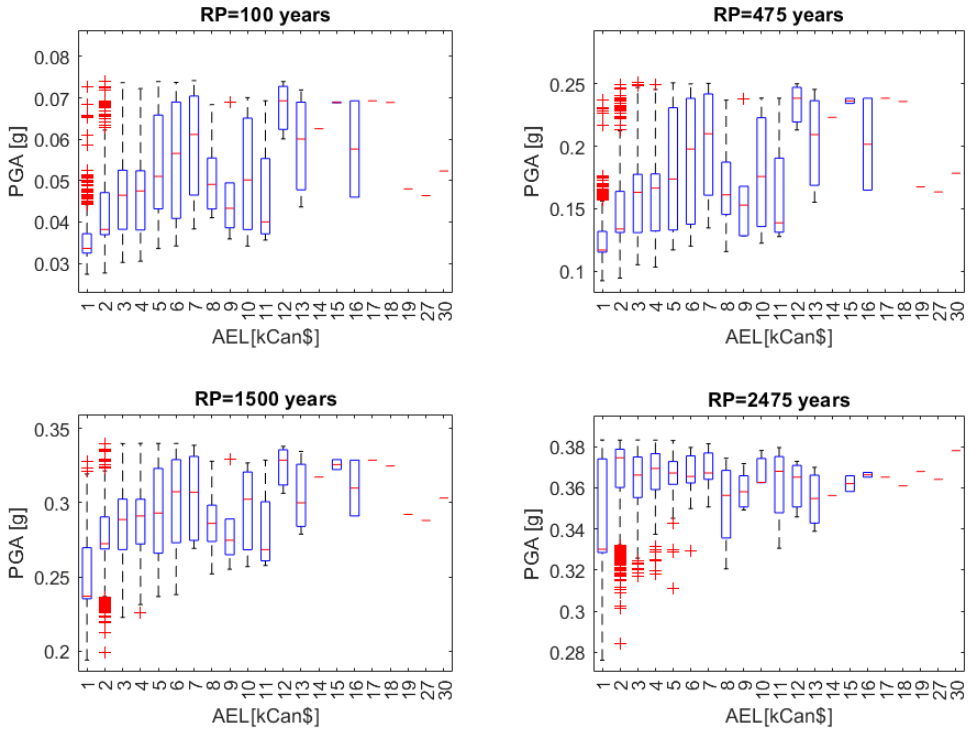

Figure 47. Relationship between the PGA value (in g) for the return periods of 100, 475, 1500 and 2,475 years and the value of AEL (in kCan$)

[*box represents the median value, the 25 and 75 percentiles, the maximum and minimum of the number of buildings, red cross represent outliers]

4.2.2 Building values

Figure 49 shows the relationship between AEL or AELR that are grouped in intervals of 1,000 Can$ and the total building count. The box represents the median value, the 25 and 75 percentiles, the maximum and minimum of the number of buildings, and the red circle represents the mean value. The blue dots represented the outliers for each group. There is a clear positive relationship between the AEL and the number of buildings by DA. For AELR, which represents the ratio between AEL and building value, it is approximately constant regardless of the building count. The average building count in each DA is around 150-180 buildings across all the AELR intervals.

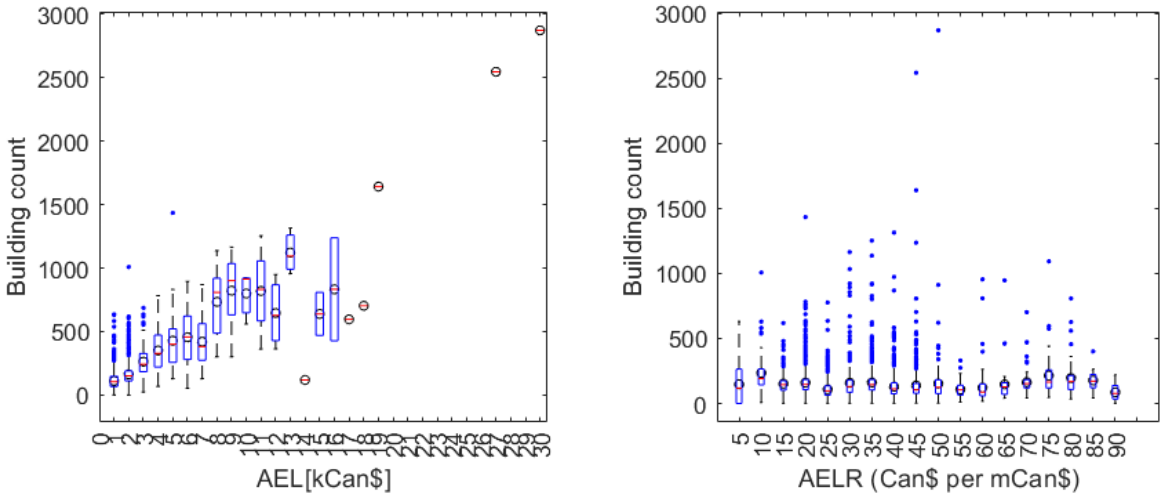

Figure 48. AEL (Left) or AELR (right) grouped against total building count

The graphs in Figure 50 show the relationship between AEL or AELR values grouped in intervals of 1,000 Can$ and the total building value. The symbols are the same in the Figure 49. AEL is positively correlated with the total building value. The greater the building value, the greater the replacement or repair cost for a given level of seismic stress. This relationship does not hold between AELR and the total building value, but AELR is also sensitive to the distribution of the hazard over the study area. AELR is approximately constant regardless of the building exposure because it is already calculated as AEL per unit building exposure.

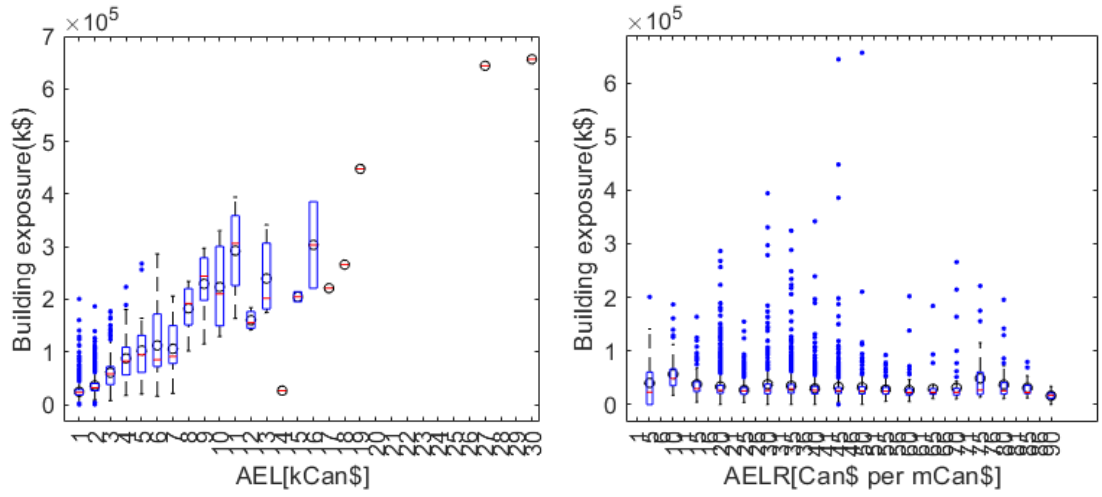

Figure 49. AEL (Left) or AELR (right) grouped against total building exposure

4.2.3 Construction Materials

A plot of AEL against building exposure for the five general building types (Figure 51) indicates the influence of building materials on seismic loss. Each point represents a DA, and

the number of buildings is represented by the color of the points. It is clear that there is a positive relationship between the building count, building exposure, and the AEL, regardless of the building type.

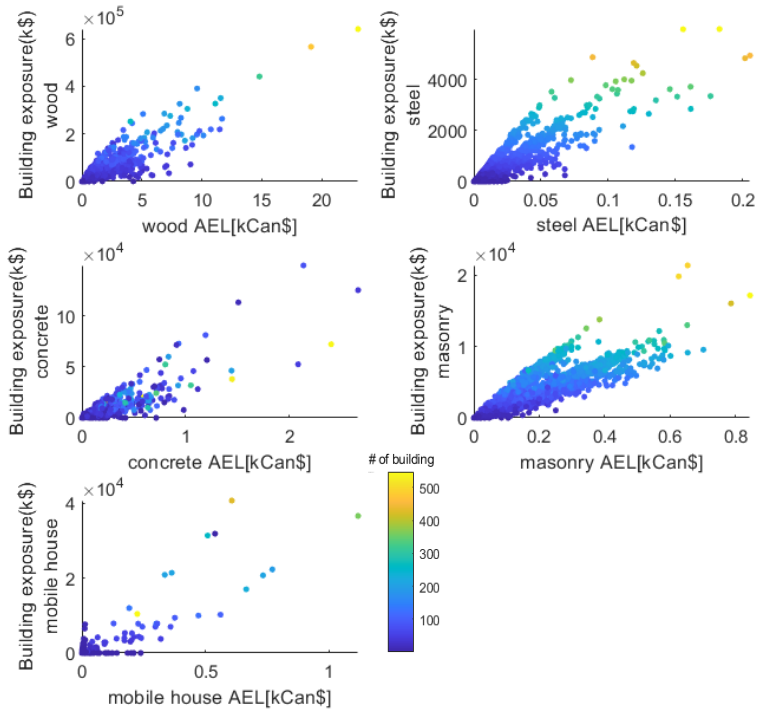

Figure 50. AEL against building exposure for the five general building type

Since a clear linear relationship is observed, linear regression is calculated for each of the building types and is drawn on Figure 52. While most of the DAs have AEL smaller than Can$ 1000, there are about 80% of the DAs with AEL larger than 10000 Canadian dollars, especially for wood and concrete buildings. The difference between these AEL values is unmanageably large, so a log-scale plot was used for better illustrate the regression. The 90% prediction interval is shown as a pink dashed line and the coefficient of determination, R^2, is calculated and shown in the graph. The closer R^2 approaches to 1, the better regression predictions fit the data. Steel buildings and masonry buildings both have a clear linear relationship and most of points are within the 90% prediction interval, which results in R^2 values close to 1.

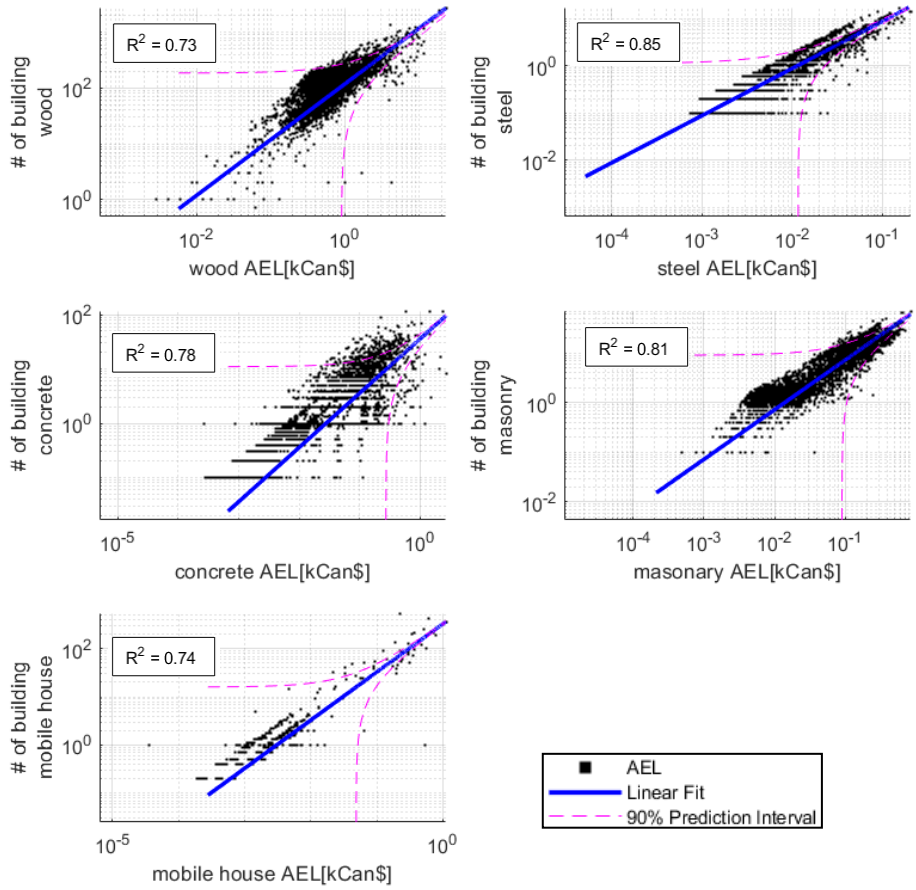

Figure 51. regression of AEL against building count for the five general building type

For the concrete buildings with low AEL, the points are very scattered because there are further breakdown categories of the concrete buildings by structure systems and height. The concrete buildings based on structure systems can be divided into moment-resisting frames (C1), shear walls (C2), and concrete frame with unreinforced masonry infill walls (C3); for each structure system, it is further divided into low-rise, medium-rise, and high-rise buildings. In total, there are 10 sub-categories of concrete buildings. It is shown below in Figure 53 that for each type of concrete building, a linear relationship exists. In general, higher building values result in a larger AEL for a given specific building type. For concrete buildings with different heights, the AEL has different sensitivity to the building exposure. For example, AEL increases more as building exposure increases for high-rise buildings (C1H and C2H) compared to for the low-rise buildings (C1L, C2L, and C3L).

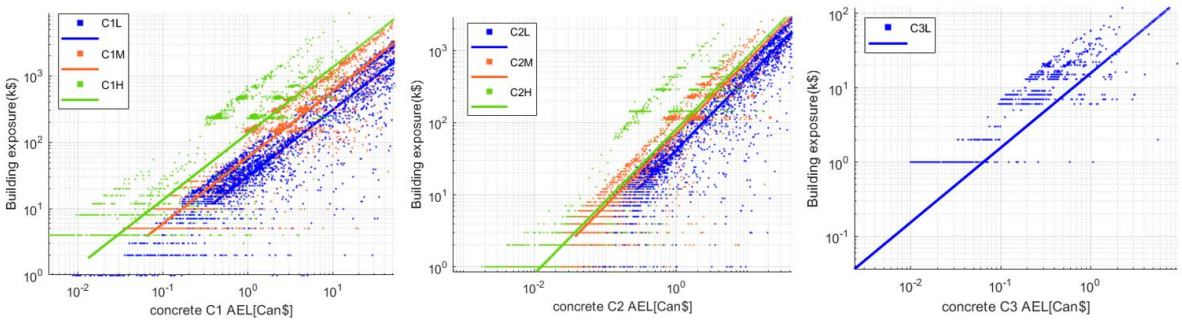

Figure 52. Building exposure versus AEL for C1, C2, and C3 building types

4.2.4 Code levels

The log-scale graphs in Figure 54 plotting building exposure against AEL by DA for wood (W1) and concrete (C1) indicate the effect of code level on AEL values. The AEL ranges from Can$ 0.1 thousand to over Can$ 10 million.

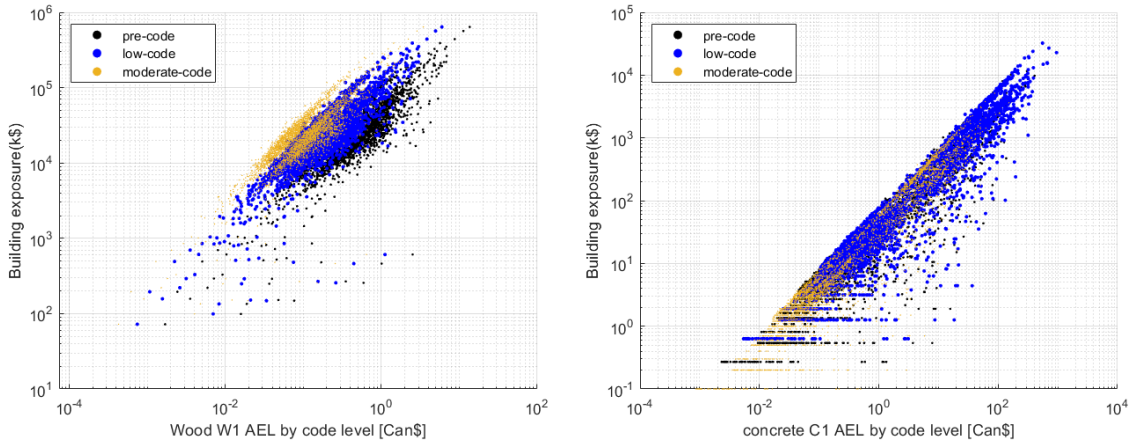

Figure 53. AEL VS building exposure by building code for W1(left) and C1L (right)

For a given building value of an area (exposure), pre-code buildings have the largest AEL, and moderate-code buildings have the smallest AEL, indicating that old buildings will experience larger damage and induce a larger AEL. Between different building types, the effect of year of construction also varies. The difference of AEL between low-code and moderate-code levels of same exposure for wood buildings is larger than for concrete buildings, by a factor of 2.3. This indicates that AEL is more sensitive to code level for wood buildings compared to concrete buildings, since wood deteriorates more and therefore is more vulnerable than concrete as time passes by (Filiatrault, 2013).

4.3 Hazus result based on SHM 6

From the result of SHM5, it is shown that the return period of 2475 years contributes the most (37%) in the total AEL (Table 20). Therefore, the loss at this probability level is the most important to consider. By calculating the seismic loss from SHM6 hazard model, it is significant to have a first glance of the impact of two versions of seismic hazard models on seismic loss. The loss of return period of 2475 years obtained from SHM6 is Can$ 8748 million. It increased 53% compared with the loss from SHM5. The seismic loss map of return period of 2475 years is shown in Figure 46. The loss range with largest number of DAs is between Can$ 700-1000 thousand. A full analysis should be conducted in future studies.

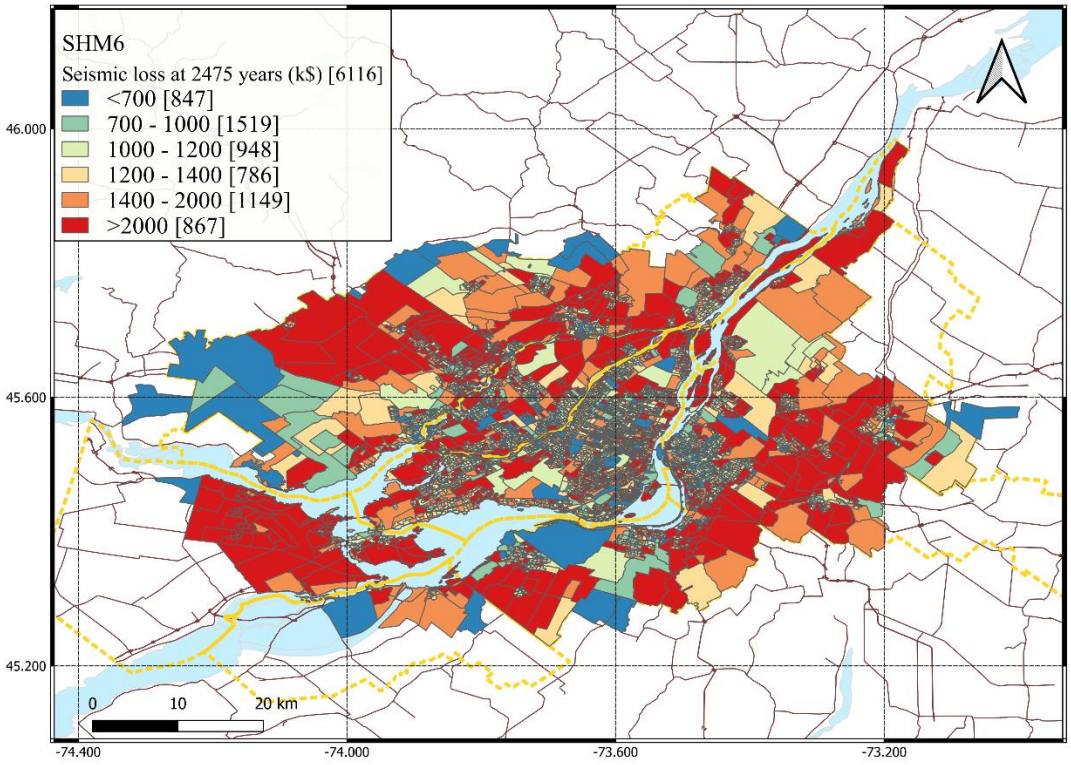

Figure 54. Seismic loss distribution by DA for the return period of 2475 years based on SHM6

5. OpenQuake Result

5.1 Damage Approach

5.1.1 AEL

OpenQuake is used to calculate AEL, combining fragility functions and consequence models. Table 22 presents the direct economic losses calculated for the eight return periods using the damage approach. The AEL is estimated around Can$ 12.4 million. It is further broken down into structural (Can$ 0.31 million), non-structural (Can$ 6.76 million), and content losses (Can$ 5.36 million).

Table 22. Direct economic losses for the eight return periods and AEL from OpenQuake using damage approavch (in Can$)

return period	structural losses for each RP(in k$)	non-structural losses for each RP (in k$)	content losses for each RP (in k$)	total
100	127.49	6,473.90	5,466.32	12,067.7
225	2948.0	162514.3	126623.9	292,086.3
475	23161.7	722133.8	565412.8	1,310,708.2
750	49345.3	1271911.8	1004656.7	2,325,913.8
1000	88823.0	1970877.8	1546166.3	3,605,867.1
1500	155583.1	3063559.5	2429484.7	5,648,627.3
2000	245978.0	4407575.9	3510698.3	8,164,252.2
2475	323030.6	5515795.4	4412280.2	10,251,106.2
total AEL	314.5	6762.9	5357.1	12,434.6

The distribution of AEL by dissemination area is shown in Figure 55. The number in the bracket in the legend represents the number of DAs in the corresponding interval. The majority of DAs (4141 DAs) has AEL between 1,000 and 3,000 Can$. Southwest of Montreal has a larger AEL than the rest of Montreal region. If the AEL distribution is correlated with the hazard map (Appendix B), it is shown that the distribution follows a similar trend. The PGA values are larger in the southwest region than the other parts of the region and decreases gradually to the northeastern of the Greater Montreal region.

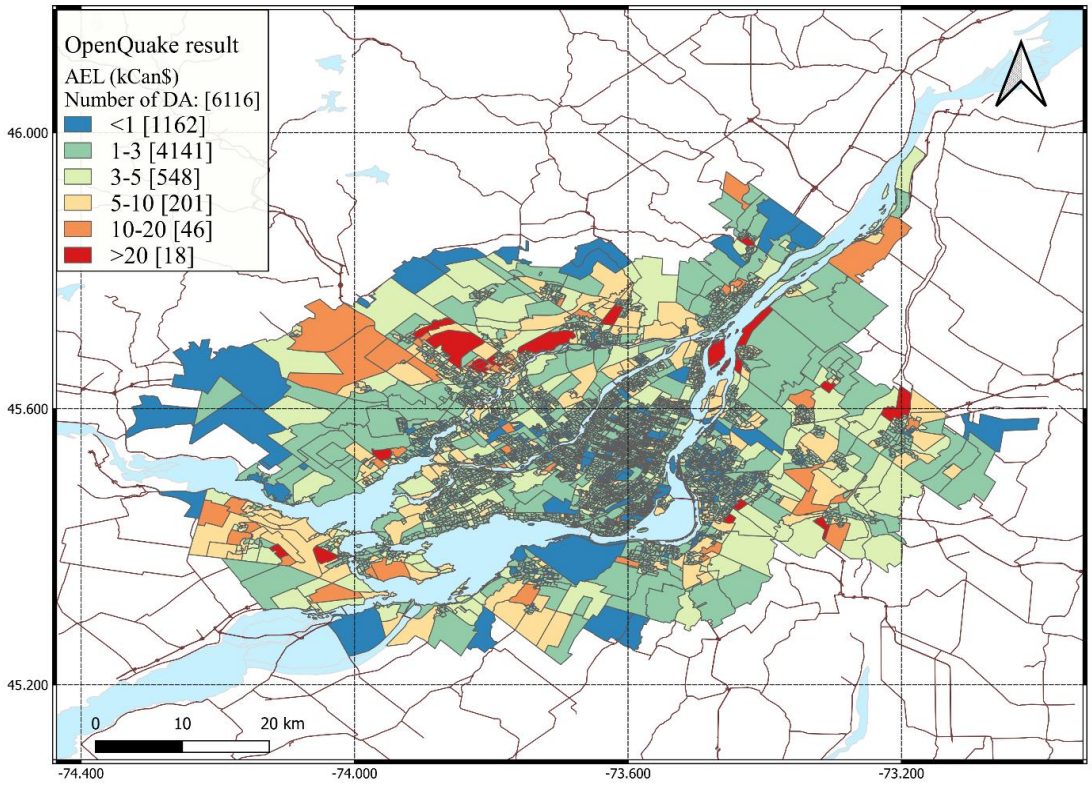

Figure 55. Distribution of AEL by Dissemination Area from OpenQuake using the damage approach

5.1.2 AELR

The distribution of AELR by dissemination area obtained from OpenQuake is shown in Figure 56. The AELR is high in two RCMs in the north and northeast region: Therese De Blainville and Les Moulins; and two RCMs in the southwest region: Vaudreuil-Soulanges and Lajemmerais. More than 80% of the DA in these municipalities have AELR higher than Can$60 per million Can$ of building value.

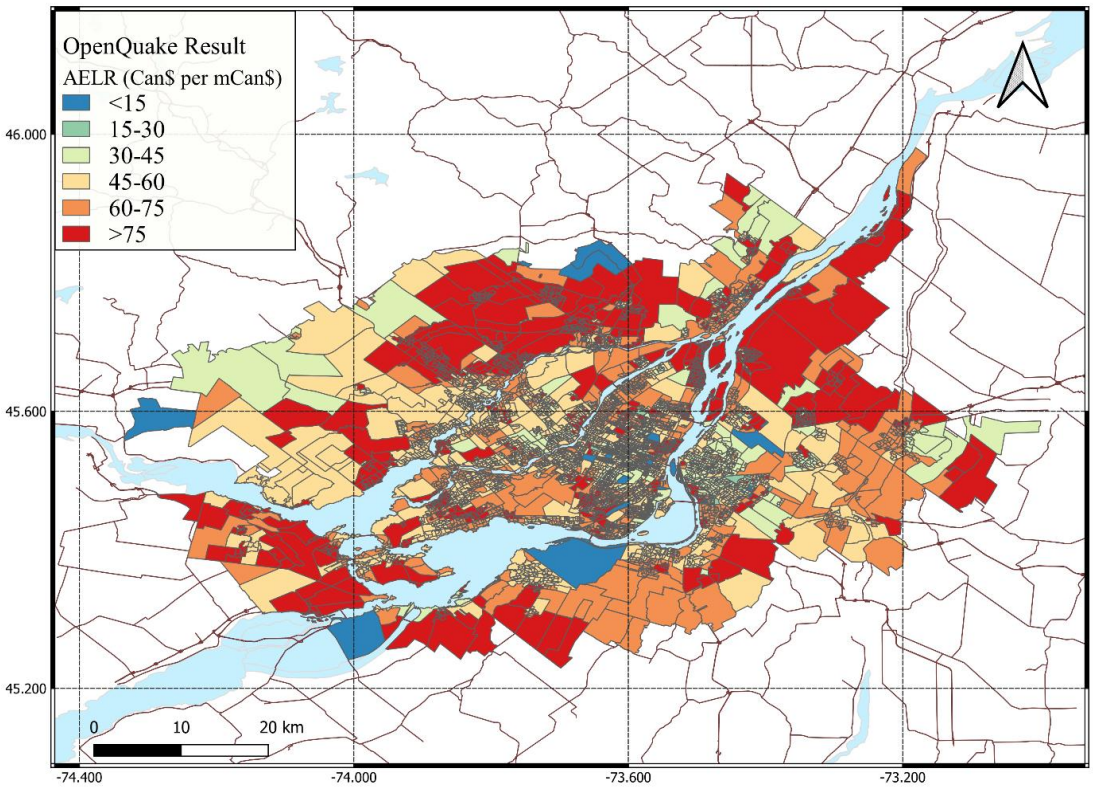

Figure 56. Distribution of AELR by Dissemination Area from OpenQuake using the damage approach

5.1.3 AEL per capita and per building

The socio-economic impact of earthquakes is also studied using the OpenQuake result. The map in Figure 57 shows the geographic distribution of AEL relative to the number of residents by dissemination area. The map in Figure 58 shows the distribution of AEL relative to the number of residential buildings by DA. The average value of AEL per capita is Can$ 3.28 and the average AEL per building is Can$ 16.98. The distribution of the AEL per capita and per building have similar spatial distribution. The largest AEL per building and per capita are concentrated in the Northern part of the Greater Montreal region.

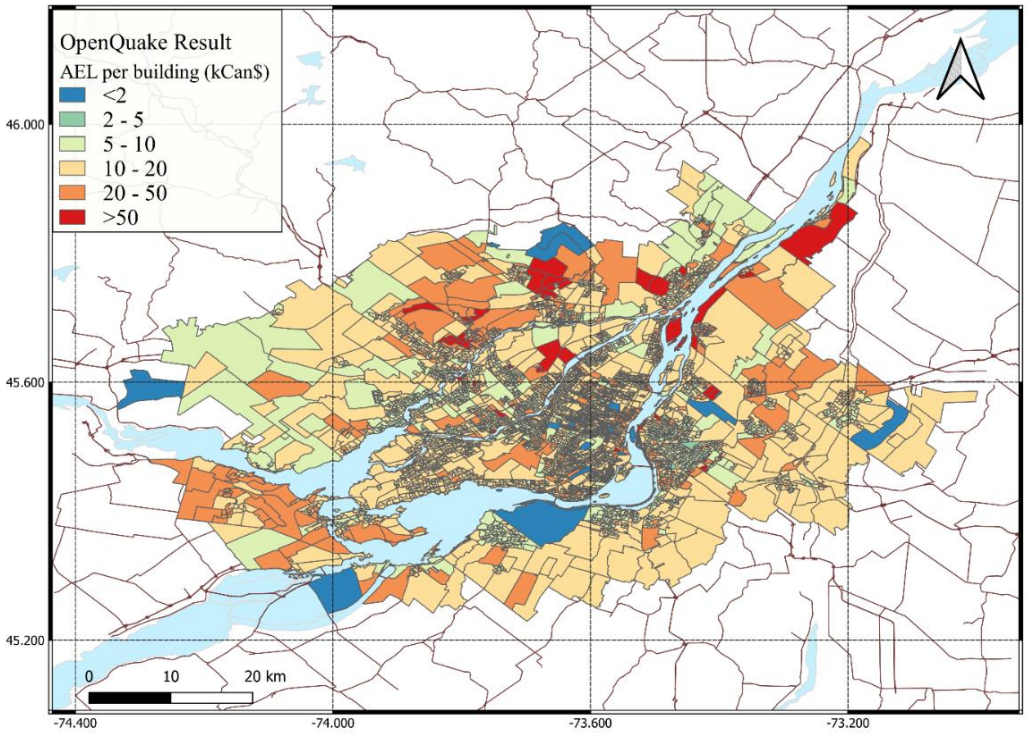

Figure 57. Distribution of AEL per capita by Dissemination Area obtained from OpenQuake using the damage approach

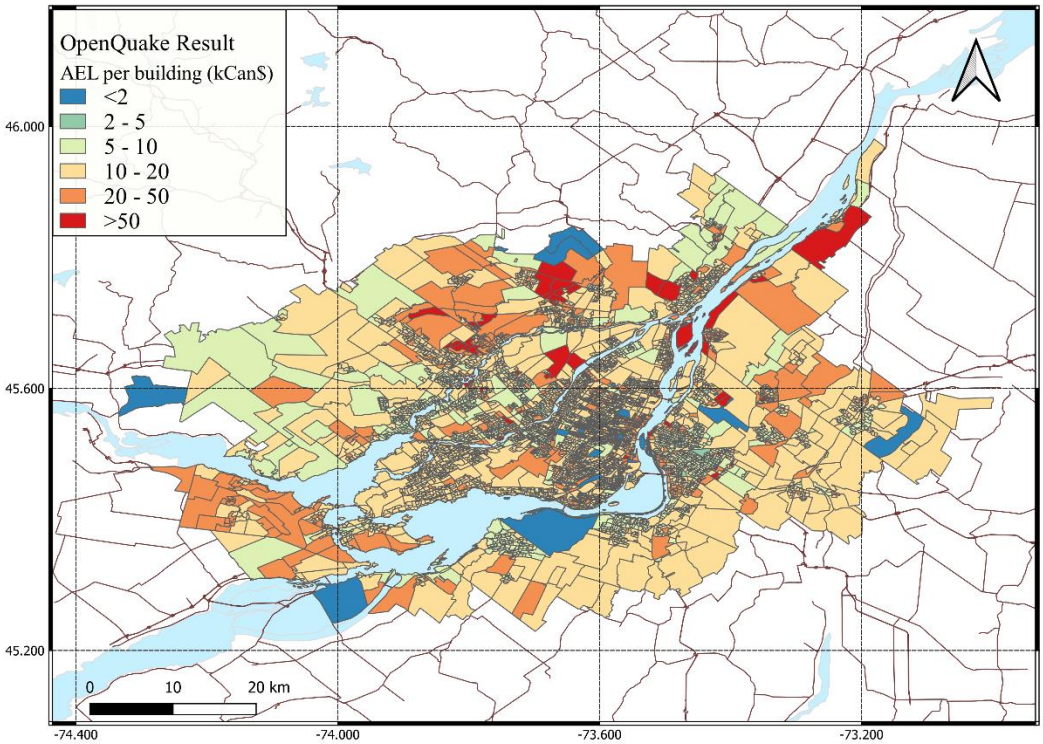

Figure 58. Distribution of AEL per capita by Dissemination Area obtained from OpenQuake using the damage approach

5.2 Risk approach

5.2.1 AEL

In the risk approach, the AEL is estimated using vulnerability functions in OpenQuake as explained in section 3.4.5. Table 23 presents the direct economic losses for the eight return periods. The total annualized earthquake loss is calculated as Can$ 6.2 million. It is further broken down into structural (Can$ 1.99 million), non-structural (Can$ 2.78 million), and content losses (Can$ 1.39 million).

Table 23. Direct economic losses for the eight return periods and AEL from OpenQuake using risk approavch (in Can$)

return period	structural losses for each RP(in k$)	non-structural losses for each RP (in k$)	content losses for each RP (in k$)	total
100	49,247	9,358	11,333	69,938
225	113,960	47,273	35,451	196,684
475	295,353	217,918	104,807	618,078
750	415,799	421,342	189,871	1,027,012
1000	517,637	712,393	299,445	1,529,475
1500	594,301	1,242,930	553,893	2,391,124
2000	682,671	1,997,520	938,857	3,619,048
2475	819,082	2,760,640	1,374,690	4,954,412
total AEL	1,986	2,777	1,393	6,156

The distribution of AEL by dissemination area is shown in Figure 59. Southeast and downtown Montreal has a larger AEL. There are only two dissemination areas that have AEL larger than Can$ 20 thousand, circled in red in Figure 59. The largest one is in Les Moulins (24071710034), Can$ 27.0 thousand, and the second largest one is in Vaudreuil-Soulanges (24064640013), Can$ 22.5 thousand.

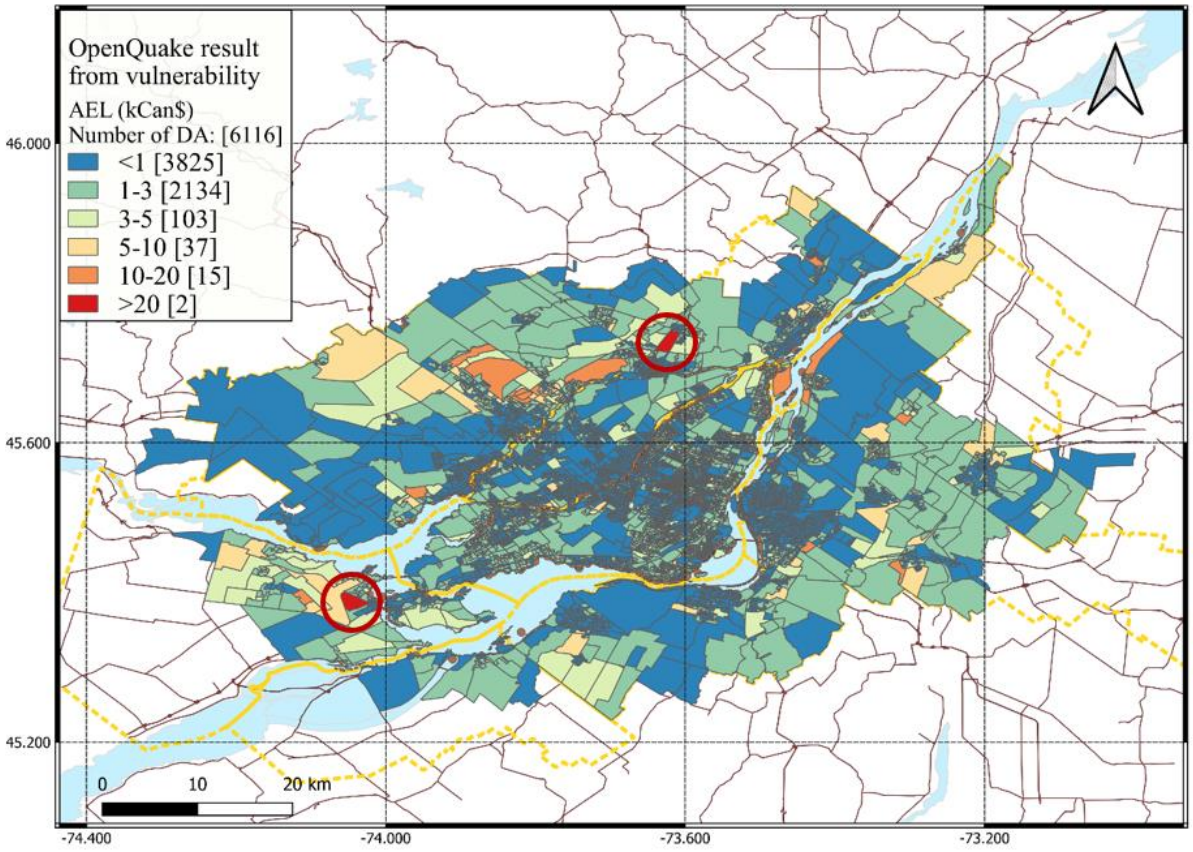

Figure 59. Distribution of AEL by Dissemination Area obtained from OpenQuake using the risk approach

5.2.2 AELR

The distribution of AELR obtained by dissemination area from OpenQuake is shown in Figure 60. The AELR is larger in northern Montreal. Although some DAs in central and southern Montreal have AELR larger than Can$45, the DAs with large AELR are mainly concentrated in three RCMs: Therese De Blainville, Les Moulins, and Lajemmerais. More than 80% of the DA in these municipalities have AELR higher than Can$60 per million Canadian dollars of building value.

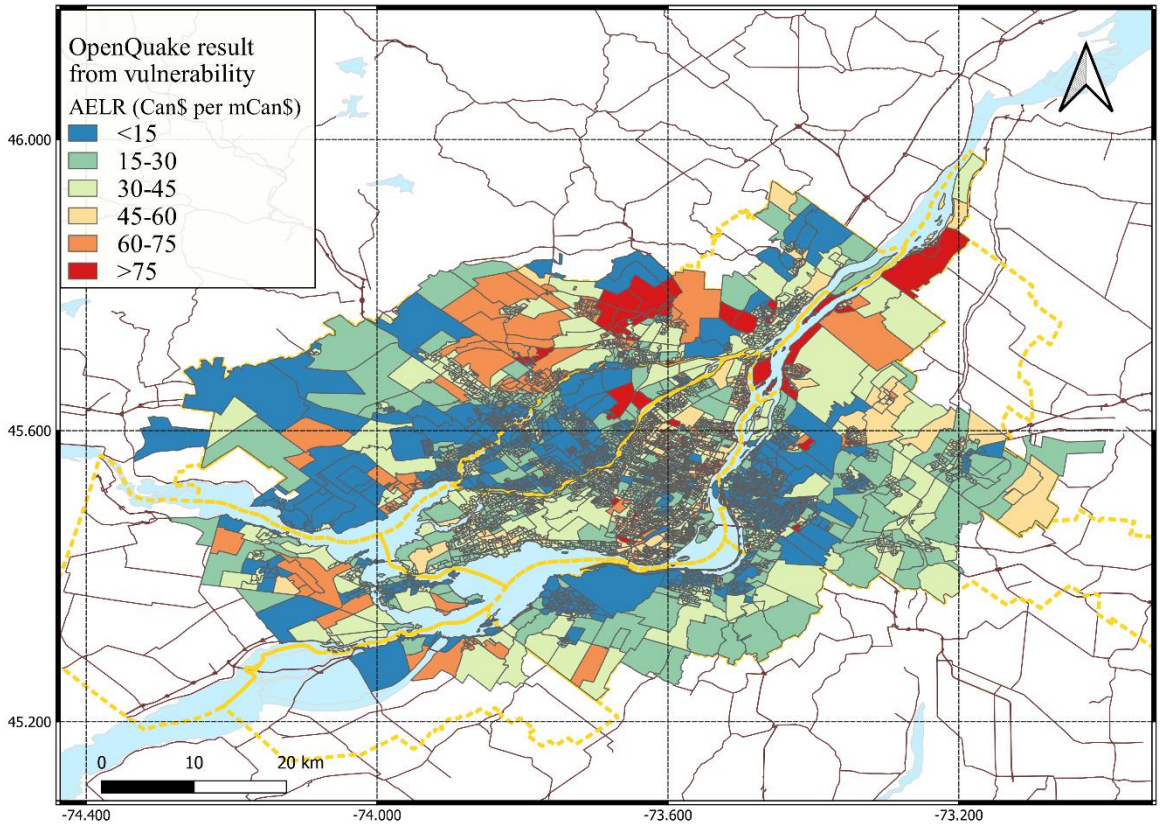

Figure 60. Distribution of AELR by Dissemination Area obtained from OpenQuake using the risk approach

5.2.3 AEL per capita and per building

The socio-economic impact of earthquakes is also analyzed from the risk analysis. The map in Figure 61 shows the geographic distribution of AEL relative to the number of residents by dissemination area. The map in Figure 62 shows the distribution of AEL relative to the number of residential buildings by DA. The average value of AEL per capita is of the order of Can$ 3.28 and the average AEL per building is Can$ 16.98. It follows a very similar spatial distribution as the results in Hazus. The largest AEL per building and per capita are concentrated in the northern part of the Greater Montreal region.

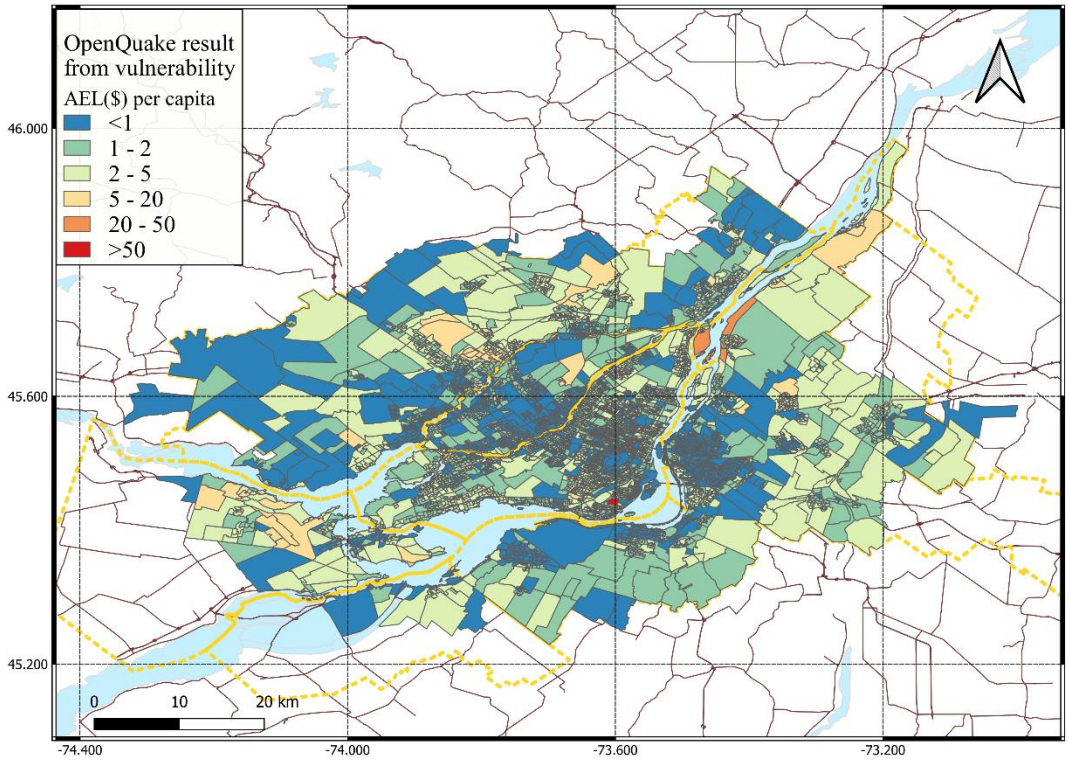

Figure 61. Distribution of AEL per capita by Dissemination Area obtained from OpenQuake using the risk approach

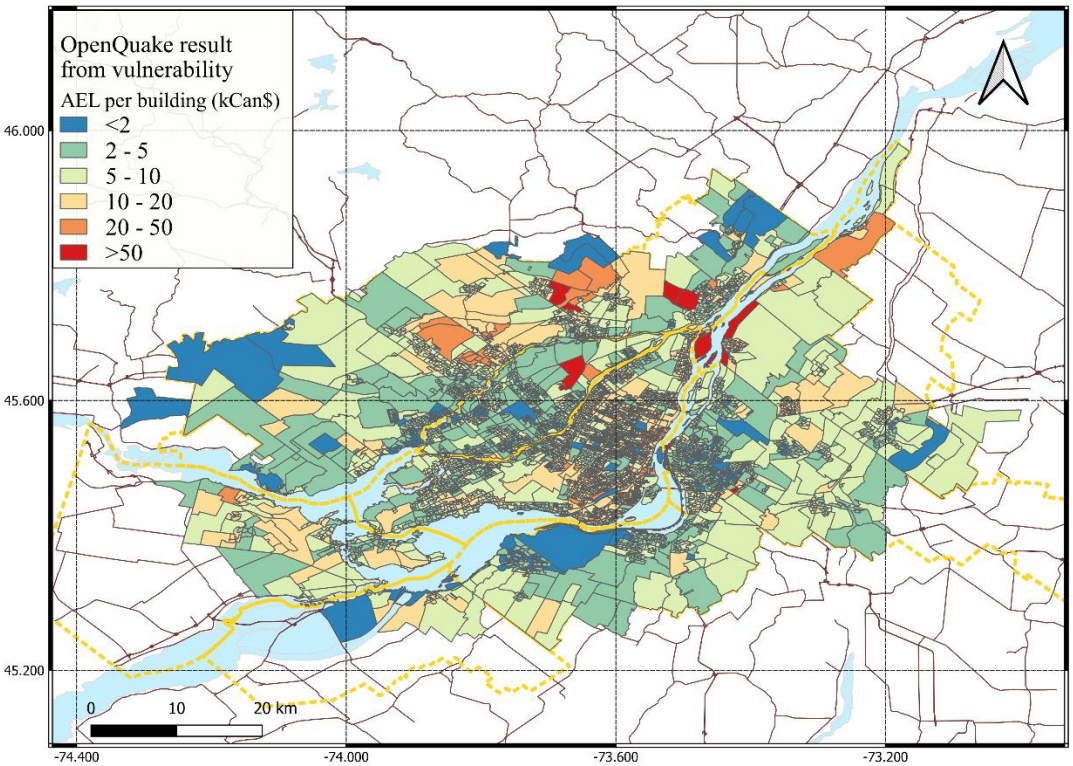

Figure 62. Distribution of AEL per building and by Dissemination Area obtained from OpenQuake using the risk approach

6. Discussion

6.1 Influence of the Seismic Hazard Model (SHM5 and SHM6) in Hazus calculations

Seismic losses calculated for the return period of 2475 years using both SHM5 and SHM6 are compared in Figure 63. For both models, the distribution of AEL approximately follows a log-normal distribution. The peak of the distribution represents the most DAs within this interval. It tends to shift to the right for the SHM6 compared to SHM5. This indicates a lower mean value in SHM6 (6.35) than SHM5 (3.22). The distribution spread is larger for SHM5 than SHM6. This indicates a larger standard deviation of the losses of all DAs from SHM6 (36.8) than SHM5 (3.86).

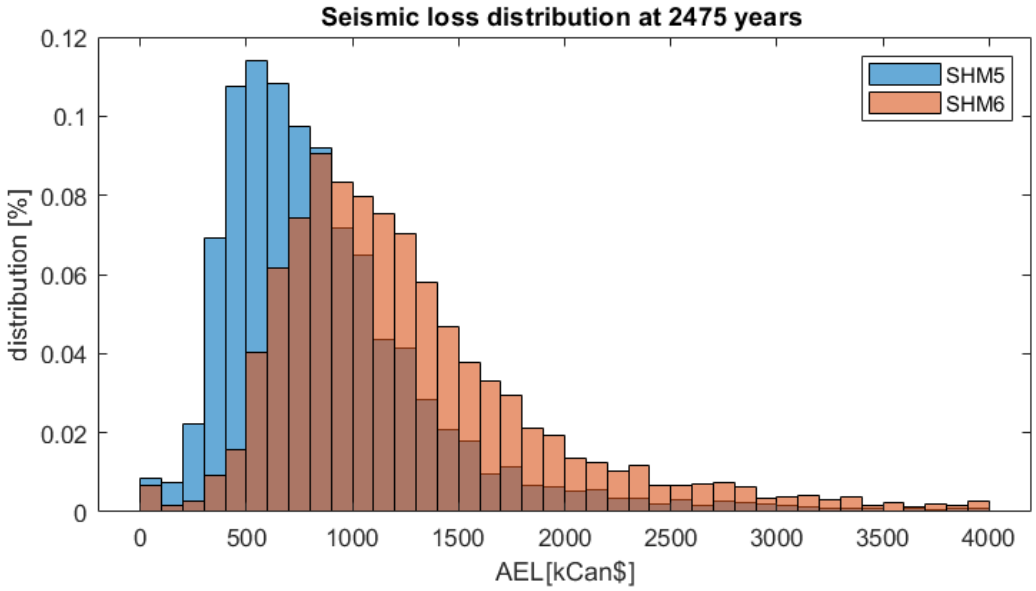

Figure 63. AEL distribution by DA from SHM5 and SHM6 models

The seismic loss maps at the return period of 2475 years from SHM5 and SHM6 are plotted in Figure 64. Comparing the two loss maps, the losses increase as the seismic hazard values increase from 5th generation to the 6th generation. In the SHM5 model, there are only 312 DAs that have losses greater than Can$ 2 million while in the 6th generation, there are 867 DAs that have losses greater than Can$ 2 million. The seismic loss of the northeastern region greatly increased from the range of Can$ 700-1000 thousand to Can$ 1400-2000 thousand.

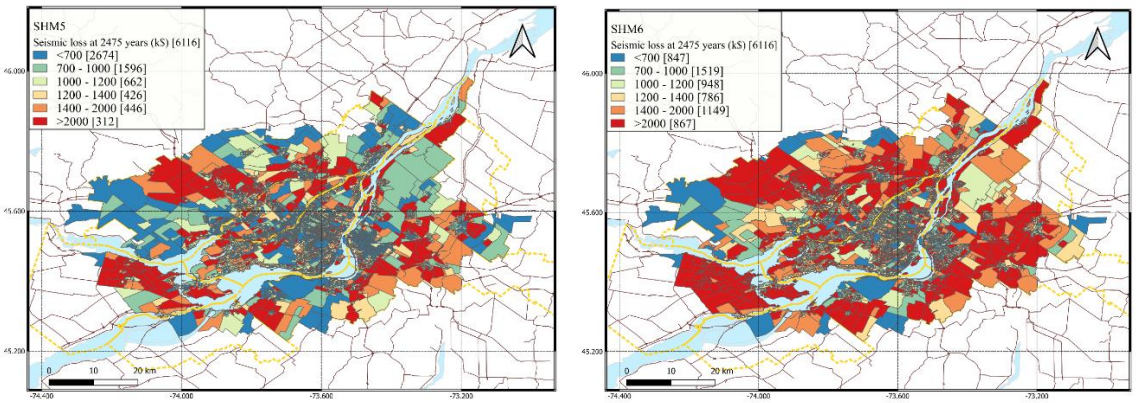

Figure 64 Seismic loss distribution by DA at 2475 years based on SHM5 (left) and SHM6 (right)

6.2 Influence of the damage or risk approaches in OpenQuake

The results based on the damage approach and risk approach share the same trend but have some discrepancies as well. Since the hazard map used is identical, the loss maps of both approaches share the same distribution. From Figure 55 and 59, the dissemination areas with high ground motion values (for example, PGA) have high AEL in both risk and damage approaches. The results from the two approaches at the same return period also share some similarities. The total AEL is from the non-structural and content losses for both approaches. The highest seismic loss from both risk models was obtained from the return period of 2475 years and the lowest from the return period of 100 years. It is clear that the losses increase as the probability of exceedance (the inverse of return period) decreases. However, the values of the AEL by DA from two approaches are very different. The AEL from the damage approach is twice the AEL from the risk approach. The discrepancy from the two loss estimations comes from the use of different risk models. Both models should be further verified so that the loss estimation can be calculated from OpenQuake. In the next section, the Hazus result will be a reference used to assess the accuracy of results obtained from OpenQuake.

6.3 Comparison of results obtained with Hazus and OpenQuake using SHM5

6.3.1 General comments

The comparison for the results from the two software provides a critical perspective on the accuracy of the OpenQuake calculation, setting Hazus as a reference since it is more developed in the past studies for Montreal region. The table 24 provides a comparative

analysis of the estimated AEL, and the association structural, non-structural, and content components, using Hazus and the damage and risk approaches in OpenQuake. The total AEL from damage approach is twice as large as the Hazus result due to the large nonstructural and content loss while the total AEL from the risk analysis is close to the AEL from Hazus (only 0.6% lower). The three results indicate that the non-structural and content losses are the major contributors of the seismic loss. This illustrates that nonstructural damage contributes more economic loss compared with structural damage. However, there are larger differences between the Hazus and OpenQuake results for each component. Admittedly, there will be a small difference between the two software due to the accuracy of calculation. There is relatively large discrepancy of the OpenQuake damage approach from the non-structural and content components and of the OpenQuake risk approach from structural component.

Table 24. Comparison of AEL from Hazus and the OpenQuake-engine

	AEL	% diff	Structural AEL	% diff	Nonstructural AEL	% diff	Content AEL	% diff
Hazus	6,190		275		3,796		2,119	
OpenQuake damage analysis	12,435	101	315	14	6,763	78	5,357	153
OpenQuake risk analysis	6,156	-0.6	1,986	622.4	2,777	-26.9	1,393	-34.3

*AEL in kCA$

6.3.2 Comparison between Hazus and OpenQuake damage approach

The total AEL calculated with OpenQuake damage approach (Can$12.4 million) is twice as high as the value provided by Hazus (Can$6.2 million). The distribution of the AEL per DA in Figure 65 shows that more than 70% of the DA has an AEL lower than Can$1,500 AEL. The lognormal AEL distribution from both calculations are similar but the AEL values calculated with OpenQuake are generally larger than the ones from Hazus.

The losses, divided in their structural, non-structural, and content components, calculated for each return period with both tools are presented in Figure 66. The structural losses from OpenQuake are around 20% larger than those from Hazus, varying $\pm$5% between all the return periods. For nonstructural and content components, this difference increases for long return period from 100 years to 2475 years.

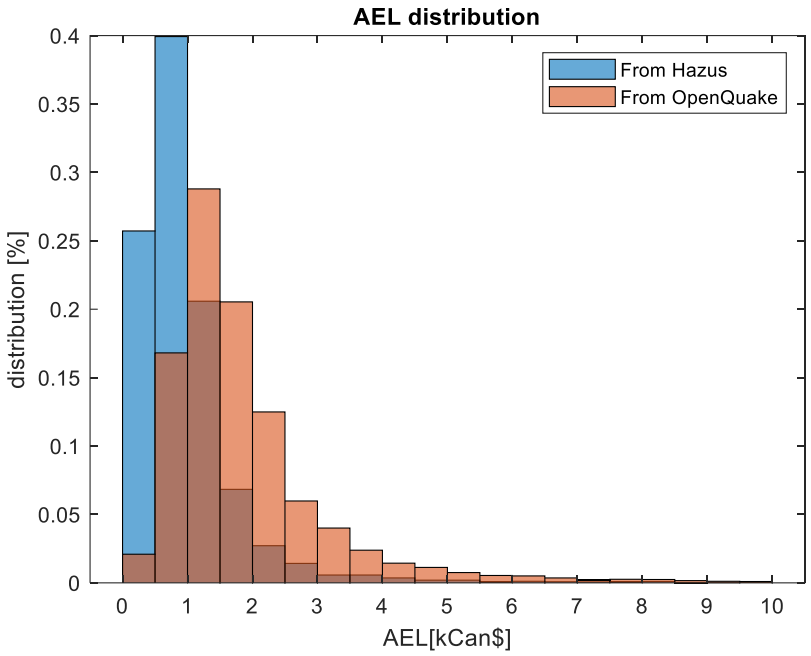

Figure 65. AEL distribution by DA obtained from Hazus and OpenQuake damage approach

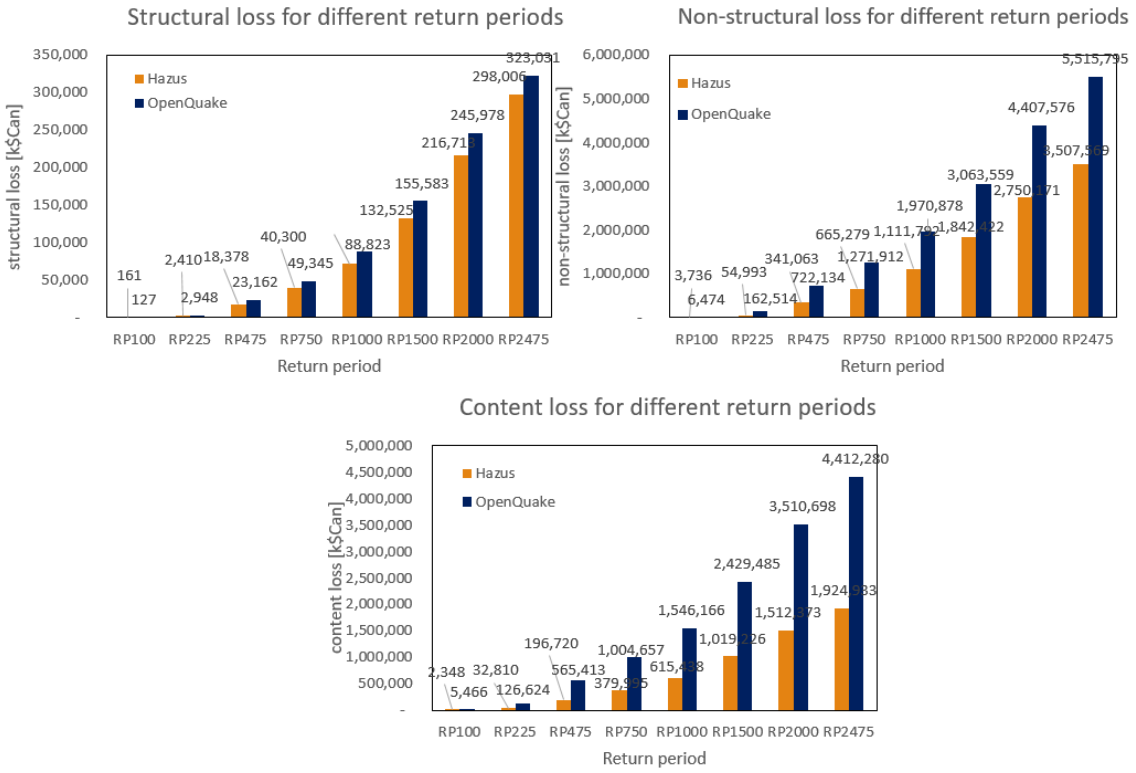

Figure 66. Seismic loss distribution for each return period obtained from OpenQuake damage approach and Hazus

The bar graphs in Figure 67 represent the percentage by components of the total calculated AEL for each return period and in both tools. In both Hazus and OpenQuake, the structural losses represent 2 to 5% of the total losses. In Hazus, the content losses are around

35% of the total as the non-structural ones count for more than 60%. In OpenQuake, the content loss consists of around 35-40% of the total losses, and structural loss consists of the largest percentage (around 55%) of the total losses.

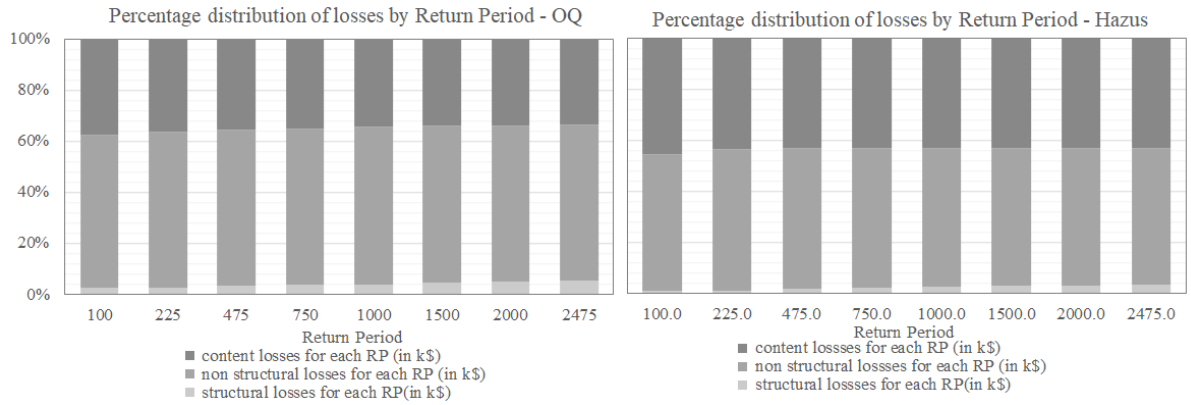

Figure 67.Distribution of losses by components and return period obtained from OpenQuake (Left), and Hazus (Right)

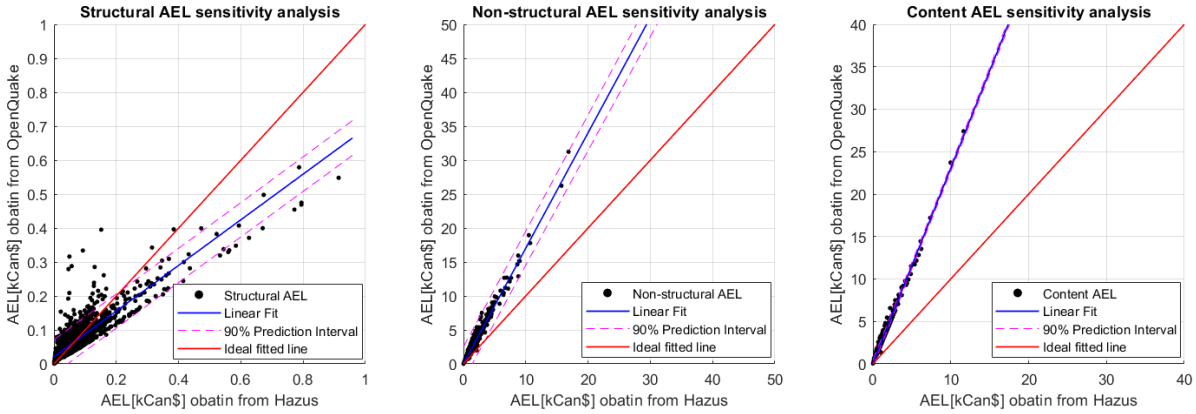

Figure 68. Comparison of results from Hazus and from OpenQuake damage approach for structural, non-structural, and content AEL

Figure 68 presents the comparison between results from OpenQuake and from Hazus by each component. The blue line represents the fitted line for the AEL ratio of OpenQuake over Hazus and the red line represents the unit line, which means the two results are equal. The 90% prediction interval in Figure 68 shows that the content loss is the largest difference between results from Hazus and OpenQuake. There are a few DAs with larger structural losses at lower AEL range from OpenQuake. This is due to the adjustment of the OpenQuake fragility functions (as section 3.4.4 discussed). However, the slope of fitted line for structural components is the closest to 1, which means the results obtained from OpenQuake is closest

to results obtained from Hazus. The discrepancies between Hazus and OpenQuake results are mostly from the nonstructural and content components.

Figure 69 shows the ratio between the acceleration-sensitive and drift-sensitive non-structural loss under different damage states obtained from Hazus. The label on the bar provides the average losses under different damage states and the y axis shows the percentage of acceleration-sensitive and drift-sensitive non-structural losses. The non-structural acceleration-sensitive losses under all four damage states are larger than the drift-sensitive ones. Although the acceleration-sensitive losses represent 99.7% of the total loss under complete damage, it is only $Can 9,400 (4,1% of the total loss). This indicates that the most severe damage state doesn't contribute the largest loss.

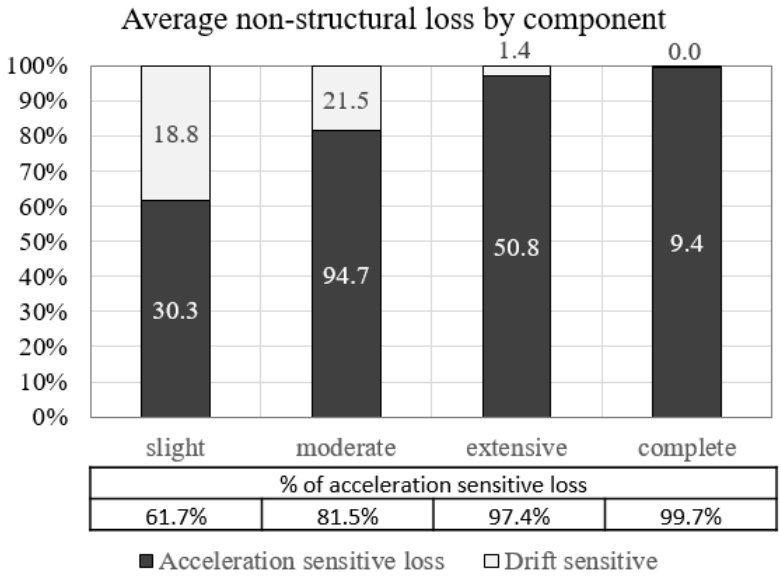

Figure 69. Average non-structural loss by component from Hazus

In OpenQuake, only the acceleration-sensitive component was considered in the calculation of non-structural damage for two reasons; the only published hazard maps from NRCan include only maps of PGA and Spectral acceleration, and unlike the CSM used in Hazus, OpenQuake does not develop fragility curves using the spectrum and capacity curve. It calculates damage using the fragility functions developed externally. Therefore, the drift-sensitive components can not be developed in OpenQuake. By default, the non-structural damage is calculated for all of the non-structural elements from only acceleration-sensitive fragility functions and the corresponding PGA. The acceleration-sensitive damage will be

100% of the non-structural loss instead of only part of the non-structural damage developed in Hazus. It is assumed that most content damage, such as overturned cabinets and equipment, or equipment sliding off tables and counters, is a function of building acceleration. Therefore, acceleration-sensitive non-structural damage is considered to be a good indicator of content damage. In this case study, the OpenQuake content loss is based on the acceleration-sensitive non-structural fragility function. Since the fragility functions developed in Hazus are used in OpenQuake without any modification, both non-structural and content loss will be overestimated as shown from the result in this approach.

6.3.3 Comparison between Hazus and OpenQuake risk approach

The losses calculated with the OpenQuake risk approach are very close to those provided by Hazus for any return period (Table 24). The total AEL obtained from Hazus is Can$6.2 million while the total AEL obtained from OpenQuake is Can$6.15 million. The distribution of the AEL for each return period (Figure 70) shows that seismic losses increase as the return periods get longer. The structural loss is significantly larger for lower return periods. For return period of 100 years and 225 years, the loss ratio between Hazus and OpenQuake is up to 300 and 50 respectively.

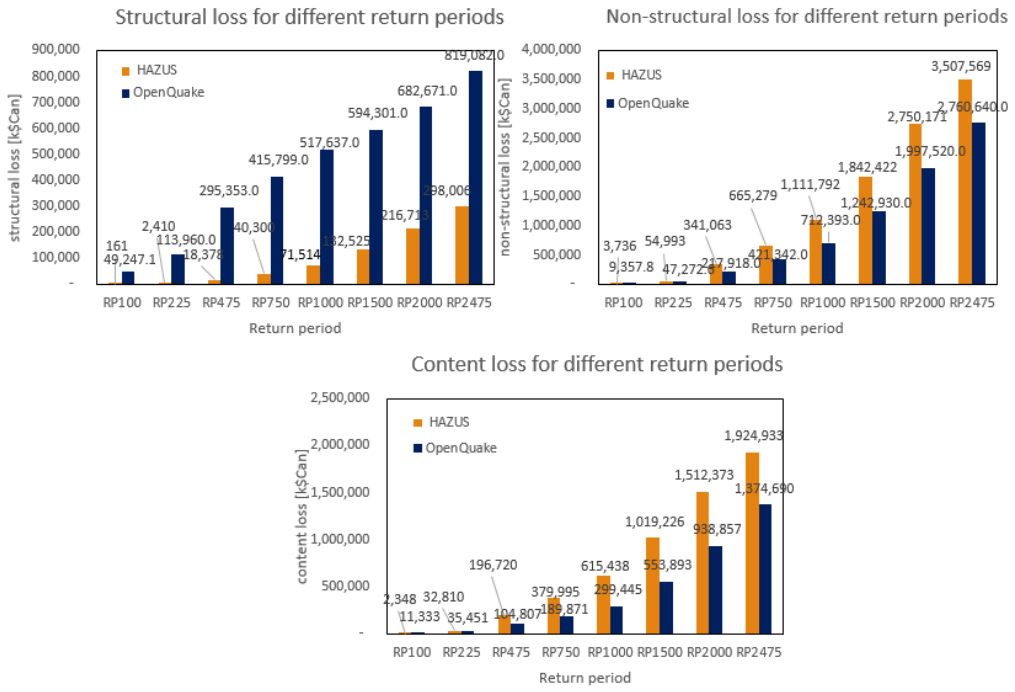

Figure 70. Seismic loss by components for each return period obtained from OpenQuake risk approach and Hazus

Figure 71 presents the comparison between the result from OpenQuake and from Hazus by each component. The blue line represents the fitted line for the AEL ratio of OpenQuake over Hazus and the red line represents the unit line, which means the two results are equal. The fitted line for structural loss in Figure 71 shows that the structural losses obtained with OQ risk approach are five times larger than the ones calculated with Hazus. Although there are some points scattered from the linear fit line, the linear fit line formed from data of non-structural and content AEL is close to the ideal curve (unit line). The fitted line indicates that the Hazus result for non-structural component is only 10% larger than OpenQuake and the Hazus result of content component is around 8% larger.

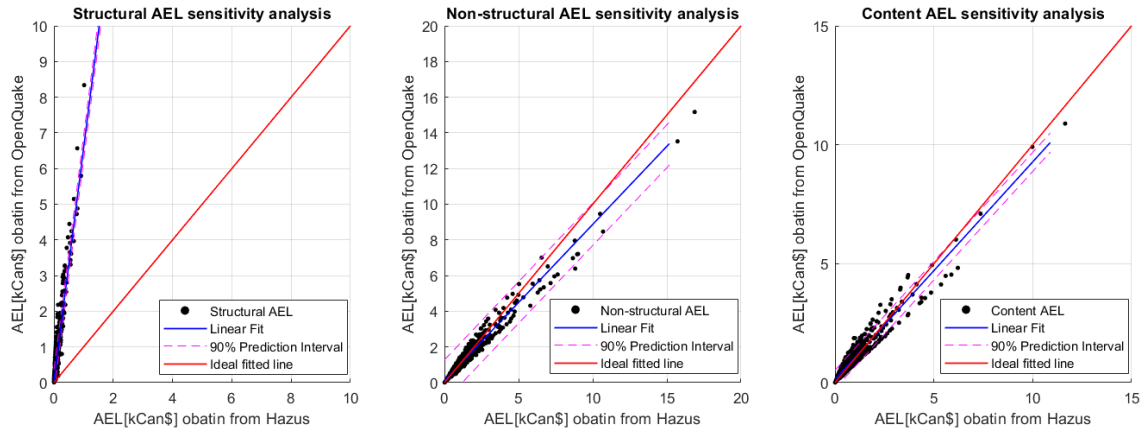

Figure 71. Comparison of results from Hazus and from OpenQuake risk approach for structural, non-structural, and content AEL

The structural loss has the largest discrepancy from the Hazus result. If the structural loss is further broken down by building types, it is shown that wood building contributes a big portion of the structural loss compared with Hazus. From Figure 72, the structural vulnerability curve for wood buildings provided a large mean loss ratio for low spectral acceleration. This leads to a large seismic loss from wood buildings. The Sa(0.3s) for Montreal region is approximately 0.05 to 0.4 from a return period of 100 years to 2475 years. The structural mean loss ratio is more than five times larger than the non-structural and content mean loss ratio for pre-code and moderate-code buildings and more than 10 times larger than the low-code buildings.

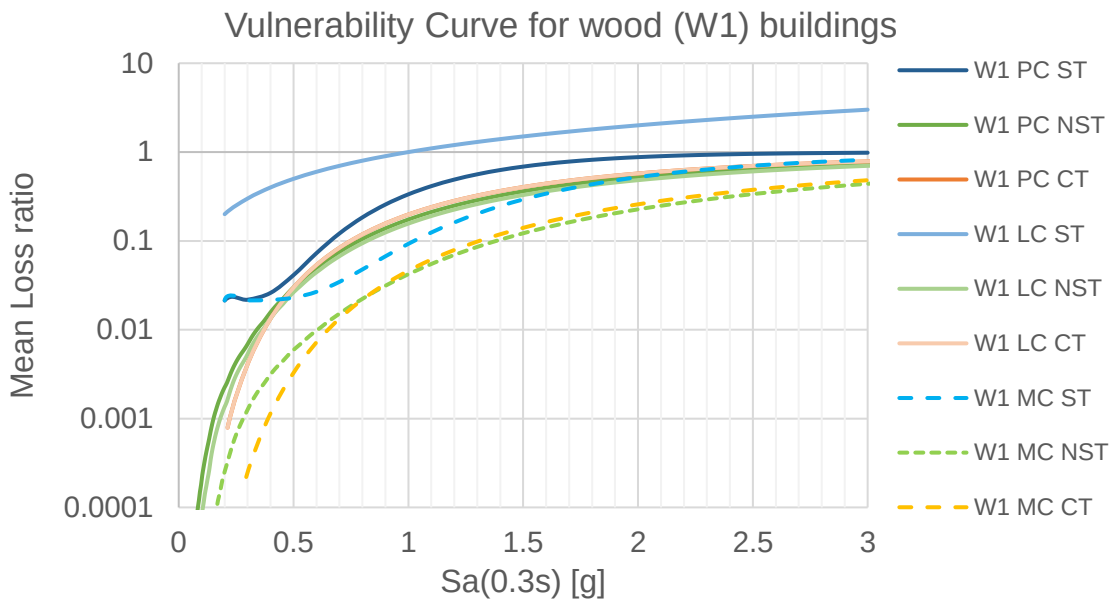

Figure 72. Structural and non-structural vulnerability functions for Wood building pre-code, low-code, and moderate-code

The other building types have very small or negligible losses for short return periods. The wood building type contributes to the majority (72.4%) of the seismic losses. Indeed, it counts for 99.97% of the total structural loss (Can$49,247 thousand). Since the vulnerability functions used by NRCan are not yet fully explained, further research needs to be done in order to calibrate them to the Montreal and Quebec building context.

7. Conclusion, Limitation and Future improvement

7.1 Overview

This thesis estimates the Annualized Earthquake Losses (AEL) for residential buildings in the Greater Montreal region using two software, Hazus and OpenQuake. The 5th generation of the Canadian Seismic Hazard Maps, building inventory, and vulnerability model are used as inputs to estimate seismic losses for eight return periods. The resulting economic losses, with the associated probability of exceedance, are used to estimate AEL. Compared to the calculation of maximum loss for an event, AEL provides a better interpretation of the expected loss because of the combination of the effects of seismic losses on probability of exceedance. The AEL can be further analyzed with building exposure to obtain AELR, as well as to calculate the loss per capita and per building count, in order to understand the regional loss distribution.

Major findings of this thesis are summarized below:

- The AEL is estimated around Can$ 6.18 million with Hazus. In OpenQuake, the AEL is calculated to be Can$12.4 million from the damage approach combining fragility and consequence functions, and to be Can$6.16 million using the risk approach using only vulnerability functions.
- The effect of the ground motion, building value, construction type, and code level on AEL from Hazus is studied by a sensitivity analysis. It is observed that all four factors have an impact on the AEL. The AEL follows a positive linear relationship with the ground motions, building value, and building type. AEL is also sensitive to building's year of construction (code level). Older buildings (pre-code) will experience larger damage and induced larger AEL than newly built ones (moderate-code).
- The structural component contributes to less than 10% of the total AEL, which indicates the significance of considering non-structural components.
- By using two software, the Hazus results has some differences from the OpenQuake results using both different approaches: results from OpenQuake are two times larger than the Hazus result using the damage approach and 0.6% larger using the risk

approach. The differences in the results using two software are due to the distinct techniques to compute vulnerability, as the same ground motion and exposure models were used.

7.2 Pros and cons of the two software

The comprehensive understanding and comparison of the two software is possible in the case study of Montreal.

Hazus has been used in various past research for Eastern Canada with the Canadian version HazCan. The Capacity Spectrum method embedded is commonly acknowledged (Freeman, 2004) and the data inputs have been well-prepared. It is also easier to compare and analyze with existing resources to draw conclusions. In terms of functionality, besides residential buildings, Hazus performs loss estimation for a variety of infrastructure including lifelines, essential facilities, and transportation systems. It also considers damage from fires following earthquakes and debris losses.

However, Hazus also has some limitations. First, it is not very up to date. The national population and building database obtained is from 2008, which is outdated with respect to the 2014 version (Ulmi et al., 2014). The most updated data included in this thesis is the 2018 data for the CMM. There are features that allows mass export of the results in the US version while HazCan is not updated to include this feature. The second limitation is that there are difficulties for practical usage and technical support of the missing feature. The input data units of the inputs are based on American standards and imperial US customary unit system (inches and feet) which requires a conversion from the international unit system applied in Canada. For example, the units of PGV are inches per second which requires some conversion when using the existing data from the Canadian database. Additionally, Hazus requires an ArcGIS license, which reduces the accessibility to the software.

For OpenQuake, the most obvious advantage is that it is a free open-source software, which does not set economic barriers for the user. The developer also hosts learning workshops and sets up discussion forums for all users to communicate and seek support (https://www.training.openquake.org/). In the long run, it has better accessibility compared to Hazus. The biggest advantage of OpenQuake compared to Hazus is the ability to model

uncertainty. For example, in OpenQuake, users can modify the standard deviation of the consequence model to account for the uncertainty of the Repair Cost Ratio. HAZUS does not explicitly include such uncertainty models. Their obtained results represent the expected values of losses and do not include uncertainty ranges that would help better understand the potential variability of the results.

One limitation of OpenQuake is the requirement of high-expertise judgement when selecting the proper input. The large flexibility of the model allows the OpenQuake software to adapt to various conditions and information from different countries. However, this also causes some difficulty for people to use it quickly, as sufficient knowledge is required to build proper models and obtain reliable results. The other limitation is the lack of a graphic user interface. Even if there are available add-on GIS tools helpful for result analysis, the lack of graphic user interface requires additional effort to navigate and run calculations on OpenQuake.

7.3 Limitation, Future improvement, and application

Canada's 6th generation seismic hazard model was introduced in 2020 (Kolaj et al., 2020) and not yet officially published in 2022. At the time of writing this thesis, only a calculation for return period of 2475 years was done. The annualized seismic loss with this new SHM6 model has not yet been estimated. By using the new model in the future, the updates on the soil condition and source model will be more accurately addressed for the 6^{th} generation hazard map and a more updated AEL should be calculated based on it.

AEL only addresses direct economic losses to buildings and Hazus has the advantage of including features assessing social losses such as casualties, as well as indirect economic losses sustained by communities and regions. In the future, a comprehensive study that includes perspectives besides direct economic loss should be envisioned in Hazus and OpenQuake if technically possible.

The use of OpenQuake is very innovative for seismic risk assessments in Canada. Overall, this study provided an introduction to the application of OpenQuake for the AEL estimation. There are various possible future applications that can be carried out. Some of the improvement and future development are discussed below:

- Only direct economic loss is compared in this study. More discussion on other factors, such as landslide, debris etc., can be evaluated from OpenQuake. The ability to examine earthquake impact in terms of other demographic parameters such as ethnicity, age, and income could also be important, like past research done by Yu (2011).
- It is concluded that there are differences between the results from Hazus and OpenQuake. In the OpenQuake damage approach, the missing drift-sensitive non-structural components give an overestimation the non-structural losses. Although OpenQuake does not have a feature to further divide the non-structural losses by more than one component, it is possible to modify the non-structural fragility function so that it will include both acceleration-sensitive and drift-sensitive components in future studies. In the OpenQuake risk approach, the vulnerability of wood buildings contributed from 80.9 % to 99.7% of the structural loss depending on the return period, and the total structural losses are around 6 times larger than the structural losses in Hazus. A future validation should be done for the vulnerability functions in order to obtain a more reliable loss estimation.

The region of Greater Montreal was studied in this thesis. In the future, study of a larger region in Quebec should be carried out to obtain estimation of regional seismic loss and to gain more comprehensive information for decision-making process by the government.

Appendix A Dissemination Area

In this Appendix, the dissemination area in this thesis is summarized in the table below by code number. The star after the name indicates that all the DAs of this RCMs are selected. For the other, only the DAs indicated below are selected for study.

Regional County Municipality (RCM)	Number of DA	Dissemination Code number
Argenteuil	1	24076760094
Beauharnois-Salaberry	22	2407070003-0004 2407070067 to 0079 and 0087 to 0092
Deux-Montagnes	162	24072720001 à 0275 (without184, 186, 187, 190, 194, 197, 201, 203-205)
La Rivière-du-Nord	4	24075750210-0211-0226-0230
La vallée de Richelieu	158	2405757 (without 215 to 225 and 235-236)
Lajemmerais *	126	2405959
L'Assomption	185	2406060 (without 199 to 212)
Laval *	637	2406565
Les Jardins-de-Napierville	2	24068680051-0053
Les Maskoutains	1	24054540135
Les Moulins *	231	2406464
Longueuil *	692	2405858
Mirabel *	47	2407474
Montcalm	4	24063630069-0109-0112-0114
Montréal *	3201	2406666
Roussillion *	252	2406767
Rouville	14	24055550075 to 0088
Thérèse-De Blainville *	238	2407373
Vaudreuil-Soulanges	139	2407171 (without 137 to143, 145, 175 to207, 216 to 220)
Total	6116	

Appendix B Contour map

In this Appendix, contour maps for the eight return periods (100, 225, 475, 750, 1000, 1500, 2000 and 2475 years) without (left) and with (right) consideration of site conditions are shown. There are three ground motion parameters that are studied: PGA, Sa(0.3s), and Sa(1.0s).

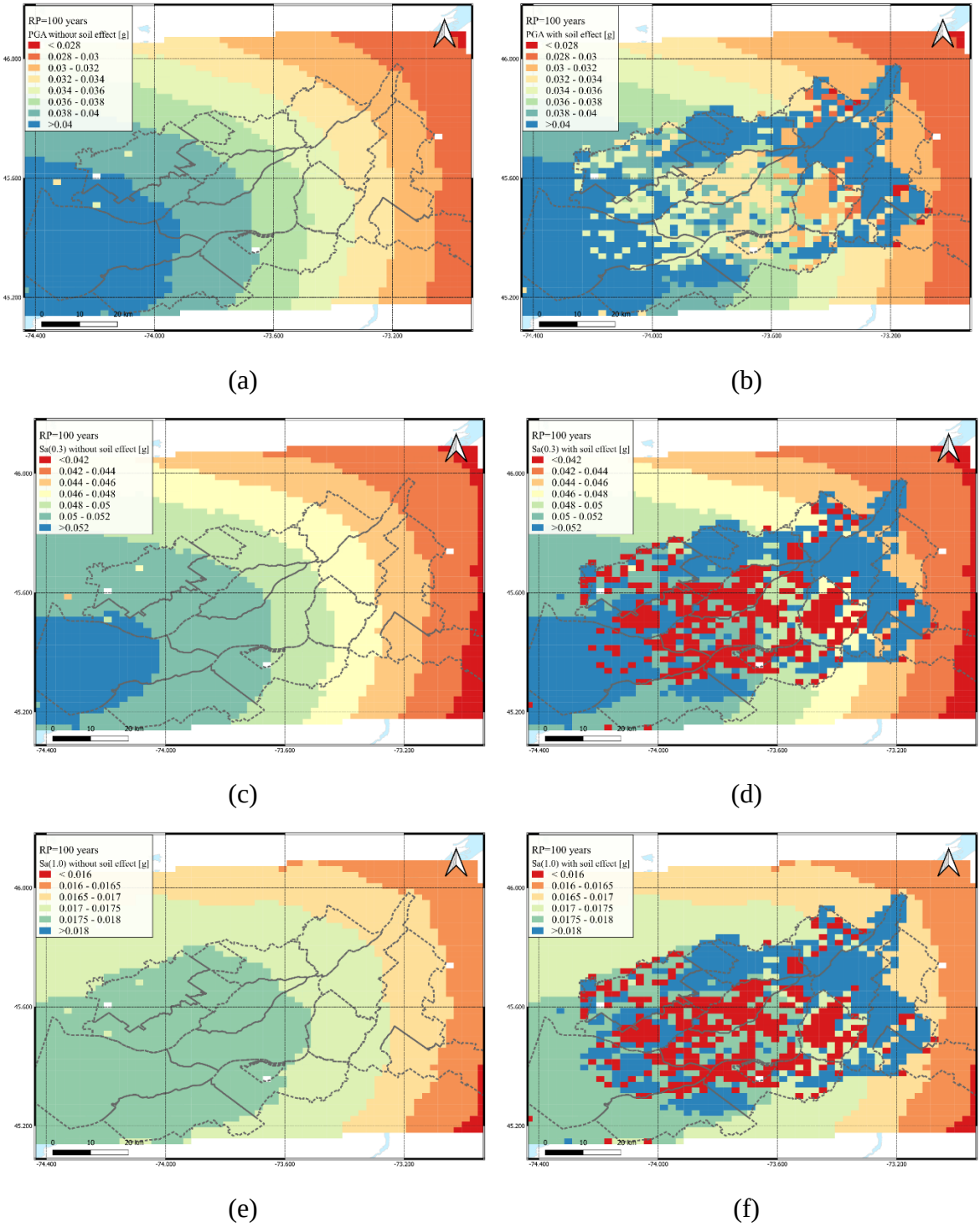

Figure 73. contour maps without (left) and with (right) consideration of site conditions for PGA (a)&(b), Sa(0.3s) (c)&(d), and Sa(1.0s) (e)&(f) for return period of 100 years

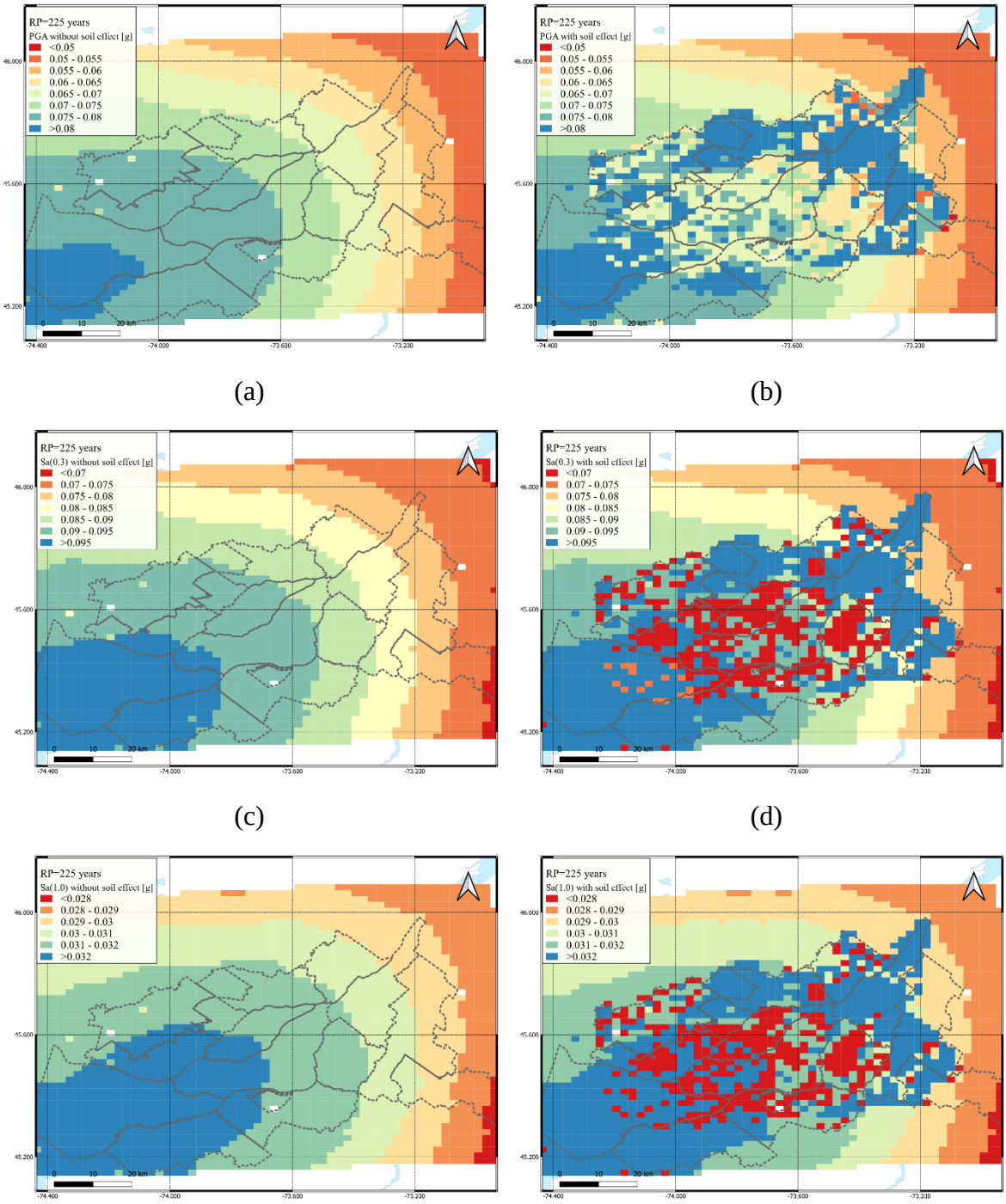

Figure 74. contour maps without (left) and with (right) consideration of site conditions for PGA (a)&(b), Sa(0.3s) (c)&(d), and Sa(1.0s) (e)&(f) for return period of 225 years

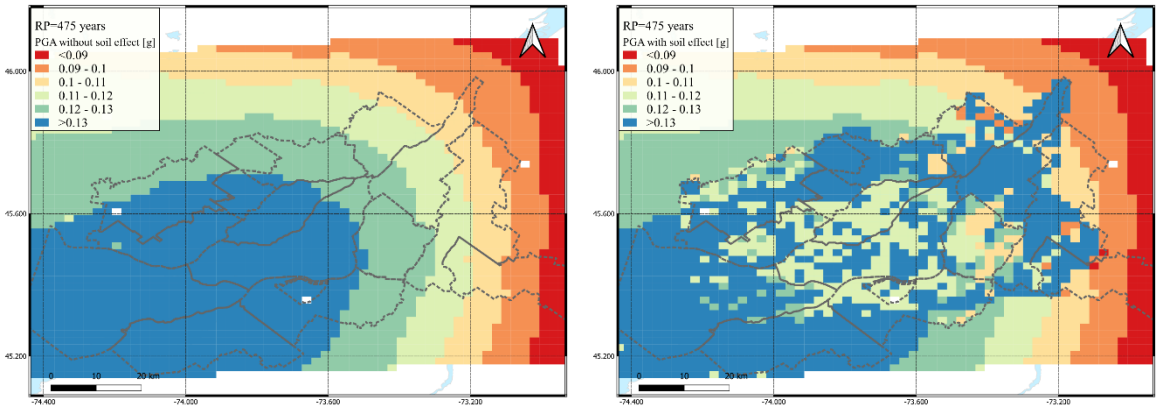

(a) (b)

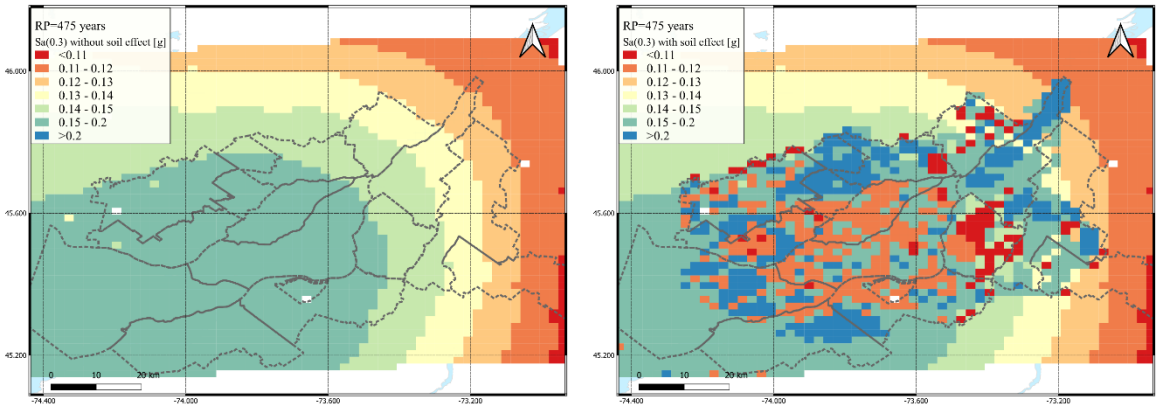

(c) (d)

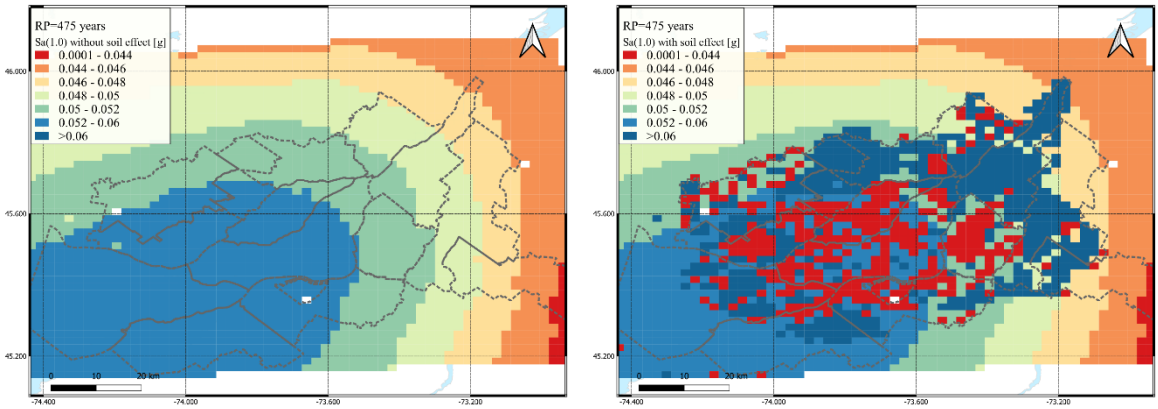

(e) (f)

Figure 75. contour maps without (left) and with (right) consideration of site conditions for PGA (a)&(b), Sa(0.3s) (c)&(d), and Sa(1.0s) (e)&(f) for return period of 475 years

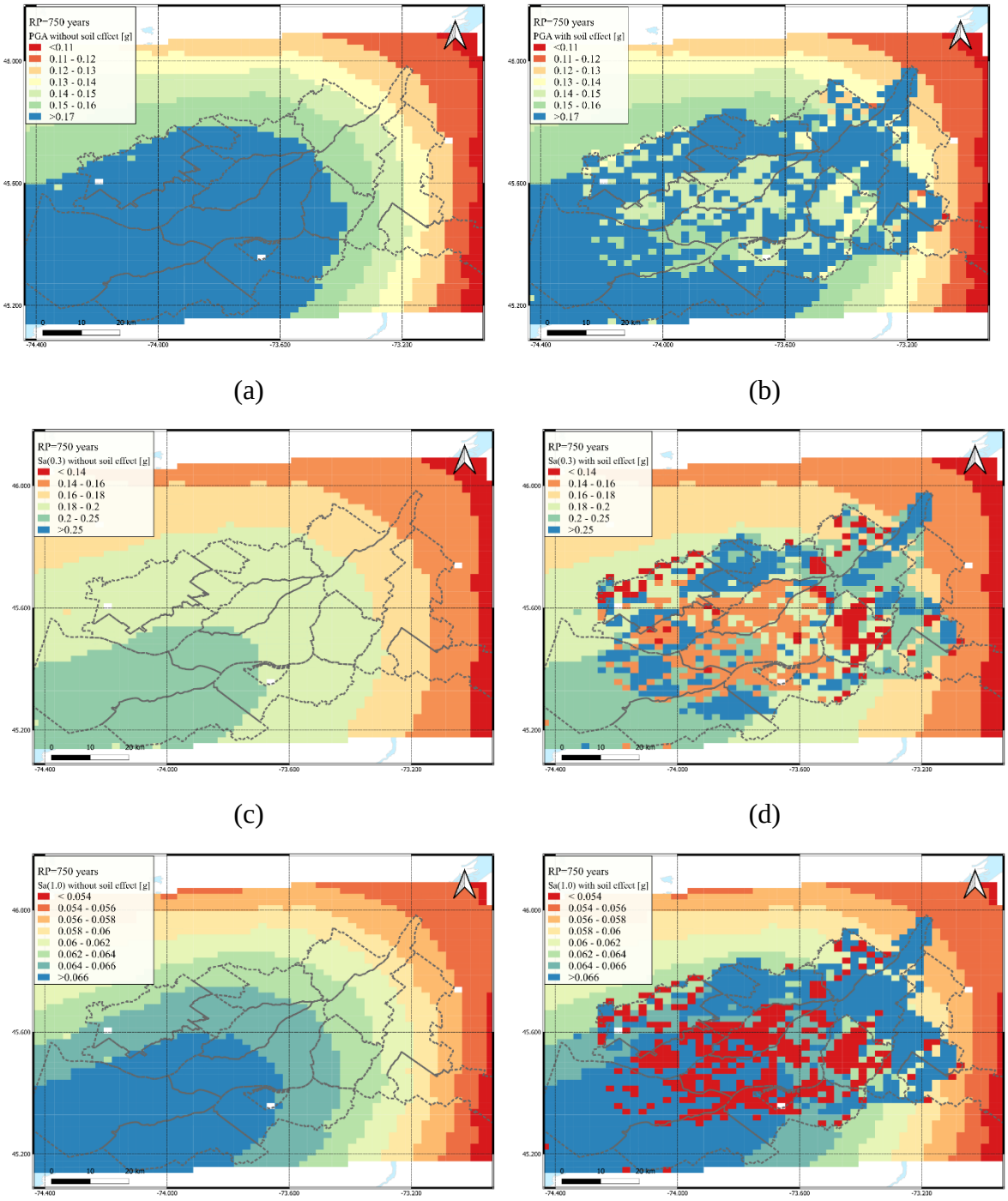

Figure 76. contour maps without (left) and with (right) consideration of site conditions for PGA (a)&(b), Sa(0.3s) (c)&(d), and Sa(1.0s) (e)&(f) for return period of 750 years

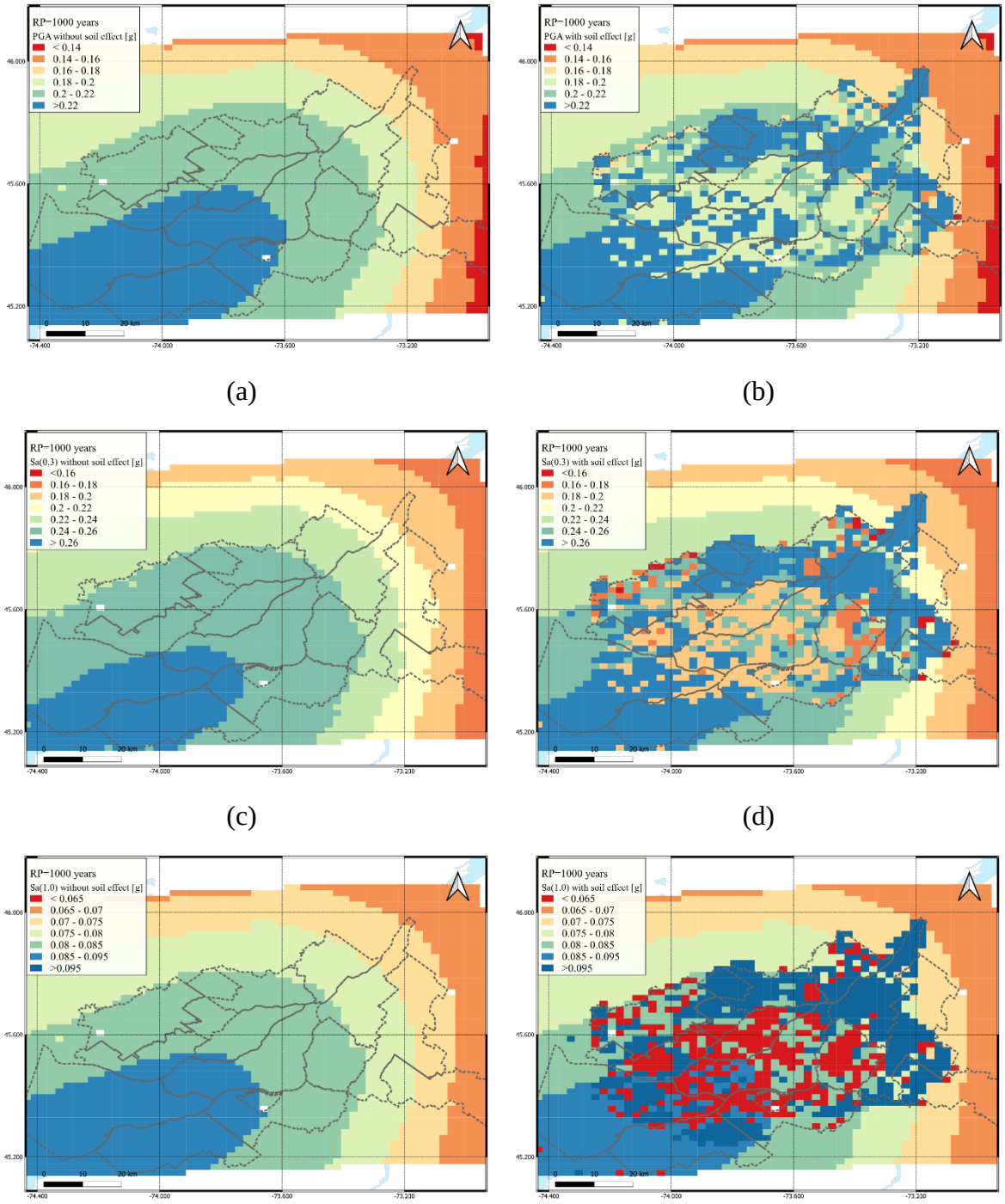

Figure 77. contour maps without (left) and with (right) consideration of site conditions for PGA (a)&(b), Sa(0.3s) (c)&(d), and Sa(1.0s) (e)&(f) for return period of 1000 years

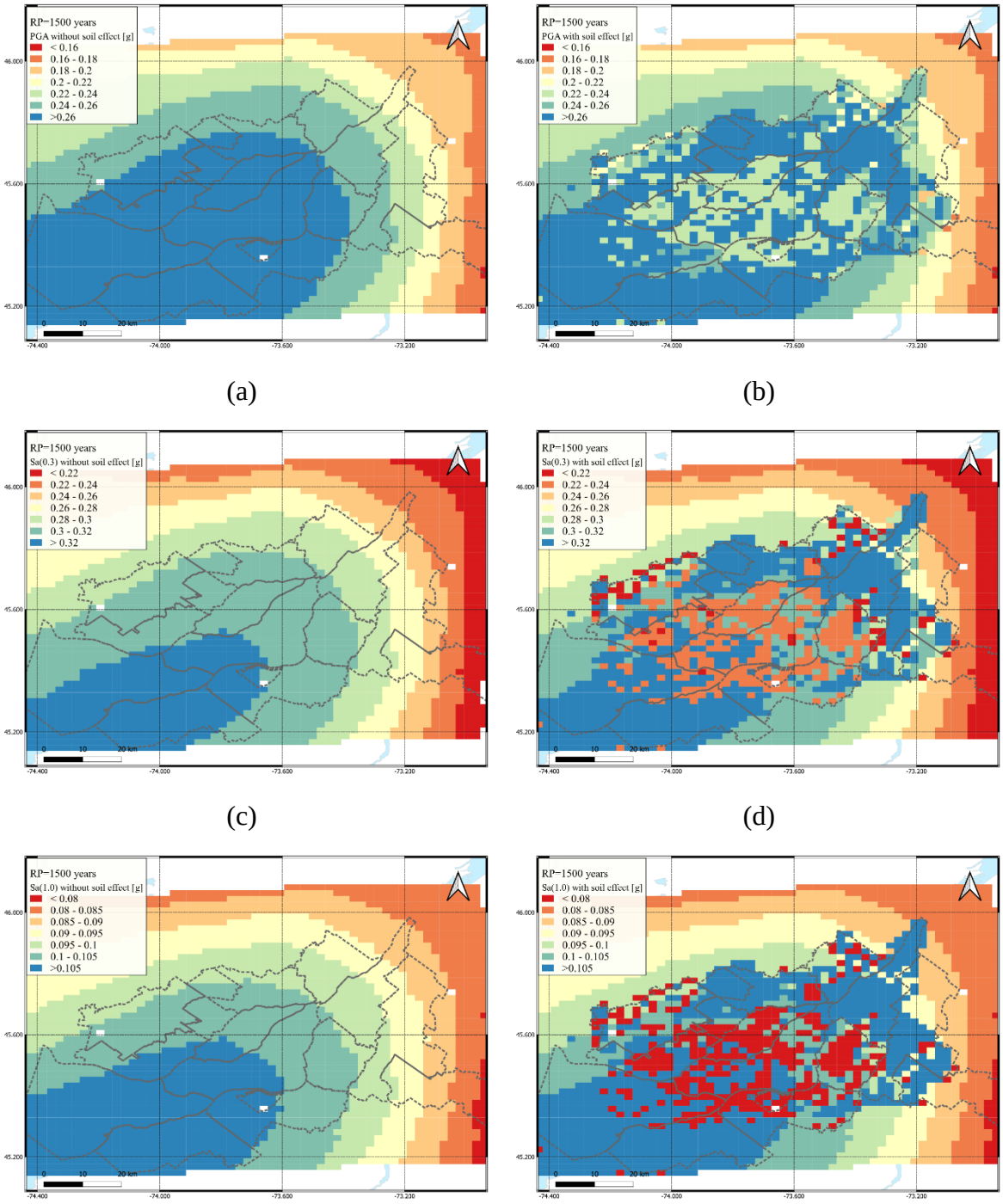

Figure 78. contour maps without (left) and with (right) consideration of site conditions for PGA (a)&(b), Sa(0.3s) (c)&(d), and Sa(1.0s) (e)&(f) for return period of 1500 years

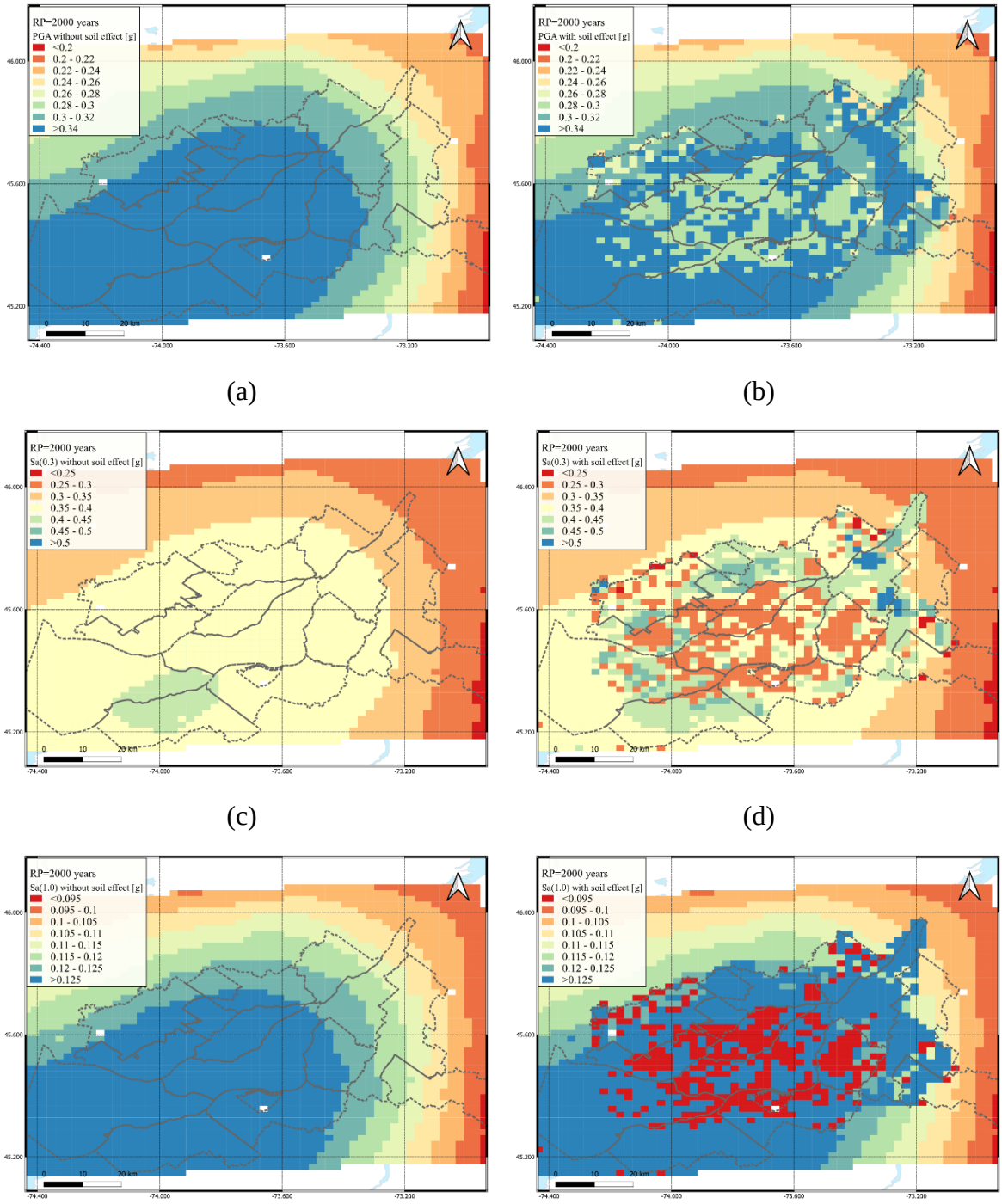

Figure 79. contour maps without (left) and with (right) consideration of site conditions for PGA (a)&(b), Sa(0.3s) (c)&(d), and Sa(1.0s) (e)&(f) for return period of 2000 years

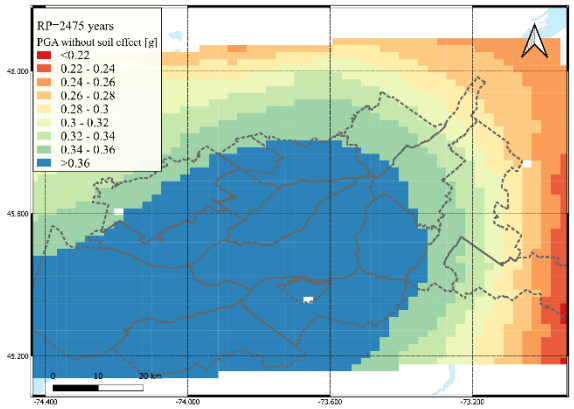

(a)

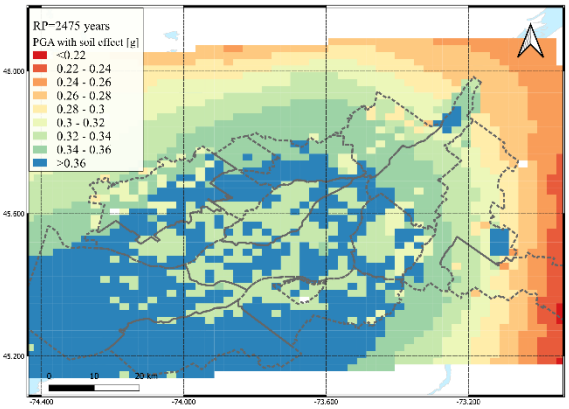

(b)

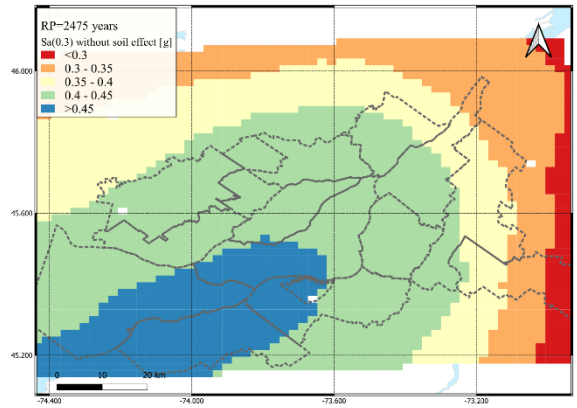

(c)

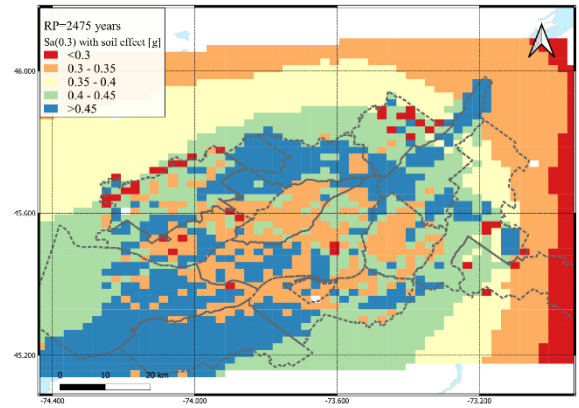

(d)

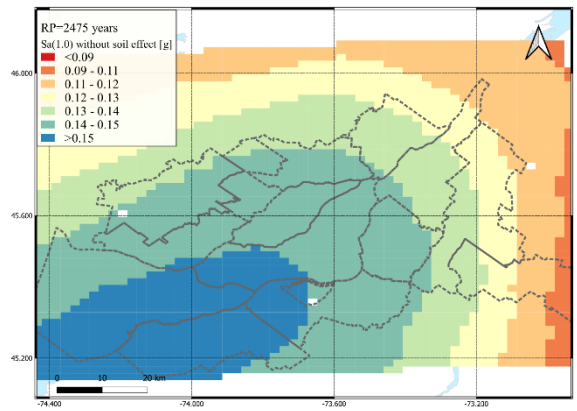

(e)

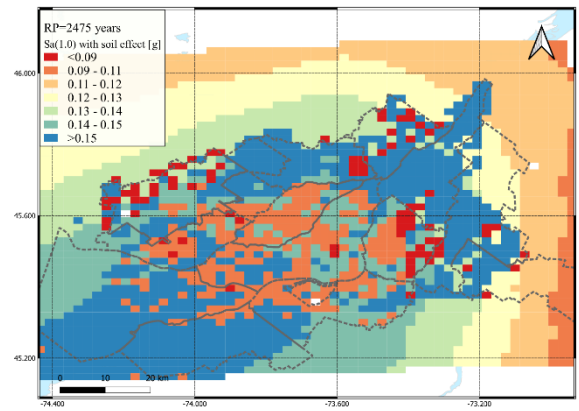

(f)

Figure 80. contour maps without (left) and with (right) consideration of site conditions for PGA (a)&(b), Sa(0.3s) (c)&(d), and Sa(1.0s) (e)&(f) for return period of 2475 years

Appendix C Equivalent PGA Fragility function

Table 5-29 Equivalent-PGA Structural Fragility -Moderate-Code Seismic Design Level

Building Type	Median Equivalent-PGA (g) and Logstandard Deviation (Beta)							
	Slight		Moderate		Extensive		Complete	
	Median	Beta	Median	Beta	Median	Beta	Median	Beta
W1	0.24	0.64	0.43	0.64	0.91	0.64	1.34	0.64
W2	0.20	0.64	0.35	0.64	0.64	0.64	1.13	0.64
S1L	0.15	0.64	0.22	0.64	0.42	0.64	0.80	0.64
S1M	0.13	0.64	0.21	0.64	0.44	0.64	0.82	0.64
S1H	0.10	0.64	0.18	0.64	0.39	0.64	0.78	0.64
S2L	0.20	0.64	0.26	0.64	0.46	0.64	0.84	0.64
S2M	0.14	0.64	0.22	0.64	0.53	0.64	0.97	0.64
S2H	0.11	0.64	0.19	0.64	0.49	0.64	1.02	0.64
S3	0.13	0.64	0.19	0.64	0.33	0.64	0.60	0.64
S4L	0.19	0.64	0.26	0.64	0.41	0.64	0.78	0.64
S4M	0.14	0.64	0.22	0.64	0.51	0.64	0.92	0.64
S4H	0.12	0.64	0.21	0.64	0.51	0.64	0.97	0.64
S5L* S5M* S5H*								
C1L	0.16	0.64	0.23	0.64	0.41	0.64	0.77	0.64
C1M	0.13	0.64	0.21	0.64	0.49	0.64	0.89	0.64
C1H	0.11	0.64	0.18	0.64	0.41	0.64	0.74	0.64
C2L	0.18	0.64	0.30	0.64	0.49	0.64	0.87	0.64
C2M	0.15	0.64	0.26	0.64	0.55	0.64	1.02	0.64
C2H	0.12	0.64	0.23	0.64	0.57	0.64	1.07	0.64
C3L* C3M* C3H*								
PC1	0.18	0.64	0.24	0.64	0.44	0.64	0.71	0.64
PC2L	0.18	0.64	0.25	0.64	0.40	0.64	0.74	0.64
PC2M	0.15	0.64	0.21	0.64	0.45	0.64	0.86	0.64
PC2H	0.12	0.64	0.19	0.64	0.46	0.64	0.90	0.64
RM1L	0.22	0.64	0.30	0.64	0.50	0.64	0.85	0.64
RM1M	0.18	0.64	0.26	0.64	0.51	0.64	1.03	0.64
RM2L	0.20	0.64	0.28	0.64	0.47	0.64	0.81	0.64
RM2M	0.16	0.64	0.23	0.64	0.48	0.64	0.99	0.64
RM2H	0.12	0.64	0.20	0.64	0.48	0.64	1.01	0.64
URML* URMM*								
MH	0.11	0.64	0.18	0.64	0.31	0.64	0.60	0.64

**Shaded boxes and building types with an asterisk (*) indicate types that are not permitted by current seismic codes.*

Table 5-30 Equivalent-PGA Structural Fragility - Low-Code Seismic Design Level

Building Type	Median Equivalent-PGA (g) and Logstandard Deviation (Beta)							
	Slight		Moderate		Extensive		Complete	
	Median	Beta	Median	Beta	Median	Beta	Median	Beta
W1	0.20	0.64	0.34	0.64	0.61	0.64	0.95	0.64
W2	0.14	0.64	0.23	0.64	0.48	0.64	0.75	0.64
S1L	0.12	0.64	0.17	0.64	0.30	0.64	0.48	0.64
S1M	0.12	0.64	0.18	0.64	0.29	0.64	0.49	0.64
S1H	0.10	0.64	0.15	0.64	0.28	0.64	0.48	0.64
S2L	0.13	0.64	0.17	0.64	0.30	0.64	0.50	0.64
S2M	0.12	0.64	0.18	0.64	0.35	0.64	0.58	0.64
S2H	0.11	0.64	0.17	0.64	0.36	0.64	0.63	0.64
S3	0.10	0.64	0.13	0.64	0.20	0.64	0.38	0.64
S4L	0.13	0.64	0.16	0.64	0.26	0.64	0.46	0.64
S4M	0.12	0.64	0.17	0.64	0.31	0.64	0.54	0.64
S4H	0.12	0.64	0.17	0.64	0.33	0.64	0.59	0.64
S5L	0.13	0.64	0.17	0.64	0.28	0.64	0.45	0.64
S5M	0.11	0.64	0.18	0.64	0.34	0.64	0.53	0.64
S5H	0.10	0.64	0.18	0.64	0.35	0.64	0.58	0.64
C1L	0.12	0.64	0.15	0.64	0.27	0.64	0.45	0.64
C1M	0.12	0.64	0.17	0.64	0.32	0.64	0.54	0.64
C1H	0.10	0.64	0.15	0.64	0.27	0.64	0.44	0.64
C2L	0.14	0.64	0.19	0.64	0.30	0.64	0.52	0.64
C2M	0.12	0.64	0.19	0.64	0.38	0.64	0.63	0.64
C2H	0.11	0.64	0.19	0.64	0.38	0.64	0.65	0.64
C3L	0.12	0.64	0.17	0.64	0.26	0.64	0.44	0.64
C3M	0.11	0.64	0.17	0.64	0.32	0.64	0.51	0.64
C3H	0.09	0.64	0.16	0.64	0.33	0.64	0.53	0.64
PC1	0.13	0.64	0.17	0.64	0.25	0.64	0.45	0.64
PC2L	0.13	0.64	0.15	0.64	0.24	0.64	0.44	0.64
PC2M	0.11	0.64	0.16	0.64	0.31	0.64	0.52	0.64
PC2H	0.11	0.64	0.16	0.64	0.31	0.64	0.55	0.64
RM1L	0.16	0.64	0.20	0.64	0.29	0.64	0.54	0.64
RM1M	0.14	0.64	0.19	0.64	0.35	0.64	0.63	0.64
RM2L	0.14	0.64	0.18	0.64	0.28	0.64	0.51	0.64
RM2M	0.12	0.64	0.17	0.64	0.34	0.64	0.60	0.64
RM2H	0.11	0.64	0.17	0.64	0.35	0.64	0.62	0.64
URML	0.14	0.64	0.20	0.64	0.32	0.64	0.46	0.64
URMM	0.10	0.64	0.16	0.64	0.27	0.64	0.46	0.64
MH	0.11	0.64	0.18	0.64	0.31	0.64	0.60	0.64

Table 5-31 Equivalent-PGA Structural Fragility - Pre-Code Seismic Design Level

Building Type	Median Equivalent-PGA (g) and Logstandard Deviation (Beta)							
	Slight		Moderate		Extensive		Complete	
	Median	Beta	Median	Beta	Median	Beta	Median	Beta
W1	0.18	0.64	0.29	0.64	0.51	0.64	0.77	0.64
W2	0.12	0.64	0.19	0.64	0.37	0.64	0.60	0.64
S1L	0.09	0.64	0.13	0.64	0.22	0.64	0.38	0.64
S1M	0.09	0.64	0.14	0.64	0.23	0.64	0.39	0.64
S1H	0.08	0.64	0.12	0.64	0.22	0.64	0.38	0.64
S2L	0.11	0.64	0.14	0.64	0.23	0.64	0.39	0.64
S2M	0.10	0.64	0.14	0.64	0.28	0.64	0.47	0.64
S2H	0.09	0.64	0.13	0.64	0.29	0.64	0.50	0.64
S3	0.08	0.64	0.10	0.64	0.16	0.64	0.30	0.64
S4L	0.10	0.64	0.13	0.64	0.20	0.64	0.36	0.64
S4M	0.09	0.64	0.13	0.64	0.25	0.64	0.43	0.64
S4H	0.09	0.64	0.14	0.64	0.27	0.64	0.47	0.64
S5L	0.11	0.64	0.14	0.64	0.22	0.64	0.37	0.64
S5M	0.09	0.64	0.14	0.64	0.28	0.64	0.43	0.64
S5H	0.08	0.64	0.14	0.64	0.29	0.64	0.46	0.64
C1L	0.10	0.64	0.12	0.64	0.21	0.64	0.36	0.64
C1M	0.09	0.64	0.13	0.64	0.26	0.64	0.43	0.64
C1H	0.08	0.64	0.12	0.64	0.21	0.64	0.35	0.64
C2L	0.11	0.64	0.15	0.64	0.24	0.64	0.42	0.64
C2M	0.10	0.64	0.15	0.64	0.30	0.64	0.50	0.64
C2H	0.09	0.64	0.15	0.64	0.31	0.64	0.52	0.64
C3L	0.10	0.64	0.14	0.64	0.21	0.64	0.35	0.64
C3M	0.09	0.64	0.14	0.64	0.25	0.64	0.41	0.64
C3H	0.08	0.64	0.13	0.64	0.27	0.64	0.43	0.64
PC1	0.11	0.64	0.14	0.64	0.21	0.64	0.35	0.64
PC2L	0.10	0.64	0.13	0.64	0.19	0.64	0.35	0.64
PC2M	0.09	0.64	0.13	0.64	0.24	0.64	0.42	0.64
PC2H	0.09	0.64	0.13	0.64	0.25	0.64	0.43	0.64
RM1L	0.13	0.64	0.16	0.64	0.24	0.64	0.43	0.64
RM1M	0.11	0.64	0.15	0.64	0.28	0.64	0.50	0.64
RM2L	0.12	0.64	0.15	0.64	0.22	0.64	0.41	0.64
RM2M	0.10	0.64	0.14	0.64	0.26	0.64	0.47	0.64
RM2H	0.09	0.64	0.13	0.64	0.27	0.64	0.50	0.64
URML	0.13	0.64	0.17	0.64	0.26	0.64	0.37	0.64
URMM	0.09	0.64	0.13	0.64	0.21	0.64	0.38	0.64
MH	0.08	0.64	0.11	0.64	0.18	0.64	0.34	0.64

Appendix D Repair Cost Ratio

In this Appendix, the Table of building repair cost ratio and the content damage ratio from (FEMA, 2015) for each component is shown below.

Structural Repair Cost Ratios (in % of building replacement cost)

No.	Label	Occupancy Class	Structural Damage State			
			Slight	Moderate	Extensive	Complete
1	RES1	Single-family Dwelling	0.5	2.3	11.7	23.4
2	RES2	Mobile Home	0.4	2.4	7.3	24.4
3-8	RES3A-F	Multi-family Dwelling	0.3	1.4	6.9	13.8
9	RES4	Temporary Lodging	0.2	1.4	6.8	13.6
10	RES5	Institutional Dormitory	0.4	1.9	9.4	18.8
11	RES6	Nursing Home	0.4	1.8	9.2	18.4

Acceleration-Sensitive Non-structural Repair Cost Ratios (in % of building replacement cost)

No.	Label	Occupancy Class	Acceleration-Sensitive Nonstructural Damage State			
			Slight	Moderate	Extensive	Complete
1	RES1	Single-family Dwelling	0.5	2.7	8.0	26.6
2	RES2	Mobile Home	0.8	3.8	11.3	37.8
3 - 8	RES3A-F	Multi-family Dwelling	0.8	4.3	13.1	43.7
9	RES4	Temporary Lodging	0.9	4.3	13.0	43.2
10	RES5	Institutional Dormitory	0.8	4.1	12.4	41.2
11	RES6	Nursing Home	0.8	4.1	12.2	40.8

Drift-Sensitive Non-structural Repair Cost Ratios (in % of building replacement cost)

No.	Label	Occupancy Class	Drift-Sensitive Nonstructural Damage State			
			Slight	Moderate	Extensive	Complete
1	RES1	Single-family Dwelling	1.0	5.0	25.0	50.0
2	RES2	Mobile Home	0.8	3.8	18.9	37.8
3 – 8	RES3A-F	Multi-family Dwelling	0.9	4.3	21.3	42.5
9	RES4	Temporary Lodging	0.9	4.3	21.6	43.2
10	RES5	Institutional Dormitory	0.8	4.0	20.0	40.0
11	RES6	Nursing Home	0.8	4.1	20.4	40.8

Contents Damage Ratios (in % of contents replacement cost)

Occupancy Class	Acceleration Sensitive Nonstructural Damage State			
	Slight	Moderate	Extensive	Complete
All Occupancies	1	5	25	50

Appendix E Site Amplification Factor

This Table 4-7 below is the Table used to account for soil amplification in FEMA, (2020). For different return period, the S_{A1} is different, so Fv varies accordingly. However, soil class C is assumed for the region studied, Fv is 1.5 for different value of S_{A1}.

Table 4-7 Site Amplification Factors

Spectral Acceleration	Site Class				
	A	B	C	D	E
Short-Period, S_{AS} (g)	**Short-Period Amplification Factor, F_A**				
< 0.25	0.8	0.9	1.3	1.6	2.4
0.50	0.8	0.9	1.3	1.4	1.7
0.75	0.8	0.9	1.2	1.2	1.3
1.0	0.8	0.9	1.2	1.1	1.1
1.25	0.8	0.9	1.2	1.0	0.9
> 1.5	0.8	0.9	1.2	1.0	0.8
1-Second Period, S_{A1} (g)	**Mid-Period Amplification Factor, F_V**				
< 0.1	0.8	0.8	1.5	2.4	4.2
0.2	0.8	0.8	1.5	2.2	3.3
0.3	0.8	0.8	1.5	2.0	2.8
0.4	0.8	0.8	1.5	1.9	2.4
0.5	0.8	0.8	1.5	1.8	2.2
> 0.6	0.8	0.8	1.4	1.7	2.0
Peak Ground Acceleration (g)	**Peak Ground Acceleration Amplification Factor, F_{PGA}**				
< 0.1	0.8	0.9	1.3	1.6	2.4
0.2	0.8	0.9	1.2	1.4	1.9
0.3	0.8	0.9	1.2	1.3	1.6
0.4	0.8	0.9	1.2	1.2	1.4
0.5	0.8	0.9	1.2	1.1	1.2
> 0.6	0.8	0.9	1.2	1.1	1.1

** Source: Stewart and Seyhan, 2013*

Appendix F Average Consequence

	Structural			
	slight	**moderate**	**extensive**	**complete**
W	0.0046	0.0212	0.1074	0.2148
S	0.0030	0.0140	0.0690	0.1380
C	0.0030	0.0140	0.0690	0.1380
URMM	0.0030	0.0140	0.0690	0.1380
URML	0.0034	0.0158	0.0786	0.1572
MH	0.0040	0.0240	0.0730	0.2440

	Non-Structural			
	slight	**moderate**	**extensive**	**complete**
W	0.0077	0.0394	0.1664	0.3926
S	0.0085	0.0430	0.1720	0.4310
C	0.0085	0.0430	0.1720	0.4310
URMM	0.0085	0.0430	0.1720	0.4310
URML	0.0083	0.0421	0.1706	0.4214
MH	0.0080	0.0380	0.1510	0.3780

	Contents			
	slight	**moderate**	**extensive**	**complete**
W	0.01	0.05	0.25	0.5
S	0.0100	0.0500	0.2500	0.5000
C	0.0100	0.0500	0.2500	0.5000
URMM	0.0100	0.0500	0.2500	0.5000
URML	0.01	0.05	0.25	0.5
MH	0.0100	0.0500	0.2500	0.5000

Appendix G Building Damage by Building type

In this Appendix, a summary of the building damage under four damage states for eight return period are summarized below. Both the damage by building count and by percentage of the total damage under each damage state are presented.

	None		Slight		Moderate		Extensive		Complete	
	Return Period 2475 years									
	Count	%	Count	%	Count	%	Count	%	Count	%
Wood	620,635	93.56	163504	88.06	11,977	52.9	63	6.34	0	0
Steel	2,870	0.43	562	0.3	213	0.94	7	0.75	0	0.35
Concrete	12,855	1.94	1641	0.88	584	2.58	20	2.07	0	1.14
URM	24,202	3.65	18502	9.96	9,295	41.05	877	88.76	25	97.92
MH	2,815	0.42	1472	0.79	574	2.53	21	2.09	0	0.58
	Return Period 2000 years									
Wood	663,254	93.21	125524	86.35	7,373	48.44	28	5.01	0	0
Steel	3,114	0.44	414	0.28	123	0.8	3	0.51	0	0.43
Concrete	13,439	1.89	1260	0.87	391	2.57	11	2	0	1.45
URM	28,581	4.02	16891	11.62	6,911	45.4	506	90.25	10	97.37
MH	3,167	0.45	1278	0.88	424	2.79	13	2.24	0	0.76
	Return Period 1500 years									
Wood	712,051	92.7	80500	83.81	3,620	43.48	9	3.56	0	0
Steel	3,369	0.44	232	0.24	51	0.61	1	0.33	0	0
Concrete	14,087	1.83	796	0.83	212	2.55	5	2.04	0	1.1
URM	34,888	4.54	13583	14.14	4,203	50.49	222	92.17	4	98.44
MH	3,696	0.48	941	0.98	240	2.88	5	1.9	0	0.45
	Return Period 1000 years									
Wood	750,497	92.3	44274	79.77	1,407	35.31	1	1.51	0	0
Steel	3,524	0.43	111	0.2	17	0.43	0	0.13	0	0
Concrete	14,556	1.79	449	0.81	94	2.35	2	1.62	0	1.96
URM	40,469	4.98	10010	18.03	2,333	58.53	88	94.52	1	97.05
MH	4,087	0.5	659	1.19	135	3.38	2	2.23	0	0.99
	Return Period 750 years									
Wood	770,117	91.89	25304	77.76	758	36.46	1	3.35	0	0
Steel	3,596	0.43	50	0.15	6	0.3	0	0.11	0	0
Concrete	14,762	1.76	273	0.84	64	3.06	1	3.28	0	8.66
URM	45,248	5.4	6451	19.82	1,166	56.12	36	90.52	0	89.6
MH	4,333	0.52	464	1.43	84	4.05	1	2.74	0	1.74

	Return Period 475 years									
Wood	784,604	91.63	11331	72.6	244	29.38	0	0	0	0
Steel	3,631	0.42	19	0.12	2	0.22	0	0	0	0
Concrete	14,954	1.75	125	0.8	21	2.54	0	1.77	0	0
URM	48,500	5.66	3860	24.73	529	63.75	11	96.96	0	100
MH	4,576	0.53	272	1.74	34	4.12	0	1.26	0	0

	Return Period 225 years									
Wood	794,874	91.32	1292	58.55	13	15.41	0	0	0	0
Steel	3,651	0.42	2	0.08	0	0.1	0	0	0	0
Concrete	15,086	1.73	13	0.59	1	1.16	0	0.08	0	0
URM	51,991	5.97	843	38.19	66	78.68	1	99.92	0	0
MH	4,821	0.55	57	2.59	4	4.66	0	0	0	0

	Return Period 100 years									
Wood	796,114	91.24	65	42.91	0	0	0	0	0	0
Steel	3,652	0.42	0	0.03	0	0	0	0	0	0
Concrete	15,100	1.73	1	0.37	0	0.38	0	0	0	0
URM	52,814	6.05	81	53.26	5	95.9	0	0	0	0
MH	4,877	0.56	5	3.43	0	3.72	0	0	0	0

Reference

Adams, J. (2011). Seismic hazard maps for the National Building Code of Canada. *Proceedings, Annual Conference - Canadian Society for Civil Engineering*, *2*, 896–905.

Adams, J., Allen, T., Halchuk, S., & Kolaj, M. (2019). Canada's 6th generation seismic hazard model, as prepared for the 2020 National Building Code of Canada. *The 12th Canadian Conference on Earthquake Engineering*.

Adams, J., Halchuk, S., Allen, T., & Rogers, G. (2015). Canada's 5th Generation Seismic Hazard Model, As Prepared For the 2015 National Building Code of Canada. *The 11th Canadian Conference on Earthquake Engineering*, *2003*, 21–24.

AIR. (2013). *Study of impact and the insurance and economic cost of a major earthquake in British Columbia and Ontario / Québec*. *October*, 264.

Allen, T.I., Halchuk, S., Adams, J., & Rogers, G. C. (2017). Canada's 5th Generation Seismic Hazard Model: 2015 Hazard Values and Future Updates. *16th World Conference on Earthquake Engineering*, 12. http://www.wcee.nicee.org/wcee/article/16WCEE/WCEE2017-3494.pdf

Allen, Trevor I., Halchuk, S., Adams, J., & Weatherill, G. A. (2020). Forensic PSHA: Benchmarking Canada's Fifth Generation seismic hazard model using the OpenQuake-engine. *Earthquake Spectra*, *36*(1_suppl), 91–111. https://doi.org/10.1177/8755293019900779

Ansal, A., Akinci, A., Cultrera, G., Erdik, M., Pessina, V., Tönük, G., & Ameri, G. (2009). Loss estimation in Istanbul based on deterministic earthquake scenarios of the Marmara Sea region (Turkey). *Soil Dynamics and Earthquake Engineering*, *29*(4), 699–709.

Atkinson, G. M., & Adams, J. (2013). Ground motion prediction equations for application to the 2015 Canadian national seismic hazard maps. *Canadian Journal of Civil Engineering*, *40*(10), 988–998. https://doi.org/10.1139/cjce-2012-0544

Atkinson, G. M., & Boore, D. M. (2011). Modifications to existing ground-motion prediction equations in light of new data. *Bulletin of the Seismological Society of America*, *101*(3), 1121–1135.

Bagatini Cachuço, F. (2021). *Seismic performance evaluation of steel building systems in Canada*. University of British Columbia.

Baker, J. W. (2013). An introduction to probabilistic seismic hazard analysis. *White Paper Version*, *2*(1), 79.

Bendito, A., Rozelle, J., & Bausch, D. (2014). Assessing Potential Earthquake Loss in Mérida State, Venezuela Using Hazus. *International Journal of Disaster Risk Science*, *5*(3), 176–191. https://doi.org/10.1007/s13753-014-0027-0

Burton, C. G., & Silva, V. (2016). Assessing integrated earthquake risk in OpenQuake with an application to Mainland Portugal. *Earthquake Spectra*, *32*(3), 1383–1403. https://doi.org/10.1193/120814EQS209M

Calderon, A., & Silva, V. (2019). Probabilistic seismic vulnerability and loss assessment of the residential building stock in Costa Rica. *Bulletin of Earthquake Engineering*, *17*(3), 1257–1284. https://doi.org/10.1007/s10518-018-0499-1

Campbell, K. W., & Bozorgnia, Y. (2008). NGA ground motion model for the geometric mean horizontal component of PGA, PGV, PGD and 5% damped linear elastic response spectra for periods ranging from 0.01 to 10 s. *Earthquake Spectra*, *24*(1), 139–171.

CCBFC. (2015). *National Building Code of Canada: 2015*. National Research Council of Canada.

https://doi.org/10.4224/40002005

Chaulagain, H., Rodrigues, H., Silva, V., Spacone, E., & Varum, H. (2015). Seismic risk assessment and hazard mapping in Nepal. *Natural Hazards*, *78*(1), 583–602. https://doi.org/10.1007/s11069-015-1734-6

Chen, R., Jaiswal, K. S., Bausch, D., Seligson, H., & Wills, C. J. (2016). Annualized earthquake loss estimates for California and their sensitivity to site amplification. *Seismological Research Letters*, *87*(6), 1363–1372. https://doi.org/10.1785/0220160099

Chien, J., Peña-Castro, A. F., Onwuemeka, J., Liu, Y., Pollet, J., Rosset, P., & Chouinard, L. (2021). Earthquake source parameter inversion and seismic hazard model in the western Quebec Seismic Zone. *AGU Fall Meeting 2021*.

Dargush, A. S., Augustyniak, M., Deodatis, G., Jacob, K. H., Laura McGinty, George Mylonakis, Guy J.P. Nordenson, Daniel O'Brien, Scott Stanford, B. S., & Wear, M. W. T. and S. (2001). *Estimating Earthquake Losses for the Greater New York City Area*. 173–184.

Dell'Acqua, F., Gamba, P., & Jaiswal, K. (2013). Spatial aspects of building and population exposure data and their implications for global earthquake exposure modeling. *NATURAL HAZARDS*, *68*(3), 1291–1309. https://doi.org/10.1007/s11069-012-0241-2

Dowrick, D. J. (2009). *Earthquake resistant design and risk reduction*. John Wiley & Sons.

Federal Emegency Management Agency (FEMA). (2001). *Hazus®99 Estimated Annualized Earthquake Losses for the United States Federal Emergency Management Agency Mitigation Directorate*. FEMA.

Federal Emegency Management Agency (FEMA). (2008). *HAZUS MH Estimated Annualized Earthquake Losses for the United States*. FEMA.

Felsenstein, D., Elbaum, E., Levi, T., & Calvo, R. (2021). Post-processing HAZUS earthquake damage and loss assessments for individual buildings. *Natural Hazards*, *105*(1), 21–45. https://doi.org/10.1007/s11069-020-04293-1

FEMA-USGS-PDC. (2017). Estimated annualized earthquake losses for the United States: FEMA P-366. *Federal Emergency Management Agency (FEMA), United States Geologic Survey (USGS), and the Pacific Disaster Center (PDC), April*, 78.

FEMA. (2015). Earthquake Model Hazus-MH 2.1 User Manual. *Federal Emergency Management Agency*, 121. www.fema.gov/plan/prevent/hazus

FEMA. (2020). Hazus Earthquake Model Technical Manual - 4.2 SP3. *Federal Emergency Management Agency*, *October*, 1–436.

Field, E. H., Jordan, T. H., & Cornell, C. A. (2003). A developing community-modeling environment for seismic hazard analysis. *Seismological Research Letters*, *74*(4), 406–419.

Field, E. H., Seligson, H. A., Gupta, N., Gupta, V., Jordan, T. H., & Campbell, K. W. (2005). Loss estimates for a Puente Hills blind-thrust earthquake in Los Angeles, California. *Earthquake Spectra*, *21*(2), 329–338.

Filiatrault, A. (2013). *Elements of earthquake engineering and structural dynamics*. Presses inter Polytechnique.

Firuzi, E., Ansari, A., Amini Hosseini, K., & Rashidabadi, M. (2019). Probabilistic earthquake loss model for residential buildings in Tehran, Iran to quantify annualized earthquake loss. *Bulletin of Earthquake Engineering*, *17*(5), 2383–2406. https://doi.org/10.1007/s10518-019-00561-z

Freeman, S. A. (2004). Review of the development of the capacity spectrum method. *ISET Journal of Earthquake Technology*, *41*(1), 1–13.

GEM. (2021). *OQ User Manual v3.11.2*. 208. http://globalquakemodel.org/openquake

Halchuk, S., Adams, J., Kolaj, M., & Allen, T. (2019). Deaggregation of NBCC 2015 seismic hazard for selected Canadian cities. *12th Canadian Conference on Earthquake Engineering*, 9.

Halchuk, S., Allen, T. I., Adams, J., & Rogers, G. C. (2014). Fifth generation seismic hazard model input files as proposed to produce values for the 2015 National Building Code of Canada. *Geological Survey of Canada Open File 7576*, 18. https://doi.org/10.4095/293907

HAZUS-MH, N. (2004). Users's manual and technical manuals. report prepared for the federal emergency management agency. *National Institute of Building Sciences. Federal Emergency Management Agency (FEMA). Washington, DC*.

Hobbs, T. E., Journeay, J. M., Rotheram, D., Hobbs, T. E., Journeay, J. M., & Rotheram, D. (2021). *An earthquake scenario catalogue for Canada : a guide to using scenario hazard and risk results*. *GEOLOGICAL SURVEY OF CANADA*.

Hosseinpour, V., Saeidi, A., Nollet, M. J., & Nastev, M. (2021). Seismic loss estimation software: A comprehensive review of risk assessment steps, software development and limitations. *Engineering Structures*, *232*(January). https://doi.org/10.1016/j.engstruct.2021.111866

Hunter, J. A. M., & Crow, H. L. (2015). *Shear wave velocity measurement guidelines for Canadian seismic site characterization in soil and rock*. Natural Resources Canada.

Kazantzidou-Firtinidou, D., Kyriakides, N., Votsis, R., & Chrysostomou, C. (2022). Seismic risk assessment as part of the National Risk Assessment for the Republic of Cyprus: from probabilistic to scenario-based approach. In *Natural Hazards* (Issue 0123456789). Springer Netherlands. https://doi.org/10.1007/s11069-021-05200-y

Khaheshi Banab, K., Kolaj, M., Motazedian, D., Sivathayalan, S., Hunter, J. A., Crow, H. L., Pugin, A. J., Brooks, G. R., & Pyne, M. (2012). Seismic site response analysis for Ottawa, Canada: A comprehensive study using measurements and numerical simulations. *Bulletin of the Seismological Society of America*, *102*(5), 1976–1993.

Kolaj, M., Adams, J., & Halchuk, S. (2020). The 6th Generation seismic hazard model of Canada. *17th World Conference on Earthquake Engineering*, 1–12.

Kolaj, M., Halchuk, S., Adams, J., & Allen, T. (2020). Sixth Generation Seismic Hazard Model of Canada: input files to produce values proposed for the 2020 National Building Code of Canada. *Geological Survey of Canada, Open File 8630*, 15. https://doi.org/10.4095/327322

Lamontagne, M., Halchuk, S., Cassidy, J. F., & Rogers, G. C. (2008). Significant Canadian earthquakes of the period 1600-2006. *Seismological Research Letters*, *79*(2), 211–223. https://doi.org/10.1785/gssrl.79.2.211

Levi, T., Bausch, D., Katz, O., Rozelle, J., & Salamon, A. (2015). Insights from Hazus loss estimations in Israel for Dead Sea Transform earthquakes. *Natural Hazards*, *75*(1), 365–388. https://doi.org/10.1007/s11069-014-1325-y

Lu, G. Y., & Wong, D. W. (2008). An adaptive inverse-distance weighting spatial interpolation technique. *Computers & Geosciences*, *34*(9), 1044–1055.

McKinley, S., & Levine, M. (1998). *Cubic spline interpolation*.

Moffatt, S. F., & Cova, T. J. (2010). Parcel-scale earthquake loss estimation with HAZUS: A case study in salt Lake County, Utah. *Cartography and Geographic Information Science*, *37*(1), 17–29. https://doi.org/10.1559/152304010790588106

Parisi, M. A., & Piazza, M. (2015). Seismic strengthening and seismic improvement of timber structures. *Construction and Building Materials*, *97*, 55–66.

Parvez, I. A., & Rosset, P. (2014). The role of microzonation in estimating earthquake risk. In *Earthquake hazard, risk and disasters* (pp. 273–308). Elsevier.

Pezeshk, S., Zandieh, A., & Tavakoli, B. (2011). Hybrid empirical ground-motion prediction equations for eastern North America using NGA models and updated seismological parameters. *Bulletin of the Seismological Society of America*, *101*(4), 1859–1870.

Ploeger, S. K., Atkinson, G. M., & Samson, C. (2010). Applying the HAZUS-MH software tool to assess seismic risk in downtown Ottawa, Canada. *Natural Hazards*, *53*(1), 1–20. https://doi.org/10.1007/s11069-009-9408-x

Powers, P. M., Rezaeian, S., Shumway, A. M., Petersen, M. D., Luco, N., Boyd, O. S., Moschetti, M. P., Frankel, A. D., & Thompson, E. M. (2021). The 2018 update of the US National Seismic Hazard Model: Ground motion models in the western US. *Earthquake Spectra*, *37*(4), 2315–2341.

Rao, A., Dutta, D., Kalita, P., Ackerley, N., Silva, V., Raghunandan, M., Ghosh, J., Ghosh, S., Brzev, S., & Dasgupta, K. (2020). Probabilistic seismic risk assessment of India. *Earthquake Spectra*, *36*(1_suppl), 345–371. https://doi.org/10.1177/8755293020957374

Rodrigues, D., Crowley, H., & Silva, V. (2018). Earthquake loss assessment of precast RC industrial structures in Tuscany (Italy). *Bulletin of Earthquake Engineering*, *16*(1), 203–228. https://doi.org/10.1007/s10518-017-0195-6

Rosset, P., Bent, A. L., & Chouinard, L. E. (2020). Correlating DYFI Data With Seismic Microzonation in the Region of Montreal. *Earth Science Research*, *9*(2), 85. https://doi.org/10.5539/esr.v9n2p85

Rosset, P., Bour-Belvaux, M., & Chouinard, L. (2015). Microzonation models for Montreal with respect to VS30. *Bulletin of Earthquake Engineering*, *13*(8), 2225–2239. https://doi.org/10.1007/s10518-014-9716-8

Rosset, P., & Chouinard, L. (2009). Characterization of site effects in Montreal, Canada. *Natural Hazards*, *48*(2), 295–308. https://doi.org/10.1007/s11069-008-9263-1

Rosset, P., Chouinard, L. E., & Nollet, M. (2022a). *Consequences on Residential Buildings in Greater Montreal for a Repeat of the 1732 M5.8 Montreal Earthquake* (Vol. 2).

Rosset, P., Chouinard, L., & Nollet, M. (2022b). *Internal Report - Evaluation du Dommage Moyen Annuel du Bati Residentiel Pour la Communaute Metropolitaine De Montreal*.

Rosset, P., Kert, M., Youance, S., Nollet, M., & Chouinard, L. (2019a). Could Montreal residential buildings suffer important losses in case of major earthquakes? *In Proceedings of the 12th Canadian Conference on Earthquake Engineering*, *Mmi*, 2–8.

Rosset, P., Kert, M., Youance, S., Nollet, M. J., & Chouinard, L. (2019b). The use of Hazcan to assess the earthquake risk of residential buildings in Montreal, Canada. *Proceedings, Annual Conference - Canadian Society for Civil Engineering*, *2019-June*(Mmi).

Rozelle, J., Bausch, D., & Seligson, H. A. (2019). Hazus Earthquake Model. FEMA Standard Operating Procedure for Hazus Earthquake Data Preparation and Scenario Analysis. In *Fema*. https://www.fema.gov/sites/default/files/2020-09/fema_hazus_earthquake-sop.pdf

Rozman, M., & Fajfar, P. (2009). Seismic response of a RC frame building designed according to old and modern practices. *Bulletin of Earthquake Engineering*, *7*(3), 779–799.

Saretta, Y., Sbrogio, L., & Valluzzi, M. R. (2021). Seismic response of masonry buildings in historical centres struck by the 2016 Central Italy earthquake. Calibration of a vulnerability model for strengthened conditions. *Construction and Building Materials*, *299*, 123911.

Silva, V., Amo-Oduro, D., Calderon, A., Costa, C., Dabbeek, J., Despotaki, V., Martins, L., Pagani, M., Rao, A., & Simionato, M. (2020). Development of a global seismic risk model. *Earthquake Spectra*, *36*(1_suppl), 372–394.

Silva, V., Crowley, H., Pagani, M., Monelli, D., & Pinho, R. (2014). Development of the OpenQuake engine, the Global Earthquake Model's open-source software for seismic risk assessment. *Natural Hazards*, *72*(3), 1409–1427. https://doi.org/10.1007/s11069-013-0618-x

Silva, W., Gregor, N., & Darragh, R. (2002). Development of regional hard rock attenuation relations for central and eastern North America. *Pacific Engineering and Analysis, El Cerrito, CA*.

Tamima, U., & Chouinard, L. (2016). Development of evacuation models for moderate seismic zones: A case study of Montreal. *International Journal of Disaster Risk Reduction*, *16*, 167–179. https://doi.org/10.1016/j.ijdrr.2016.02.003

Wieland, M., Pittore, M., Parolai, S., Begaliev, U., Yasunov, P., Niyazov, J., Tyagunov, S., Moldobekov, B., Saidiy, S., Ilyasov, I., & Abakanov, T. (2015). Towards a cross-border exposure model for the earthquake model Central Asia. *Annals of Geophysics*, *58*(1). https://doi.org/10.4401/ag-6663

Wyss, M., Rosset, P., Tolis, S., & Speiser, M. (2021). Earthquake loss alerts to save victims. *EGU General Assembly Conference Abstracts*, EGU21-6311.

Yilmaz, C., Silva, V., & Weatherill, G. (2021). Probabilistic framework for regional loss assessment due to earthquake-induced liquefaction including epistemic uncertainty. *Soil Dynamics and Earthquake Engineering*, *141*(May 2020), 106493. https://doi.org/10.1016/j.soildyn.2020.106493

Yu, K. (2011). *Seismic Vulnerability Assessment for Montreal -An Application of HAZUS-MH4 By*. *February*.

Yu, K., Chouinard, L. E., & Rosset, P. (2016). Seismic vulnerability assessment for Montreal. *Georisk*, *10*(2), 164–178. https://doi.org/10.1080/17499518.2015.1106562